LUND UNIVERSITY

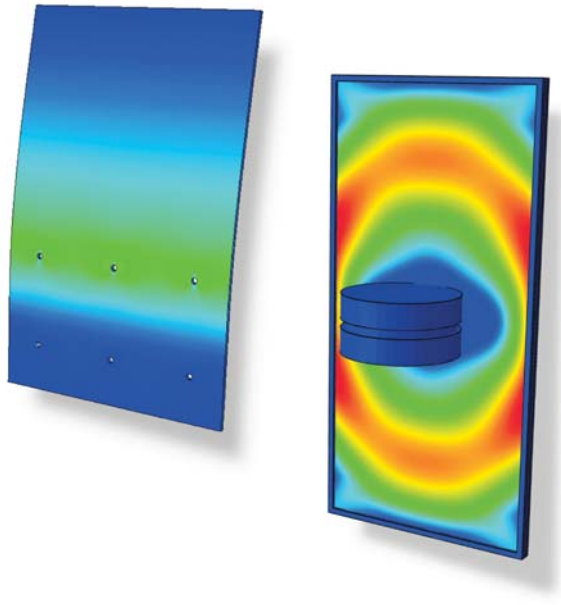

STRENGTH DESIGN METHODS FOR GLASS STRUCTURES

MARIA FRÖLING

Structural Mechanics

Doctoral Thesis

DEPARTMENT OF CONSTRUCTION SCIENCES
DIVISION OF STRUCTURAL MECHANICS

ISRN LUTVDG/TVSM--13/1025--SE (1-178) | ISSN 0281-6679
ISBN 978-91-7473-599-4 (print) | ISBN 978-91-7473-600-7 (pdf)
DOCTORAL THESIS

STRENGTH DESIGN METHODS FOR GLASS STRUCTURES

MARIA FRÖLING

Printed by Media-Tryck LU, Lund, Sweden, September 2013 *(Pl)*.

For information, address:
Division of Structural Mechanics, LTH, Lund University, Box 118, SE-221 00 Lund, Sweden.
Homepage: http://www.byggmek.lth.se

Acknowledgements

The work in this thesis has been performed at the Department of Construction Sciences, at Lund University. The financial support from the Swedish Research Council FORMAS, Glasbranschföreningen and Svensk Planglasförening is gratefully acknowledged.
I would like to thank my supervisors Anne Landin, Kent Persson and Per-Erik Austrell for their guidance, support and encouragement. I owe gratitude to Kent Persson for his genuine support through all stages of the research work including determining the research direction, generating ideas, practical advice, help with technical details and giving useful feedback. Per-Erik Austrell is acknowledged for his useful suggestions and cooperation on the fourth paper of this thesis.
The reference group of this project is acknowledged for their interest in the project, support and advice.
Technical help from personnel at the center for scientific and technical computing at Lund University, LUNARC, is acknowledged. Especially Anders Sjöström, Magnus Ullner and Joachim Hein who were of great help when it comes to issues relating to the computer systems. Anders Sjöström deserves a special thanks for helping with details regarding LATEX and Matlab. I would also like to thank Bo Zadig for help with graphical details. A thanks is directed to Johan Lorentzon for technical assistance. Håkan Hansson and Christina Glans are acknowledged for their excellent administrative skills that greatly simplify worklife.
I would like to thank the whole Department of Construction Sciences, and especially the Division of Structural Mechanics, for providing a supportive, open and creative work atmosphere.
I thank my family that was there for me to encourage when it was needed the most and that always supports me. Finally, thanks to all my friends for support, friendship and for making my leisure time more worthwile.

Abstract

In this thesis, user friendly and efficient methods for the design of glass structures are developed. The glass structures comprise various boundary conditions. Several types of glass are considered: single layered glass as well as laminated and insulated glass units. Typical load cases for strength design of glass are applied.
A recently developed finite element is suggested to be suitable for the modeling of laminated glass structures. It is shown that the new finite element is superior to standard solid elements for modeling of laminated glass. The results show that the element provides excellent capabilities for modeling of complex laminated glass structures with several bolted or adhesive joints.
The new element is utilized in the development of a method to compute stress concentration factors for laminated glass balustrades with two horizontal rows with two bolt fixings. The stress concentration factors are represented graphically in design charts. The use of the design charts allow the maximum principal stresses of the balustrade to be determined without using finite element analysis or advanced mathematics.
The shear-capacity of adhesive glass-joints is tested in a short-term load-case. Commonly used stiff and soft adhesives are considered. Finite element models of the test are developed to determine the material models of the adhesives. The material models are verified through large-scale tests. For the stiff adhesives and the main part of the soft adhesives, the material models are experimentally validated for both small-scale and large-scale tests. For a group of the soft adhesives, further research is necessary to validate the material models for a large-scale joint.
A reduced model for determining the maximum principal stresses of a glass subjected to dynamic impact load is developed and validated. The developed model is general in the sense that it is applicable to arbitrary location of the impact as well as to structures of arbitrary boundary condition. The validation is made for a four-sided supported glass pane and centric applied impact as well as excentric applied impact. It is shown that the model is applicable to small and medium sized structures. Finally it is proven that the model performs very well for a laminated glass balustrade of standard dimensions and with clamped fixings.
Finally, insulated glass subjected to soft body impact is analyzed be means of structure-acoustic analysis. A parametric study is made with respect to in-plane dimensions, glass thickness and thickness of the gas layer. For quadratic panes, a larger glass has a larger center displacement but lower stresses than a smaller glass. A single layered glass is proven to have only marginally greater stresses than the corresponding double glass. The air layer thickness has almost no influence on the stresses of the insulated glass but the thickness of the glass has a large influence. Finally, there is almost nothing to be gained to add a third glass pane to the insulated unit.

Keywords: finite element, computational techniques, laminated glass, stress concentration factor, design chart, bolt fixing, adhesive joint, balustrade, shear-capacity, dynamic impulse load, insulated glass.

Populärvetenskaplig sammanfattning

Glas som konstruktionsmaterial är relativt nytt och har blivit mer utbrett på grund av tekniska framsteg inom produktion av planglas, för vidarebearbetning av det tillverkade glaset och utvecklingen inom datorbaserade analysmetoder som finita elementmetoden. Jämfört med andra konstruktionsmaterial, till exempel betong, är kunskapen om glasets mekaniska egenskaper och strukturmekaniska beteende mindre.

Standarddimensioneringsmetoden inom konstruktion går ut på att dimensionerna hos en struktur bestäms genom att se till att de högsta spänningarna inte är större än materialets hållfasthet någonstans i strukturen. Den här typen av dimensionering är vanlig vid glaskonstruktion. Vid användning av den här metoden är det viktigt att de maximala spänningarna bestäms med tillförlitlighet.

Glas är ett sprött material som inte deformeras plastiskt innan brott. Spänningskoncentrationer som uppstår vid exempelvis ett borrhål reduceras därför inte. Det finns ett stort intresse för att bygga med glas i bärande delar av konstruktioner och att i glaskonstruktioner använda så lite annat material som möjligt. För att uppnå detta används infästningstyper som bultförband och limfogar. Tyvärr saknas det enkla och säkra dimensioneringskriterier och verktyg för att konstruera med glas utom för fall med enkla geometrier, infästningtyper och laster. Att utföra experiment är möjligt men det blir dyrt och inte så effektivt att utföra dimensionering på det sättet.

Syftet med det här arbetet är att utveckla metoder för att utföra effektiv dimensionering av avancerade glasstrukturer med olika infästningstyper och som utsätts för olika lastfall. En ny metod baserad på finita elementmetoden implementeras för att beräkna spänningsfördelningarna i avancerade strukturer av laminerat glas korrekt och effektivt. Den här metoden utgör en bas för utvecklingen av en analytisk dimensioneringsmetod för bultinfästa balustrader av laminerat glas. Metoden utgör ett komplement för att dimensionera den här typen av struktur och är lättare att använda än finita elementmetoden. Med hjälp av metoden kan spänningarna i balustraden bestämmas med hjälp av enkla formler och diagram.

En del av avhandlingen fokuserar på limfogar. Limfogar belastas ofta i skjuvning. Därför analyseras vanligt använda limmers skjuvkapacitet och finita elementmodeller tas fram så att limfogarna ska kunna analyseras med hjälp av beräkningar.

Glasstrukturer kan behöva dimensioneras för så kallad tung stöt. Det innebär att en vikt släpps i en pendelrörelse mot glaset. Inom ramen för detta arbete utvecklas en förenklad metod för att dimensionera glas för tung stöt. Förenklingarna går mestadels ut på att skapa mindre modeller. Fördelen med metoden är att den är flexibel och kan användas för olika glastyper och för olika typer av infästningar.

I bland annat fönster och fasader är det vanlig att använda isolerglas. Ett isolerglas består av två eller flera glas med mellanliggande gasspalt(er). I den här avhandlingen används strukturakustisk analys för att modellera isolerglas utsatt för tung stöt. Förutom att visa att den föreslagna metoden utgör ett hjälpmedel vid dimensionering, så används metoden för att utöka kunskapen om det strukturmekaniska beteendet hos isolerglas när det utsätts för stöt.

Contents

APPENDED PAPERS

Paper 1
Computational Methods for Laminated Glass
Maria Fröling and Kent Persson

Paper 2
Designing Bolt Fixed Laminated Glass with Stress Concentration Factors
Maria Fröling and Kent Persson

Paper 3
Shear-Capacity in Adhesive Glass Joints
Maria Fröling, Kent Persson and Oskar Larsson

Paper 4
A Reduced Model for the Design of Glass Structures Subjected to Dynamic Impulse Load
Maria Fröling, Kent Persson and Per-Erik Austrell

Paper 5 *Numerical Analysis of Insulated Glass Subjected to Soft Body Impact*
Maria Fröling and Kent Persson

Part 1: Introduction and overview of present work

1 Introduction

1.1 Background

During the past decades mass production of flat glass, development of new techniques to post-process the manufactured glass and the use of computational structural analyses by means of the finite element method have allowed for an increased use of glass as a structural material, [24]. Compared to other structural materials, for instance concrete, there is a lack in knowledge about mechanical properties and structural behaviour that has led to failure of several glass structures during the last years, [21].
Glass is a brittle material which means that it is not deformed plastically before failure. The stress concentrations that occur at for instance a bore hole edge are therefore not reduced. There is an increased interest in constructing with glass as a load bearing material and then the brittleness of the material must be accounted for in the design process. There is also an increased interest in constructing with glass using as little other materials as possible. This can be accomplished using joints of bolt fixed type or adhesive joints.
The design of innovative glass structures requires careful strength design due to the brittle characteristics of the material. However, there is a lack of simple design guidelines and tools for performing strength design of glass structures apart from when standard geometries, boundary condition and loading are used. There is always the opportunity to perform experimental tests. Full-scale testing is however time consuming and expensive and is not well suited for strength design when different design alternatives must be evaluated fast. Another possibility is to use finite element computations. The drawbacks are that it is time consuming and requires advanced skills in finite element modeling as well as access to commercial finite element software.
There is an apparent lack of knowledge when it comes to simple and reliable design tools for the design of advanced glass structures. This thesis deals with the development of efficient and user-friendly tools for the design of glass and laminated glass. The support conditions can be advanced, for instance bolt fixings, and the load conditions are different types of common static and dynamic loads.

1.2 Aim

The aim of this thesis is to provide means of efficiently designing advanced glass structures subjected to various loads and boundary conditions. More specifically, the aim is to develop simple numerical and analytical design tools for the design of those glass structures.

1.3 Limitations

In the studies performed in this thesis, some limitations are necessary. In the development of simpler design tools for structural design of glass, the effect of geometric nonlinearities are left out for the sake of increasing the computational efficiency. When the accurate

modeling of nonlinear geometry is of significant importance it is recommended to account for this feature in the modeling.
It is known, [29], that the PVB material often used in the intermediate layer of laminated glass is highly viscoelastic and strongly temperature dependent. However, if both the temperature and the loading rate are constant, the properties of PVB may be linearized. For the structures considered in this thesis the temperature is constant and the loads are short-term loads. Thus, the PVB can be modeled as a linear elastic material.
For the cases when bolt fixings are considered, only one type of bolt is considered, namely a bolt for a cylindrical bore hole.
The analytical design tool developed in this thesis is limited in applicability to indoor bolt fixed laminated glass balustrades subjected to a line load. The tool is further restricted in application to balustrades with fixed values of the thickness of the intermediate PVB layer, the bore hole diameter, thickness of the bush between bolt and glass and the material parameters. The tool is only developed for one bush material.
For the part of the thesis when adhesive joints are investigated, the thermal expansion of the adhesives is disregarded.

2 Glass in the Structural Design Process

2.1 General Remarks

In the design of structural glass, Eurocodes EN 1991-1-1: 2002, [19], prescibe the loads that act on glass structures and prEN 16612: 2013, [41], the maximum allowed stress of the glass in terms of the maximum positive principal stress. When prescribed, the structure should withstand dynamic impact load.
To increase safety in a glass structure, laminated glass may be used instead of single layered glass. Laminated glass consists of two or more glass layers bonded with plastic interlayers. The most common material used for the interlayer is polyvinylbutyral, PVB. The use of laminated glass should allow for the glass panes to break while the remaining layers can continue to carry the design loads, and the scattered glass pieces can stick onto the plastic interlayers, and thereby prevent injury.
However, laminated glass displays a complicated mechanical behavior due to the combination of a very stiff material (glass) and a very soft material (PVB), [4]. A laminated glass-PVB plate is less stiff than a monolithic glass structure of corresponding dimensions, which leads to larger displacements. Furthermore, under certain loads and boundary conditions, discontinuous stress distributions develop in laminated glass structures, ([10], [33]).
Regions close to supports and connections are often subjected to concentrated forces. Since glass is a brittle material that not shows plastic deformations before failure, the ability to distribute stresses at load is limited and thus stress concentrations easily develops. Glass fails under tension and in reality the tensile strength is much less than its theoretical counterpart. This is due to the impact of defects on the surface. The defects are created during manufacturing, treatment (such as hole drilling and cutting) and the use of the glass, [10].
The discontinuities of the stress distributions of laminated glass structures are most pronounced around holes and edges, that is, in the regions where the largest stress concentrations often occur, since these regions often are subjected to concentrated forces and may have larger amounts of defects. In order to illustrate the discontinuous stress distributions that may arise in a laminated glass structure, a simple example is provided. In Figure 1 below a cantilever laminated glass beam subjected to bending by a point load at its free end is displayed. The thickness direction of the laminated glass beam is in the z-direction.

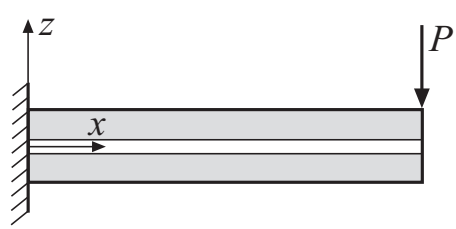

Figure 1: A cantilever laminated glass beam subjected to a point load.

The structure in Figure 1 is modeled by means of the finite element method using two dimensional plane stress elements. Both glass and PVB are modeled as linear elastic materials, since it is assumed that the beam is subjected to a short term load and that the temperature is constant. The material parameters $E = 78$ GPa, $\nu = 0.23$ (glass) and $E = 6$ MPa, $\nu = 0.43$ (PVB) are used, where E denotes modulus of elasticity and ν denotes Poisson's ratio. The distribution of normal stress along the thickness direction at a cross section located at the center of the beam is shown in Figure 2.

As one can see from the figure, the normal stress distributions of the two glass layers are linear as expected. At the glass/PVB interfaces there are discontinuities in the stress distribution and the normal stress in the PVB layer is almost zero. The large difference in stiffness between glass and PVB leads to a shear deformation of the PVB layer and thus to a partial shear force transfer between the glass layers.

It is important for the purpose of safe and cost efficient strength design, that the structural behavior in terms of displacements and stress distributions are accurately determined. Classical design methods, such as simple analytical formulas, do not provide sufficient information in order to determine the stress distributions around bolt connections and determine the load bearing capacity of glass, [24], especially laminated glass. Instead, a finite element model may be used for stress predictions. In order to sufficiently well describe the stress distributions around the bolt connections, a very fine mesh around the bolt holes is required. In comparison to bolted connections, adhesive connections may distribute the load over a greater surface of the glass, leading to a reduction in stress concentrations. Despite this advantage, there are few examples of load bearing adhesive connections used in glass structures and appropriate design guidelines are lacking, [50]. For load bearing adhesive connections, the maximum stresses occur in edge regions of the adhesive layer and for accurate design of the connection it is important to achieve accurate enough stress predictions in these critical regions. Finite element analysis is recommended as a tool for stress prediction, [1].

Accurate predictions of laminated glass strength can be obtained through finite element

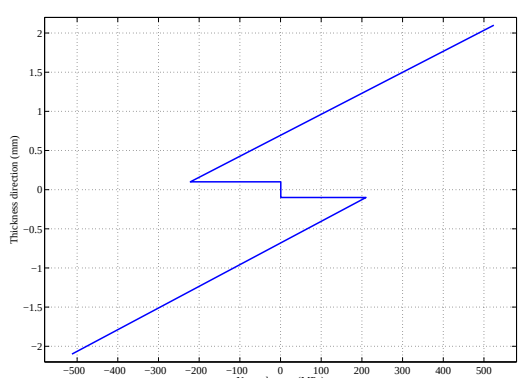

Figure 2: Distribution of normal stress along thickness.

analyses using three dimensional solid elements. However, to make precise prediction of the stress distribution several elements must be employed in the thickness direction of each layer resulting in that standard computational resources limit the scope of the analyses that can be made. Large real world structures with several bolt connections are thus practically impossible to analyze, since it easily needs millions of degrees of freedom for a correct result. Furthermore, the use of the finite element method in general is advanced, time consuming and may require access to commerical finite element software.
In many cases, companies have been using experimental tests to perform strength design of glass structures. This method is not desirable in the glass design process when engineers and architects cooperate to evaluate different design alternatives. It is also an expensive method.
Common for the methods developed in this thesis is that they are aimed at being used as design tools in the glass design process. The methods developed are both accurate and efficient to use when evaluating different design alternatives. One example of such a design tool is the glass design program ClearSight.
In [33] a first version of the finite element based glass design program ClearSight was developed. Originally, ClearSight was developed to calculate deformations and stresses in laminated glass with bolt fixings subjected to a uniformly distributed load or a uniform line load along the top edge. Recently a large number of capabilities have been added to the program including some of the results of this thesis. The program is very time efficient which means that the solve time is a few seconds. There is a strong demand that the numerical procedures used are very time efficient. In the next subsections it is described how results from this thesis are used in ClearSight and a brief description of how ClearSight is used is provided as an illustration. The example aims to show that tools such as ClearSight are practical to use when evaluating different design alternatives in glass design.

2.2 New Features of the Glass Design Program ClearSight

In this thesis, a recently developed finite element is proven to be accurate and efficient in the modeling of glass and especially laminated glass. The computational efficiency is increased through the use of a special reduced integration scheme so that only one element layer per material layer in thickness is required. The finite element is implemented in ClearSight and has made the program even more time efficient and the solution is obtained almost instantly. The time saving is especially prominent for the case of laminated glass which consists of several material layers.
In the parts of the thesis where the modeling of bolt fixings is treated, a modeling technique is implemented. The bolts used consist of a steel part and a rubber ring. Only the rubber ring is modeled and a spring model is used to model the rubber. Results from simulations of a baseline example show that the results obtained in terms of stresses are in good agreement with results from the commercial FE-software ABAQUS.
A part of the thesis deals with developing a reduced model for glass structures subjected to dynamic impact load. Several simplifications are made in the modeling. First of all, the model is reduced by means of a model reduction technique so that the reduced model

is much smaller than the full model. Further, simplifications are made when modeling material and geometric nonlinearities and when modeling contact. The simplifications cater for a computationally efficient model. The model developed is to be integrated into ClearSight for the program to handle dynamic impact load.
For a quick check of the results and to provide an alternative solution method for comparison of results, an analytical method for determining stresses for a glass balustrade with two horizontal rows with two or three bolt fixings in each row subjected to a line load is developed in the thesis. The method uses simple formulas and diagrams to compute the maximum stress of the structure.
The most recent version of ClearSight is intended for determination of strength of glass due to various loads and boundary conditions. The program consists of a user interface, a simulation module, a result viewer and a result report window. The user interface consists of a form with six pages (tabs) that should be filled in. The simulation module computes the displacements and stresses of the structure. The result viewer could be used to graphically examine the resulting stresses and displacements. In the result report window the maximum principal stress is compared with the allowed stresses.

2.3 Example of the Use of ClearSight

To demonstrate the practical use of ClearSight, an example is adopted. The example concerns a balustrade glass with four bolt fixings according to Figure 3.
It is intended for use in a common room in a residential building The glass should be laminated with two glass panes and an intermediate PVB layer of thickness 0.76 mm. The bolt type is cylindrical with an outer diameter of 60 mm and the glass bore hole has

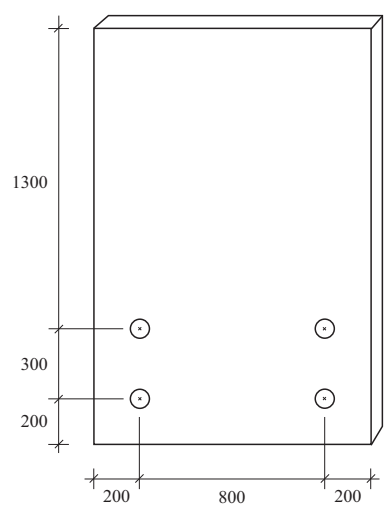

Figure 3: Geometry of glass balustrade.

the diameter 22 mm. The bolt is made of steel and has an EPDM (Ethylene-Propylene Rubber) ring that is in direct contact with the glass. The EPDM has shore hardness 70.
The task is to determine the necessary glass thickness at a certain load.
The use of ClearSight starts with filling in each of the six input tabs. An example of an input tab is displayed in Figure 4.
For instance, the following input is given

- Number of glasses: 2
- Type of support: Bolt fixing
- Height: 1800 mm, Width: 1200 mm
- Interlayer material: PVB, Interlayer thickness: 0.76 mm
- Bolt diameter: 60 mm, Hole diameter: 22 mm
- Bolt rubber thickness: 3 mm, Shore hardness: 70

The glass thickness is to be determined. A first a computation is made with a glass thickness of 8 mm.

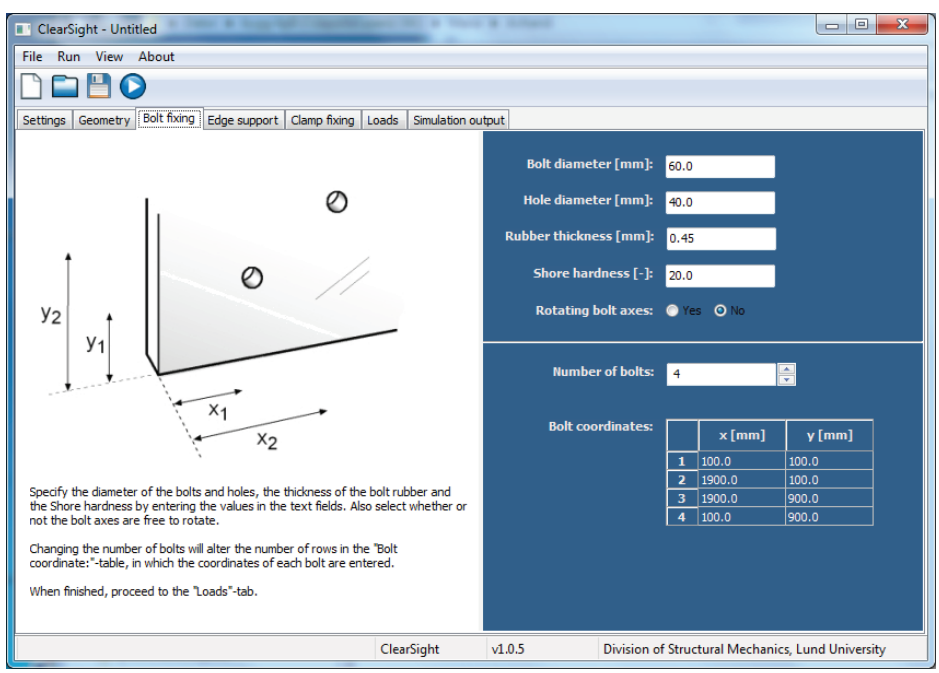

Figure 4: Example of input tab in ClearSight.

With all six tabs filled in the analysis can be run and the result file can be opened. In the report the yield stresses for different types of glass are displayed. For toughened glass, maximum allowed stresses are 84.75 MPa. Below the yield stresses, analysis results are shown. The inner glass has maximum stresses of 92.44 MPa which means that the stresses are greater than the maximum allowed stresses. Visualisation can be chosen in order to visualize the results. The visualized results are shown in Figure 5.
It is apparent from the visualization that the greatest stresses are located at the bolt holes of the inner glass.
The task was to determine the glass thickness. Since the current value of the glass thickness yields too large stresses in the glass, a glass thickness of 10 mm is tried. This glass thickness gives a value of the maximum stress which is smaller than the allowed one, as desired.
This example has demonstrated how ClearSight can be used as a helpful tool in glass design and that the program is user friendly. It does not require a lot of extra effort to run the analysis a second time with a greater glass pane thickness so that the maximum stress does not exceed the allowed one.

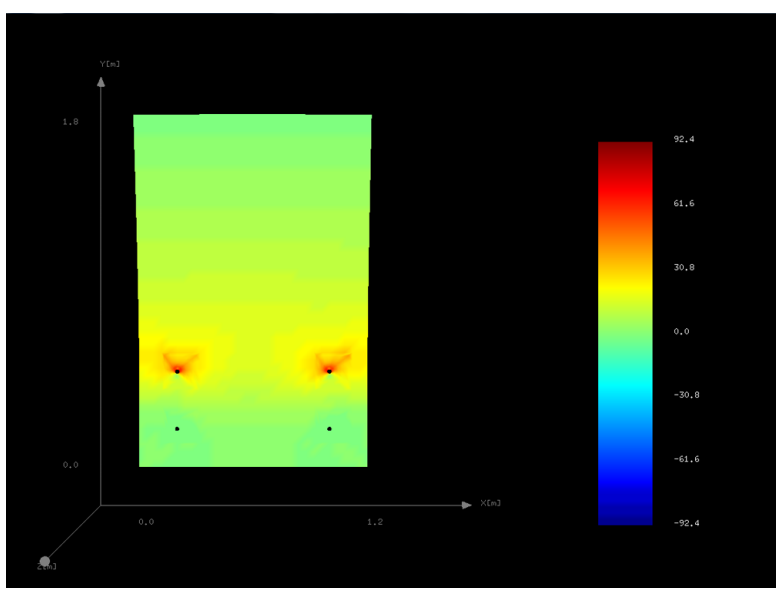

Figure 5: Visualization of results from ClearSight.

3 Structural Glass

3.1 General Remarks

In this chapter theory and properties of the material glass is presented.

3.2 The Material Glass

Generally, glass forms when a liquid is cooled down in such a way that "freezing" happens instead of crystallization, [31]. Glasses do not consist of a geometrically regular network of crystals, but of an irregular network of silicon and oxygen atoms with alkaline parts in between, [24]. The most common oxide glass, silica-soda-lime glass, is used to produce glazing, [31]. Table 1 shows the chemical composition of silica-soda-lime glass according to European construction standards, [24].
When manufacturing glass, four primary operations can be identified: batching, melting, fining and forming, [31]. While the three first operations are used in all glass manufacturing processes, the forming and the subsequent post-process depend on which end product that is manufactured. During the batching process, the correct mix of raw materials is selected based on chemistry, purity, uniformity and particle size, [31]. When melting the raw materials, glass furnaces are used. Different furnaces are used for producing different end products. The aim of the glass fining process is to produce a molten glass that is uniform in terms of composition and temperature and also bubble free.
Flat glass (which could be used for architectural glazing) is produced by the float process, which was introduced by Pilkington Brothers Ltd in the 1950s, [31]. It is noteworthy that this mass production process, together with continuously improved post-processes, have made glass cheap enough to allow it to be used extensively in the construction industry and to grow in importance as construction material during the past 50 years. Within the last two decades, further development within the field of post-processing operations, together with numerical analyses of structures (finite element analyses) have enabled glass to be used as structural elements in architectural glazing, [24]. In the start of the float process, the raw materials are melted in a furnace. Then, a fining process is used to eliminate bubbles. Later, the melt is poured onto a pool of molten tin, float, under a nitrogen atmosphere in order to prevent corrosion of the tin bath. Tin has higher specific weight (weight per unit volume) than glass, so that the glass floats on the tin. The glass spreads

Table 1: Chemical composition of silica-soda-lime glass (mass %).

Component	Chemical formula	Content (mass %)
Silica sand	SiO_2	69-74
Lime (calcium oxide)	CaO	5-14
Soda	Na_2O	10-16
Magnesia	MgO	0-6
Alumina	Al_2O_3	0-3
Others		0-5

out and forms a smooth flat sheet at an equilibrium thickness of 6-7 mm. In order to produce various glass thicknesses, rollers working from the top of the glass are used. The speed of the rollers controls the glass thickness. The range of commercial glass thickness is 2-19 mm, [31]. During this phase, the glass is gradually cooled. The next step of the process is the annealing lehr, which slowly cools the glass in order to prevent that residual stresses are induced within the glass. After the lehr, the glass is inspected and it is ensured that visual defects and imperfections are removed. The glass is cut to a typical size of 3.21 $\times$ 6.00 m, [24], and then stored.
The standard flat glass produced through the float process is called annealed glass, [24]. Often further post-processing of the glass is required in order to produce glass products with different properties. For instance lamination of the glass and hole drilling are made at this stage.

3.3 Types of Glass

During the post-processing phase, glass types and products with different properties can be manufactured. Below, the most common glass types are described.

3.3.1 Annealed Glass

Annealed glass is standard float glass that is produced by slowly cooling glass to avoid internal stresses. At breakage, annealed glass splits into large fragments, [24].

3.3.2 Fully Tempered Glass

Another commonly used term for fully tempered glass is toughened glass. During tempering, float glass is heated and then cooled rapidly (quenched) by cold air jets. The aim of the tempering process is to create a parabolic residual stress field in the thickness direction that has tensile stresses in the core and compressive stresses at the surfaces of the glass. The residual stress field in tempered glass in shown in Figure 6.
The surface of the glass always contains some cracks. Under a tensile stress field, the cracks are allowed to grow. If the glass is subjected to loads, cracks will not grow unless there is a net tensile stress field at the surface of the glass. Fully tempered glass usually breaks into small harmless pieces and therefore fully tempered glass is also termed safety glass, [24].

3.3.3 Heat Strengthened Glass

Heat strengthened glass is produced similarly as fully tempered glass, but the cooling rate is lower. The resulting residual stress is lower, and thus the tensile strength is lower than for fully tempered glass. At fracture, the fragments are larger than for fully tempered glass. On the other hand, the larger glass fragments can allow for a greater post-breakage load capacity in compression than for fully tempered glass, [24].

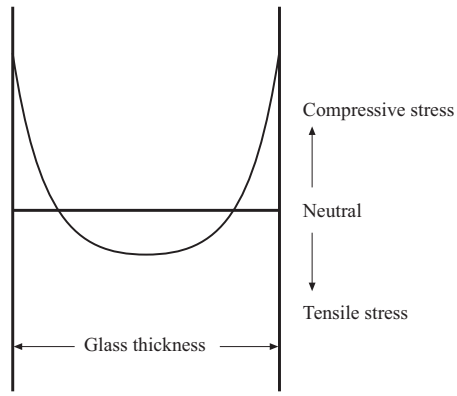

Figure 6: The residual stress profile in a tempered glass, [33].

3.3.4 Laminated Glass

Laminated glass consists of two or more glass panes bonded by a plastic interlayer. A laminated glass unit is displayed in Figure 7.
The glass panes can have different thicknesses and heat treatments. Most common among the lamination processes is autoclaving, [24]. The use of laminated glass in architectural glazing is of great advantage for two reasons. Firstly, if one glass pane breaks, the remaining panes can continue to carry the applied loads given that the structure is properly designed. Secondly, the scattered glass pieces can stick to the interlayer and thereby serve to prevent people from getting injured. The interlayer is most often made of polyvinylbutyral, PVB. The nominal thickness of a single foil of PVB is 0.38 mm. It is common that

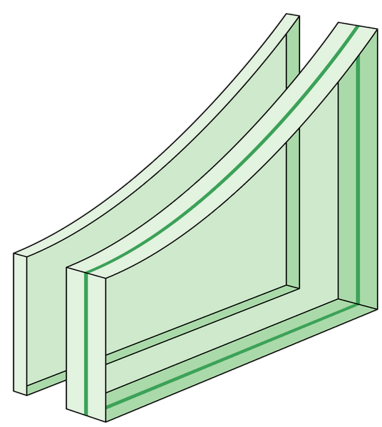

Figure 7: A single glass pane and a laminated glass unit, [39].

two (0.76 mm) or four (1.52 mm) foils form one PVB interlayer, [24]. PVB is a viscoelastic material whose physical properties depend on the temperature and the load duration. PVB behaves nonlinearily when subjected to large deformations, but can be treated as a linear elastic material when subjected to small deformations. Other interlayer materials are for instance Ethylene Vinyl Acetate (EVA) and resins, [37], as well as ionoplast interlayers as SentryGlas.

3.3.5 Insulated Glass

An insulated glass consists of two or more glass panes with intermediate gas space(s). An insulated glass unit is shown in Figure 8.
Insulated glasses are often used due to their thermal insulation properties. The gas space is sealed so that it is considered air tight and is filled with dehydrated air or another gas e.g. argon, krypton or xenon, [24]. The glass panes are connected using a spacer and a sealant. It is possible to use all types of monolithic glasses, for instance annealed glass, and laminated glasses in insulated glass, [24].

3.4 Linear-elastic Materials

Glass is regarded as a linear elastic isotropic material. The mechanical relations of a linear elastic material are described in [36]. Here, a brief description of the derivations therein is presented.
In one dimension, linear elasticity is expressed by Hooke's law

$$\sigma = E\varepsilon, \tag{1}$$

where σ is the normal stress, ε is the strain of the material and E is the modulus of elasticity. The shear-stress, τ, and the shear-strain, γ, are related through

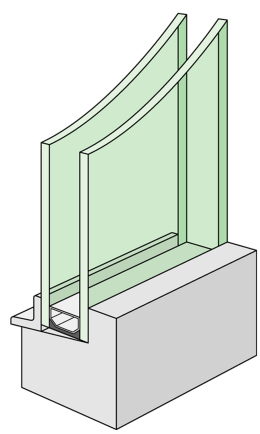

Figure 8: An insulated glass unit, [39].

$$\tau = G\gamma, \tag{2}$$

where G is the shear modulus given by

$$G = \frac{E}{2(1+\nu)}. \tag{3}$$

ν is the Poisson's ratio.
In three dimensions, the stresses and strains of an isotropic material are related by the generalized Hooke's law

$$\sigma = \mathbf{D}\varepsilon, \tag{4}$$

where

$$\sigma = \begin{bmatrix} \sigma_{xx} \\ \sigma_{yy} \\ \sigma_{zz} \\ \tau_{xy} \\ \tau_{xz} \\ \tau_{yz} \end{bmatrix}, \tag{5}$$

$$\varepsilon = \begin{bmatrix} \varepsilon_{xx} \\ \varepsilon_{yy} \\ \varepsilon_{zz} \\ \varepsilon_{xy} \\ \varepsilon_{xz} \\ \varepsilon_{yz} \end{bmatrix}, \tag{6}$$

and

$$\mathbf{D} = \frac{D}{(1+\nu)(1-2\nu)} \begin{bmatrix} 1-\nu & \nu & \nu & 0 & 0 & 0 \\ \nu & 1-\nu & \nu & 0 & 0 & 0 \\ \nu & \nu & 1-\nu & 0 & 0 & 0 \\ 0 & 0 & 0 & \frac{1}{2}(1-2\nu) & 0 & 0 \\ 0 & 0 & 0 & 0 & \frac{1}{2}(1-2\nu) & 0 \\ 0 & 0 & 0 & 0 & 0 & \frac{1}{2}(1-2\nu) \end{bmatrix}. \tag{7}$$

3.5 Mechanical Properties of Glass

Glass is an elastic, isotropic material and exhibits brittle fracture. In contrast to other construction materials, no plastic deformation occurs prior to failure. Therefore, local stress concentrations, occurring for instance close to bolt holes, are not reduced. The brittle characteristic of glass is of concern when constructing with glass as a load bearing element.

Glass has a very high theoretical tensile strength, up to 32 GPa is possible, [24]. However, the actual tensile strength depends on the influence of mechanical surface flaws. The compressive strength of glass is considerably higher than the tensile strength, since there is no surface flaw growth or failure under compression, [24]. In Table 2, relevant material properties of silica-soda-lime glass are summarized, [20], and Table 3 summarizes strength values that could be used for structural design, [22].

Table 2: Material properties of silica-soda-lime glass.

Density	2500 kg/m^3
Young's modulus	70 GPa
Poisson's ratio	0.23

Table 3: Strength values for glass design.

Compressive strength	880-930 MPa
Tensile strength	30-90 MPa
Bending strength	30-100 MPa

The standard prEN 16612: 2013, [41], prescribes a characteristic value of the bending strength of annealed glass to 45 MPa. For prestressed glass, the characteristic bending strength value is 70 MPa for heat strengthened glass and 120 MPa for fully tempered glass.

3.6 Fracture Criterion

Linear elastic fracture mechanics (LEFM) could be applied to describe the fracture strength behavior of glass, [24]. Using this theory, cracks are included in the material behavior modeling. The crack can be localized at the surface (surface crack) or within the material (volume crack). For structural glass, only surface cracks are considered.
In a previous section, it was stated that the theoretical tensile strength of glass is much less than the practical one. This difference was explained already in year 1920 by [23]. The main argument was that fracture starts from existing flaws, Griffith flaws, on a surface. Such flaws sevearly weaken brittle materials because of very high stress concentrations at the crack tip. According to the Griffith theory, based on [27] and expanded by [28], the practical tensile stress of glass, σ_f, can be written as

$$\sigma_f = \sqrt{\frac{2E\gamma}{\pi a_c}}, \tag{8}$$

where E is the Young's modulus, γ is the fracture surface energy and a_c is the critical crack length.
Irwin's version of the fracture criterion is

$$K_1 = Y\sigma_n\sqrt{\pi a} \geq K_{1c}, \tag{9}$$

where K_1 is the stress intensity factor for mode 1 loading (an opening mode where the crack walls are separated due to tensile stresses), Y is a correction factor, σ_n is the nominal tensile stress normal to the crack's plane, a represents the size of the crack and K_{1c} is the fracture toughness or the critical stress intensity factor. Y depends on the depth and geometry of the crack, the geometry of the structure, the stress field and the proximity of the crack to the boundary of the structure, [24]. As an example, a long, straight plane edge crack in a semi-infinite specimen has a value of Y equal to 1.12, [24]. K_{1c} is a material constant and its value ranges between 0.72 and 0.82 for silica-soda-lime glass at room temperature, but the value 0.75 can be used in practise, [24].
In construction, the standard (elastic) design method that is mostly utilized is the maximum stress approach, [24]. In the maximum stress approach, the engineer determines the dimensions of a structure through ensuring that the maximum stresses do not exceed the strength of the material at any position of the structure. The elastic design method is frequently used in glass structure design. Glass fails due to too high tensile stresses on the surface of the glass, i.e. the maximum positive principal stress exceeds the permissable tensile strength.

4 Review on Laminated Glass Subjected to Static Loads

4.1 Introduction

Past research on glass has focused mainly on monolithic (single-layered) glass, whereas the properties of laminated glass remain less well understood. The aim of this section is to review past research on the properties and structural behavior of laminated glass for architectural glazing. The survey is limited to static loading and standard support conditions. Research dealing with glass subjected to dynamic impact load is partly reported in this thesis. For brief reviews of glass structures with point supports, the reader is referred to the first parts of this thesis. Research on the strength properties of laminated glass is largely omitted. Similarly, studies on failure behavior and post-failure behavior are not included to a great extent. The results are presented as summaries of the authors' main findings and a critical assessment is not made. Suggested recommendations and directions for future work are those of respective author. The review is subdivided into sections, where the first section deals with experimental testing, the second with analytical methods and the last section reviews numerical testing results. In the last section, emphasis is on Finite Element Method (FEM) analyses. It is shown that a clear cut division of previous research findings into these distinct categories is difficult, but the subdivision is rather a means of providing a structured presentation of the available knowledge.

4.2 Experimental Results

Most analyses on laminated glass units are experimental. This is particularly the case for plates, since the behavior is very complex, [3]. In this review we consider test results for both beams and plates. Studies on glass beams are often used to approximate the behavior of glass plates. According to Aşik (2003), [3], this methodology is (generally) not acceptable, since the two structures have different stress and displacement fields.
One of the first studies on the behavior of architectural laminated glass subjected to structural loading is conducted by Hooper (1973), [26]. In that study, the fundamental behavior of architectural laminates in bending is assessed. This is done by means of studies of laminated glass beams subjected to four-point bending. First, analytical formulas are derived for the shear force at the interface between glass and the interlayer and the central deflection respectively. These expressions are then used in combination with experimental bending tests in order to provide general understanding about the behavior of laminated glass beams subjected to bending as well as to produce data on interlayer shear stiffnesses (shear moduli) for various loading and temperature conditions. The experimentally investigated beams have a length of 0.559 m and a width of 0.051 m. Short-term load tests are performed at a temperature of 21°C. Various glass pane thicknesses ranging between 3 and 12 mm and PVB layer thicknesses of 0.38, 0.76 or 1.02 mm are utilized. Creep tests are performed for beams of the same dimensions as for the short-term tests and for various temperatures: 1.4, 25.0 and 49.0°C. Results show that the bending resistance of the laminated glass is dependent on the thickness and shear modulus of the interlayer. The physical properties of the interlayer are dependent on the temperature and the duration of

the loading. From an architectural designer's perspective, laminated glass which is subjected to sustained loads should be treated as consisting of two independent glass layers. For short-term loading, the bending stresses of the glass could be determined on the basis of an interlayer shear modulus corresponding to the maximum temperature at which such loading is likely to occur. When the glass is subjected to both sustained and short-term loading, the combined bending stress values in the glass layers may be calculated using the principle of superposition.

Behr et al. (1985), [6], reports on studies on the behavior of laminated glass units consisting of two glass plates with an interlayer of PVB. The glass units are subjected to lateral pressure (wind loads). Compared to the work of [26], larger scale laminated glass units are used. The units have a width of 1.524 m, a length of 2.438 m and a glass pane thickness of 3.2 mm. The PVB interlayer thickness is 0.76 mm. Experiments are conducted in order to find out whether the behavior of a laminated glass unit is similar to that of a monolithic glass unit of the same thickness or to that of a layered glass unit consisting of two glass units and no interlayer. The experiments are performed at temperatures ranging between 0 and 77°C. Results show that the glass unit behaves more like a monolithic glass unit at room temperature. When temperatures are high, the behavior approaches that of two glass units without interlayer. It is stated that care should be taken not to generalize the results obtained to other geometries than the ones analysed.

Laminated glass units (two glass plates with a PVB interlayer) under uniform lateral loads and simply supported boundary conditions are investigated experimentally in Behr et al. (1986), [7]. Compared to previous work in [26] and [6] a different shape and size of the laminated glass unit is used. The unit has almost square shape and in-plane dimensions are 1.397×1.448 mm. The glass plate thickness is 4.8 mm and the interlayer thicknesses are 0.76 and 1.52 mm. According to the results, interlayer thickness effects on the structural behavior (in terms of corner stresses and center deflections) of laminated glass units are not large. Further, long-duration (one hour) load tests at different temperatures are performed. Here, the specimen dimensions are $1.524 \times 2.438 \times 7.1$ mm. The pressure load was of magnitude 1.4 kPa. Test temperatures are 22°C, 49°C and 77°C. For this case, the response in structural behavior is increasing as a function of time at load. Rates of increase in response in structural behavior decrease with time at load. In overview, the experimental data gathered during the tests are within theoretically derived monolithic and layered bounds on stresses and deflections.

Minor and Reznik (1990), [34], study the failure behavior of laminated glass units in constrast to the nondestructive testing used in previous work, for instance [6] and [7]. Three specimen sizes are used in the tests, namely $1.524 \times 2.438 \times 6$ mm, $0.965 \times 1.93 \times 6$ mm and $1.676 \times 1.676 \times 6$ mm. The load is uniformly distributed lateral load applied as a short-term load. Annealed monolithic glass samples are used as reference specimens. Laminated glass samples of the same dimensions and thicknesses as the reference specimens are tested to failure using the same loading rates as for the failure analysis of the reference specimens. Failure strengths are evaluated as functions of several variables: glass type (heat treatment), temperature and surface condition (subjected to surface damage or not). The temperatures are room temperature, 49°C and 77°C. The most interesting result is that annealed laminated glass strengths are equal to annealed monolithic glass strengths

at room temperature. This result is valid for all three sample sizes. Another interesting result is that when temperatures are increased, laminated glass strengths decrease.
Behr et al. (1991), [8], makes a reliability analysis of the glass strength data presented in [34]. The results of this analysis support the conclusions made in [34]. However, the reliability analyses suggest that the issue of the relative strength between monolithic glass units versus laminated glass units is complex at elevated temperatures. Whereas a clear strength reduction occurs in laminated glass at 77°C, little strength reduction occurs at 49°C. This indicates the possible existence of a break point in the relation between temperature and lateral pressure strength for laminated glass at around 49°C. Thus, for temperatures above this threshold it is suggested that the structural behavior of laminated glass is not longer similar to that of monolithic glass.

4.3 Analytical Results

Analytical work on laminated glass properties is scarce. In addition, most results are derived under various simplificating assumptions, [21].
In early work by for instance Vallabhan et al. (1987), [47], a previously developed computer model based on non-linear plate theory is used in order to analyze layered and monolithic rectangular glass plates subjected to uniform lateral pressure. The plates are simply supported. The layered and monolithic plates have the same in-plane geometry and total thickness. So-called strength-factors are developed for a variety of glass plate geometries and load magnitudes. The strength-factor is defined as the ratio between maximum stresses in a monolithic plate and those in a layered plate. It is noteworthy that for certain geometries and loads, layered glass plates can possess larger maximum stresses than an equivalent monolithic glass plate. This result has an implication for the behavior of laminated glass plates, since a laminated glass plate is considered to display structural mechanical behaviour in between the limiting cases of monolithic and layered plates. It is implied that the maximum stresses in a laminated glass plate can be close to (and even exceed) the maximum stresses in an equivalent monolithic glass plate under certain conditions.
Vallabhan et al. (1993), [48], use the principle of minimum potential energy and variational calculus, [25], in order to develop a mathematical model for the nonlinear analysis of (thin) laminated glass units. The final model consists of five nonlinear differential equations which are solved numerically and validated through full-scale experiments. For validation, units of dimensions 1.524×1.524 m^2, glass thickness 4.763 mm and PVB layer thickness 1.52 mm are used. The experiments are conducted at room temperature. The plates are simply supported and subjected to lateral pressure in increments. Stresses and corresponding principal stresses are calculated as a function of the lateral pressure. The results of the mathematical model compare very well with the experimental results. It is suggested that further research focuses on testing the mathematical model for various thicknesses of the laminated glass plates.
Norville et al. (1998), [35], set up an analytical beam model that explains data on deflection and stress for simply supported laminated glass beams under uniform load. The experimental data are presented in [9]. The experiment specimens are of length 0.508 m

and glass thickness 2.69 mm. The PVB layer thickness is 0.76 mm. The test temperatures are 0, 23 and 49°C. The load duration of the experiments is long (> 60 s). In the model, the PVB interlayer performs the functions of maintaining spacing between the glass sheets and transferring a fraction of the horizontal shear force between those sheets. The PVB interlayer increases the section modulus, i.e. the ratio between the bending moment at a cross section and the stress on the outer glass fiber at that cross section, of a laminated glass beam, and the magnitude of the flexural (bending) stresses in the outer glass fibers is therefore reduced. Thus, the strength of a laminated glass beam is higher than that of a monolithic glass beam with the same nominal thickness. This observation sheds light on observed fracture strengths from experiments on laminated glass plates. Other predictions of the model are that laminated glass strength increases with interlayer thickness and decreases as temperature increases, results which also find support in the glass plate experiments.

The analytical model of [48] is used, and a numerical procedure is utilized to avoid computational efficiency problems related to matrix storage, memory and computational time, in [3] in order to provide a set of graphs that shed light on the nonlinear behavior of simply supported, laminated glass plates typically used for architectural glazing. It is argued that such plates have very thin glass plies, which results in that they may undergo large deflections solely due to their own weights. This results in complex stress fields, which the author studies extensively. The example problem used has the in-plane size 1.6×1.6 m^2. Each glass plate has a thickness of 5 mm. The thickness of the PVB layer is 1.52 mm. The load is applied using increments of 0.1 kPa and the maximum load is 10 kPa. The result of the study is that the laminated glass plate that is studied undergoes very complex and nonlinear behavior when uniformly distributed load is applied. It is shown that linear theory only gives results comparable to nonlinear theory up to a load of around 1 kPa and that the error of the linear theory increases rapidly with the magnitude of the load. A conclusion is that nonlinear analysis is the only acceptable type of analysis for laminated glass plates of similar support conditions and dimensions as in the studied example.

In [4], a theoretical model for the behavior of laminated glass beams is presented. It is assumed that the glass beams are very thin such that large deflection behavior is used in the model building. According to the authors, no previous model exist for laminated glass beams undergoing nonlinear behavior. The beam is subjected to a uniformly distributed load and a point load applied at the center of the beam. The minimum potential energy and variational principles are used in the derivations. Three coupled nonlinear differential equations are obtained and closed form solutions are presented for simply supported laminated glass beams. The model is verified for the simply supported laminated glass beam through use of experimental data and for a fixed supported laminated glass beam by means of finite element modeling. For the simply supported beam, three-point bending tests are used for verification. The beam dimensions are 1.0 m length, 0.1 m width, a 5 mm glass pane thickness and a 0.38 mm PVB interlayer thickness. The experiments are performed at room temperature. For the fixed supported beam, a beam length of 1.5 m, a width of 0.05 m, a glass pane thickness of 2.12 mm and a interlayer thickness of 0.76 mm is used. The commercial finite element code ANSYS 5.6 is used in the finite element analysis. Four node plane stress elements are used. Two versions of the model are made,

one has thickness discretization 4 + 2 + 4 elements and the other has 3 + 1 + 3 elements in the thickness direction. A point load at the center of the beam is applied. For the simply supported beam example, the behavior of laminated glass is presented in comparison with the behaviors of monolithic and layered glass beams. The behavior of the laminated glass beam is bounded by the limiting cases of the monolithic and layered glass beams, and is close to the behavior of the monolithic beam. Displacement, moment and stress functions for a simply supported laminated glass beam are given for the use in design to determine the strength of a laminated glass beam. A further test example is used where the beam has dimensions 1 m $\times$ 0.1 m, glass pane thickness 5 mm and PVB layer thickness 0.76 mm. A point load of 5 kN is applied at the midpoint of the beam. The fixed beam has behavior which is limited between layered and monolithic results, but its behavior is closer to the layered beam. It is proven analytically that the behavior of a simply supported laminated glass beam is linear even under large deflection. On the other hand, for the case of the fixed supported laminated glass beam, effects of membrane stresses are substantial and nonlinearities arise from geometric constraints. This is proven by the last test example. A discussion about the behavior of laminated glass beams versus laminated glass plates is conducted. It is concluded that as earlier work on laminated glass plates show that simply supported glass plates undergo nonlinear behavior, simply supported laminated glass beams may not be used to draw conclusions about the behavior of laminated glass plates. In contrast, it is concluded that a study of nonlinear behavior of laminated glass beams makes sense concerning the behavior of laminated glass plates due to considerable similarities between these two cases.

Foraboschi (2007), [21], sets up an analytical model for simply supported laminated glass beams under uniaxial bending. The model predicts stress developments and strength of laminated glass beams with given geometries, glass moduli of elasticity and PVB moduli of elasticity in shear. The ultimate load is determined using a design value of the glass tensile strength. The model is valid under the following assumptions: (i) plane cross sections in the whole beam, as well as in the PVB interlayer, do not remain plane and normal to the longitudinal axis (ii) glass is modeled in a linear elastic manner (iii) PVB is modeled in a linear elastic manner by means of the modulus of elasticity in shear, given that the value of this parameter is related to temperature and duration of loading. The latter assumptions allows a closed-form solution to the problem, contrary to the case when PVB is modeled in a viscoelastic manner. Since no particular simplifications are made when formulating the model, the model predictions are in excellent agreement with test results. For the verification, two-sided supported laminated glass plates with length 0.508 m and width 0.508 m are used. The thickness of each glass ply is 2.69 mm. The PVB layer thickness is 0.76 mm. The tests are performed at the temperatures 0, 23 and 49°C. In particular, no presumed strength-factor, [47], has been used in order to account for the contribution of the PVB layer to the bending capacity through its capacity to transfer horizontal shear force between the glass layers. An analysis of three cases of commercial-scale laminated glass beams is made in order to gain information regarding the rational design of laminated glass beams. The first test case is a two-sided supported laminated glass plate with length 3 m and width 1.5 m. The glass ply thickness is 12 mm. The second test case is a simply supported laminated glass beam that has length 5.2 m, width 0.61 m and glass ply

thickness 8 mm. For the third test case the laminated glass structure is that of a simply supported beam of length 1.8 m, width 0.25 m and glass ply thickness 4 mm. Different values of the PVB layer thickness ranging between 0.38 and 1.52 mm are used. The modulus of elasticity in shear is also variable within the range 0.07 to 105 MPa. Failure strengths and loads are determined for these cases. A comparison is made between the laminated glass model and monolithic and layered equivalency models respectively with respect to failure strengths and loads. Some of the major results are: 1) The greater the value of the shear modulus of elasticity of PVB and the thinner the PVB layer, the closer the prediction of the stress values are to those of the monolithic equivalency model and the greater is the tensile strength of the beam. 2) Irrespective of parameter values, the layered model is not suitable for analyzing laminated glass beams with the actual loads and boundary conditions. The conditions of the layered model is only approached as the temperature is reaching a value that prevails during fire explosure or similar conditions. 3) When the thickness of the beam is designed appropriately, the strength of the beam is raised by up to 70-80 %. 4) The historical assumption that the strength of laminated glass is equal to 60 % of the strength of monolithic glass of the same thickness is sufficiently preservative, but it doesn't represent a lower bound. The benefit of using the above relation is that it provides a simplification, but at the cost of the risk of underestimating the actual load-bearing capacity. 5) The behavior of the monolithic equivalency model is far away from that of a laminated glass beam, and the implementation of the model for design purposes is not recommended.

4.4 Numerical Results

A study of stress development and first cracking of glass-PVB (Butacite) laminates is performed in [11]. Fracture behavior is studied during loading in biaxial bending (ring loading on three-point support). Initially, experiments are made using glass disks with diameter of 0.1 m and thickness 2.246 mm. Laminates are formed by using two glass disks with an intermediate PVB layer of thickness 0.76 mm. The temperature during the tests is either room temperature, -60°C or 50°C. For the room temperature tests, loading rates vary between 10^{-3} and 10^{2} mm/s. For the tests at a low temperature, the loading rate is 10^{-2} mm/s and for the tests at a high temperature, the loading rate is 10^{0} mm/s. Both monoliths and laminates are tested. A three dimensional finite element model which incorporates the role of PVB thickness and the viscoelastic character of the PVB layer in stress development in the laminate is developed and tested. The finite element model is combined with a Weibull-description of glass strength in order to provide a failure prediction framework for the present set up. The glass is modeled using eight-node brick elements with incompatible modes for accurate capture of bending modes. The PVB layer is modeled using eight-node brick elements with incompatible modes using a hybrid formulation. The commercial finite element code ABAQUS is used in the investigations. Comparisons to experimental test data using a load rate of 10^{-3} mm/s and at a temperature of 23°C show that the finite element model is in good agreement. Stress development in the laminate is determined for a set of experimental loading rates. At a slower loading rate, each glass plate deforms nearly independently. At a faster loading rate, the over-

all stresses are higher for a certain deflection which indicates a higher overall stiffness. There is also a shift in the location and magnitude of the peak tensile stress of the laminate. This shift is expected to change the initiation of the first cracking, which is also shown in subsequent investigations. It is shown, both experimentally and through finite element modeling, that the peak stress changes locations with the loading rate. Two primary modes for the initiation of failure associated with changes in maximum stress are identified: (i) first crack located in the upper ply at the glass/PVB-surface and (ii) first crack located in the lower glass sheet at the outer glass surface. Regarding a comparison to the behavior of the corresponding monolithic and layered models, it is observed that at moderate loading rates, the stress in the laminate is higher than in the equivalent monolith. For the highest loading rates, the laminate demonstrates stress behavior similar to the monolith. Furthermore, it is shown that the peak stress locations is a complex function of loading rate, polymer thickness and load uniformity. The first-cracking sequence is affected by interlayer thickness and loading distribution: concentrated loading and thicker/softer interlayer gives first cracking in the upper ply and distributed loading and stiffer/thinner interlayer promote initial cracking in the lower glass sheet. The failure sequence is a function of loading rate and temperature: high temperatures and/or slow loading rates promotes first cracking in the upper ply whereas low temperatures and/or high loading rates lead to lower ply first cracking. The probability of first cracking can be computed by combining the finite element model with a Weibull statistical description of glass fracture. The approach used in this paper can form a foundation for laboratory tests for laminates and can be extended to encompass laminate plates used in commercial applications.

Van Duser et al. (1999), [49], present a model for stress analysis of glass/PVB laminates used as architectural glazing. The model consists of a three dimensional finite element model incorporating PVB viscoelasticity and large deformations. Studies are performed on a square, simply supported glass/PVB laminate subjected to uniform loading. The question of load-bearing capacity for first glass fracture of the plate is addressed through combinating the finite element model with a statistical (Weibull) model for glass fracture. The approach used in this paper extends the work of Bennison et al., [11], to apply to commercial-scale architectural laminated glass plates, rather than laboratory scale disks. Results from the modeling exercise are compared to experimental results from [48]. For the experiments, the plate length is equal to 1.524 m. The glass thickness is equal to 4.76 mm and the interlayer thickness is 1.52 mm. The validation is best for simulations at temperatures between 40 and 50°C. The pressure load is applied at a constant rate with a peak value of 6912 Pa. Regarding the finite element model, the glass sheets are modeled using 8-node solid elements with incompatible modes to avoid locking in bending. The PVB interlayer is modeled using eight-node solid elements with incompatible modes using a hybrid formulation in order to account for nearly incompressible deformations. The commercial program ABAQUS is used for the analysis. Accuracy of the finite element model is obtained through successively refining the mesh until mesh-independent results are obtained. One of the main findings of the study is that for most of the range of pressure used in the study, the probability of failure is lower than the monolithic limit, except at low pressures. At those pressures and stresses that would be used in design, laminate strength

for this case would be predicted to be higher than for the equivalent monolithic glass plate. Since the concept of layered and monolithic limits is defined based on small strain analysis of beams, and does not take into account the membrane-dominated stress state that develops in large deflection of plates close to glass first cracking, a stress analysis that involves comparison to these limiting states could be misleading. In fact, if the derivation of these limits are based on transition to membrane-like behavior (large deflections), the stresses and deflections for a layered system in the membrane limit are exactly the same as for the equivalent monolithic plate. Since the monolithic limit ignores the thickness of the interlayer, the first cracking strength of the laminate may be larger than that of the monolith. Further, it is shown that stress development in the laminate is temperature (or loading rate) dependent. The influence of temperature can be diminished at large deflections as membrane stresses dominate and the coupling between the glass sheets play a lesser role in the stress development. Somewhat surprisingly, for typical glass Weibull moduli (m $\sim$ 5-10) the probability of first cracking is only weakly dependent on temperature. The framework developed for stress analysis and failure prediction may be applied to laminates of arbitrary shape and size under specified loading conditions. Validated against more extensive data the method may be used to develop new design standards for laminated glass.

The model of van Duser et al. (1999), [49], is based on a three dimensional finite element formulation. Thus, the resulting model becomes very large and the computations are expensive. This is noted by Ivanov (2006), [29], who aims at investigating the effect of design parameters on the strength and stiffness of glass laminates. Another aim is to perform structural optimization of glass laminates. It is emphasized that also complicated analytical models that require numerical methods and have solutions that are computationally expensive are inappropriate for such analyses. The paper treats the case of a simply supported glass/PVB beam. The following simplifications are used: (i) only a plane beam is considered and (ii) the problem is confined to small strains and displacements. The representation of the laminated glass as a plane multilayer beam leads to a plane problem of theory of elasticity, which requires less equations although the same degree of discretization through the thickness of the beam and makes the corresponding finite element analysis more computationally efficient. The materials (glass and PVB) are both represented by linearly elastic material models. At the first stage of the analysis, a finite element model is developed. The model is used for the analysis of the case bending of a laminated glass beam under transverse forces (four point bending). The length of the beam is 1.6 m and the width is 1 mm. The glass layers have different glass thicknesses. The upper glass layer has thickness 3 mm and the lower glass has thickness 5 mm. The PVB interlayer has thickness 1 mm. The beam is analysed by means of the finite element analysis software ANSYS 6.1. A linear finite element analysis is performed and yields data on nodal deflections, strains and stresses. The analysis shows that the bending stress in the glass layers is determinant for the load-bearing capability of laminated glasses, but the shear in the PVB layer is important for glass-layer interaction. Based on this first analysis step an analytical model of a laminated glass beam is developed. The model is based on Bernoulli-Euler beam theory for each glass layer, with an additional differential equation for the PVB interlayer shear interaction. The obtained differential

equations are easily solved analytically for the case of a simply supported beam under uniform transverse load. The mathematical model is validated using two test cases. For the first case, the beam length is 1.6 m, the width is 0.8 m and the glass layer thickness is 4.5 mm (the same for both glass layers). The PVB has thickness 10^{-5} mm, which means that the first test case is a monolith. Validation against analytical models (Bernoulli beam theory and Kirchhoff's plate theory) and against the 2D finite element model give errors that are almost zero for both maximum lateral displacement and for maximum and minimum stresses. The second test case is a laminated glass beam of the same dimensions as for the first validation problem but with PVB layer thickness 1 mm, upper glass layer thickness 3 mm and lower glass layer thickness 5 mm. The results in terms of maximum lateral displacement and maximum and minimum stresses are compared to those obtained with the 2D finite element model. The obtained errors are very small. The model is used to perform a parametric study of the influence of layer thicknesses on deflections and stresses of a beam under transverse uniform load. For the study, a length of 1.6 m and a width of 0.8 m is used. The ranges of variation of the variable parameters are reasonable and correspond to architectural glazing application of laminated glasses. The influence of the PVB layer thickness on the maximum lateral displacement is weak and negligible for the maximum and minimum stresses. The maximum deflection is strongly dependent on the upper glass layer thickness and also the stresses of both glass layers are strongly dependent on this parameter. The effect of the thickness of the lower glass layer is largely similar to that of the upper glass layer. Later, the model is utilized for lightweight structure optimization of layer thicknesses when applied to a structure of same dimensions as for the parametric study. The results show that the inner layer of laminated glasses could be thinner than the external glass layer and that the optimally designed laminated glasses could be superior to monolithic glasses in all criteria.

4.5 Discussion

To summarize the review above, one can conclude that most of the investigations done consider beams and plates of regular geometries subjected to standard point loads or uniformly distributed loads. These load conditions represent the primary structural requirements that architectural glass is supposed to withstand. Some attention is directed towards the physical properties of the interlayer. A main issue is to place laminated glass structural behavior correctly in relation to the behavior of layered and monolithic equivalency models for different geometries and loading cases. The influence of the temperature is included in some contributions. Most work deal with short-term loads but some studies also take sustained loads into account. Some investigations deal with the fracture behaviour of simple structures. Analytical models of various complexity have been developed in order to describe the structural mechanic behaviour of laminated glass beams. Finite element models are mainly three dimensional and are developed for the purpose of investigating failure behaviour or for optimization purposes. In all cases the structures are simple (beams and plates) and the boundary conditions are standard. One author mentions that model size constitutes a limitation when it comes to analyzing laminated glass beams subjected to uniaxial bending for optimization purposes. The remedy is to use a plane (two

dimensional) finite element model rather than a full (three dimensional) model.

5 Theory and Methods

In this section the theory and methods used throughout the thesis are presented.

5.1 Stress Prediction of Laminated Glass Structures Subjected to Static Short-term Loads

The first part of this thesis deals with stress prediction of laminated glass structures subjected to static short-term loads. When predicting stresses in laminated glass structures subjected to static short-term load, there are two main options for stress predictions. The first possibility is to use formulas, tables or design charts. The other method consists of finite element analyses of the structure. The former method has the advantage that it is easy to use, but its use is limited to some general cases of geometry and boundary conditions, [24]. In the first part of this work, mainly bolt fixed connections are considered. For the case of bolt fixed laminated glass structures, finite element analyses must be used in most cases. In [24], an example of a design chart for a more advanced bolt fixed laminated glass structure is presented. A further review on simplified design methods for glass structures is provided by the research presented in this thesis.
When making analyses using three dimensional solid elements, analysis results become sufficiently accurate given that the discretization of the model is fine enough. When analyzing the type of structures that are relevant in this work, finite element models become too large and the demand on computational resources too heavy. There is a scope for investigating alternative methods for performing finite element analyses of those structures. According to the classification of [42], laminated glass is a so-called laminated composite, which is made up of layers of different materials. For this category, there are several theories developed including corresponding numerical treatments. One means of reducing the model size is to use two dimensional models for composite plates, so-called Equivalent Single-layer Theories, (ESL), [42]. The two dimensional models are derived through making assumptions regarding the kinematics or the stress field in the thickness direction of the laminate in a fashion such that the three dimensional model is reduced to a two dimensional one. The simplest ESL theory is the Classical Laminated Plate Theory, (CLPT). It is an extension of the classical Kirchhoff plate theory to laminated composite plates. In the CLPT theory, the assumptions regarding the displacement field are such that straight lines normal to the midsurface remain straight and normal to the midsurface after deformation. Thus, the transverse shear and transverse normal effects are neglected (plane stress). The First Order Shear Deformation Theory, (FSDT), extends the ESL theory through including a transverse shear deformation in the kinematic assumptions such that the transverse shear strain is assumed to be constant with respect to the thickness coordinate. In terms of kinematic assumptions this means that straight lines normal to the midsurface do not remain perpendicular to the midsurface after deformation. There are also higher order theories for laminated composite plates. The higher order theories may be able to more accurately describing the interlaminar stress distributions. On the other hand, they also require considerably more computational effort. In the Third Order Shear Deformation Theory, the assumption on straightness and normality of straight lines nor-

mal to the midsurface after deformation is relaxed. The result is a quadratic variation of the transverse stresses through each layer. Even higher order shear deformation theories are available, but the theories are complicated algebraically and expensive numerically, and yield a comparatively little gain in computational accuracy. The simple ESL laminate theories are often not capable of accurately determining the three dimensional stress field at ply level, which may be required for an accurate description of the stress distribution in a complex laminated glass structure.
An alternative is to use Layerwise Theories, [42]. The Layerwise Theories contain full three dimensional kinematics and constitutive relations. They also fulfill requirements on C_z^0 continuity, ([42], [14]). These requirements should necessarily be fulfilled in order to correctly describe the stress field in the thickness direction that characterizes laminated glass. Even if there are some computational advantages compared to full three dimensional element models, for instance that two dimensional finite elements could be used in the analysis, in the modeling of advanced structures the models may be computationally inefficient and difficult to implement, [42].
There exist several other layerwise models for laminated plates, see [42] and references therein. It is not the intention to provide a full review of various Layerwise Theories, so the interested reader is referred to the references provided in the reference cited above.
Another possible method, which is adopted in this work, is to use solid-shell elements. A solid-shell element is a three dimensional solid element which is modified so that shell like structures could be modeled in an appropriate manner. The basis for the solid-shell element used in this work, [13], is a conventional eight node three dimensional solid element. Since low-order three dimensional solid elements are used in order to model shell like structures, locking phenomena occur. In the solid-shell formulation, certain methods are incorporated such that locking is prevented. Through maintaining three dimensional constitutive relations and kinematic assumptions, the stress distribution of laminated glass can be accurately determined. The computational efficiency is increased due to the use of a special reduced integration scheme that only requires one integration point per material layer.

5.2 The M-RESS Solid-shell Element

M-RESS stands for Modified Reduced (in-plane) integration, Enhanced strain field, Solid-Shell element. This element is used in the major part of the analysis of laminated glass in this thesis. In this section, an overview of the theory of this element is provided. The element was originally presented in [13] for linear applications. Linear theory is used throughout this thesis and it is thus the linear version of the element that is presented.
The element has the geometry of a three-dimensional hexahadral solid element that has eight nodes and three degrees of freedom per node. The element geometry together with the involved coordinate systems and the integration point locations are displayed in Figure 9.
In the formulation of the element, the computational efficiency is increased through the use of a reduced integration scheme that has multiple integration points along the local ζ-axis only. As a downside, volumetric and Poisson locking problems as well as spurious

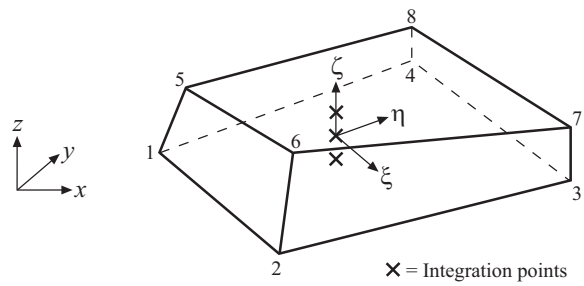

Figure 9: Element geometry.

zero-energy modes may occur. As a remedy, the element applies the Enhanced Assumed Strain (EAS) approach, [45].

5.2.1 The EAS-method

The crucial point of the EAS method is to enlarge the strain field, ε, through adding a new field of enhanced strain parameters, α. It can be shown, [2], that only one enhancing parameter, α_1, is enough in order to reduce the locking problems. This means that the locking problems can be reduced considerably, while maintaining high computational efficiency of the element formulation which is achieved through the reduced integration scheme. To overcome the hourglass modes that then may develop, hourglass stabilization is made by the Assumed Natural Strain (ANS) method, [18], for the transverse shear components whereas the membrane field were stabilized based on the stabilization vectors of [32].
In the local frame, the enhanced strain field is added to the ordinary strain field:

$$\tilde{\varepsilon} = \varepsilon + \varepsilon_\alpha = [\hat{\mathbf{B}}_\mathbf{u}\ \hat{\mathbf{B}}_\alpha] \begin{bmatrix} \mathbf{u} \\ \alpha \end{bmatrix} = \tilde{\mathbf{B}}\tilde{\mathbf{u}}. \tag{10}$$

$\hat{\mathbf{B}_\mathbf{u}}$ is the standard Finite Element Method (FEM) strain-displacement matrix, ε_α is the enhanced part of the strain field and $\mathbf{u}$ is the displacement field. In the convective coordinate system, the enhanced strain field is chosen:

$$\varepsilon^\alpha_{\zeta\zeta} = \zeta\alpha_1, \tag{11}$$

which leads to the following enhanced strain-displacement matrix in the local coordinate system:

$$\hat{\mathbf{B}}_\alpha = \mathbf{Q}_0[0\ \ 0\ \ 0\ \ \zeta\ \ 0\ \ 0]^T. \tag{12}$$

$\mathbf{Q}_0$ is a transformation matrix, see [13] and references therein. The application of the EAS method leads to the following system of equations, [45]:

$$\begin{bmatrix} \hat{\mathbf{K}}^{\mathbf{uu}} & \hat{\mathbf{K}}^{\mathbf{u}\alpha} \\ \hat{\mathbf{K}}^{\alpha\mathbf{u}} & \hat{\mathbf{K}}^{\alpha\alpha} \end{bmatrix} \begin{pmatrix} \mathbf{u} \\ \alpha \end{pmatrix} = \begin{pmatrix} \mathbf{f}^{ext} \\ \mathbf{0} \end{pmatrix}. \tag{13}$$

Static condensation of α can be performed on Equation (13) that leads to:

$$\hat{\mathbf{K}}^{\mathbf{u}+\alpha} = \hat{\mathbf{K}}^{\mathbf{uu}} - \hat{\mathbf{K}}^{\mathbf{u}\alpha}(\hat{\mathbf{K}}^{\alpha\alpha})^{-1}\hat{\mathbf{K}}^{\alpha\mathbf{u}}. \tag{14}$$

The physical stabilization procedure adds an extra part, $\hat{\mathbf{K}}^H$, to the stiffness matrix as follows:

$$\hat{\mathbf{K}} = \hat{\mathbf{K}}^{\mathbf{u}+\alpha} + \hat{\mathbf{K}}^H. \tag{15}$$

The displacement field can now be obtained as:

$$\mathbf{u} = (\hat{\mathbf{K}})^{-1}\mathbf{f}^{ext}. \tag{16}$$

5.2.2 Treatment of the Strain Field to Account for Stabilization

In order to apply the physical stabilization method, a division of the strain tensor into membrane, normal and transverse shear components is necessary. In the convective coordinate system the strain tensor can be written as:

$$\varepsilon = [\varepsilon_m ... \varepsilon_n ... \varepsilon_s]^T = [\varepsilon_{\xi\xi}\, \varepsilon_{\eta\eta}\, \varepsilon_{\xi\eta} ... \varepsilon_{\zeta\zeta} ... \varepsilon_{\xi\zeta}\, \varepsilon_{\eta\zeta}]^T, \tag{17}$$

where the strain components are defined as:

$$\varepsilon_{ab} = \frac{1}{2}(\mathbf{J}_{,a}\mathbf{u}_{,b} + \mathbf{J}_{,b}\mathbf{u}_{,a}),\ (a,b = \xi,\eta,\zeta), \tag{18}$$

where $\mathbf{J}_{,a}$ are the lines of the Jacobian matrix $\mathbf{J}$.
The strain tensor in the local coordinate system is given by

$$\hat{\varepsilon} = \mathbf{Q}_0\varepsilon. \tag{19}$$

It can be shown, [13], that the total strain field can be expanded to constant, linear and bilinear terms in the coordinates ξ, η and ζ. The constant membrane strain field is composed of a component evaluated at the center of the element and a component that depends only on the ζ coordinate:

$$\varepsilon^C_{mI} = \varepsilon^0_m + \zeta\varepsilon^\zeta_m. \tag{20}$$

The constant membrane strain tensor must be transformed to the local coordinate system through the transformation of Equation (19). For a detailed description of the corresponding strain-displacement matrices, see [13].
The reduced integration scheme with integration points only along the ζ-axis will lead to the cancellation of the contributions to the strain-displacement matrix that are corresponding to the non-constant terms of the strain field. Physical stabilization strain-displacement

relations are therefore required for those terms. The membrane part of the stabilization strain tensor is given by:

$$\varepsilon_{mI}^{H} = \xi\varepsilon_{m}^{\xi} + \eta\varepsilon_{m}^{\eta} + \xi\eta\varepsilon_{m}^{\xi\eta} + \xi\zeta\varepsilon_{m}^{\xi\zeta} + \eta\zeta\varepsilon_{m}^{\eta\zeta}. \tag{21}$$

The strain tensor is transformed to the local coordinate system through the application of Equation (19). Explicit descriptions of the corresponding strain-displacement matrices are given in [13].
For the construction of strain-displacement stabilization matrices for the normal strain component, $\varepsilon_{\zeta\zeta}$, and for the transverse shear strains $\varepsilon_{\xi\zeta}$ and $\varepsilon_{\eta\zeta}$, the ANS-method is used. For a description of the application of the ANS-method, we refer to [13].
A second stabilization method is applied to the membrane strain components as well as a method to remedy the volumetric locking that may occur to the stabilization. Details regarding these methods are out of scope of this presentation. More information is given in the first part of the thesis and in the references therein. To summarize, the resulting membrane strain tensor for the hourglass field is defined as

$$\hat{\varepsilon}_{m}^{H} = \begin{bmatrix} \hat{\varepsilon}_{\hat{x}\hat{x}} \\ \hat{\varepsilon}_{\hat{y}\hat{y}} \\ \hat{\varepsilon}_{\hat{x}\hat{y}} \end{bmatrix} = (\xi \cdot \hat{\mathbf{B}}_{mI}^{\xi} + \eta \cdot \hat{\mathbf{B}}_{mI}^{\eta} + \xi\eta \cdot \hat{\mathbf{B}}_{mI}^{\xi\eta} + \xi\zeta \cdot \hat{\mathbf{B}}_{mI}^{\xi\zeta} + \eta\zeta \cdot \hat{\mathbf{B}}_{mI}^{\eta\zeta}) \cdot \hat{\mathbf{R}}_{0} \cdot \mathbf{d}_{I}, \tag{22}$$

where the nodal degrees of freedom, $\mathbf{d}_I$, are specified in the local coordinate system. The following transformation from global coordinates to local coordinates is used:

$$\hat{\mathbf{d}}_{I} = \hat{\mathbf{R}}_{0} \cdot \mathbf{d}_{I}. \tag{23}$$

$\hat{\mathbf{R}}_0$ is defined in [13].

5.2.3 Stress Evaluation

The displacements obtained from Equation (16) are used together with Equation (10) in order to compute the strain field, $\tilde{\varepsilon}$. Once the strain distribution has been determined, the stress distribution, σ, is given by:

$$\sigma = \mathbf{D}\tilde{\varepsilon} = \mathbf{D} \cdot [\hat{\mathbf{B}}_{\mathbf{u}}\, \hat{\mathbf{B}}_{\alpha}] \begin{bmatrix} \mathbf{u} \\ \alpha \end{bmatrix}. \tag{24}$$

D is the constitutive matrix. The stresses are evaluated at the integration points. A stress smoothing procedure based on a quadratic least squares fit is used in order to extrapolate and average the stresses at the nodes, [16].

5.3 An Analytical Model for Structural Analysis of Laminated Glass in Bending

In strength design of glass there is a need for analytical methods that provide rapid solutions to certain glass structures. In this thesis, such a method is developed. The solid-shell element presented in the previous section and an analytical model used to evaluate

the structural performance of a simply supported laminated glass beam provide the basis for this method. The analytical model is presented in [15]. The model is intended to be applied to a glass balustrade and the equations are adjusted for this case. The glass balustrade consists of a plate of two laminated glass panes which can be regarded as a beam when subjected to bending around one axis. In this section, the original model is presented that deals with analytical laminated beam modeling.
Below it is derived how the stresses are determined for a laminated simply supported glass beam subjected to a point load. The beam consists of two glass layers with an intermediate PVB layer. The geometry of the beam problem is displayed in Figure 10.
In the modeling, some assumptions are made. First of all, the beam is only subjected to a bending moment due to the point load. Linear theory of elasticity is applied. For a short-term load, both glass and PVB are modeled as linear elastic materials. Small deformation theory applies. The glass plies are assumed to have equal deflections and the radiuses of curvature are approximately equal for the two plies. It is assumed that the glass plies are not subject to shear deformation, but the PVB layer is. The stiffness of the PVB is large enough so that the PVB layer acts as a connector between the glass plies without normal deformation of the PVB or separation of the plies.
The reaction forces R_1 and R_2 as well as the moment distribution $M(x)$ can be derived by equilibrium equations as

$$R_1 = P(\frac{1}{(1+\frac{l_b}{l_a})}), \tag{25}$$

$$R_2 = P(\frac{1}{(1+\frac{l_a}{l_b})}) \tag{26}$$

and

$$M(x) = R_1 x, \tag{27}$$

where the moment equation is valid on the interval $0 \leq x \leq l_b$.

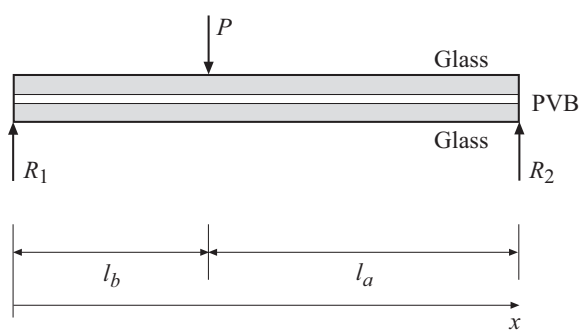

Figure 10: Geometry of beam problem.

In the course of the model development, a differential equation that governs the behavior of the laminated beam problem is derived. A full derivation is provided in [15]. The starting point of the derivation is the consideration of an infinitesimal beam element in equilibrium. The forces and displacements of the beam element are displayed in Figures 11 and 12.
It is assumed that the shear deformation, u_s, of the PVB layer is given by

$$u_s(x) = \gamma t_{PVB} = \frac{H t_{PVB}}{G_{PVB} b} = \frac{H}{k_{PVB}}, \tag{28}$$

where γ is the shear strain, $k_{PVB} = \frac{G_{PVB} b}{t_{PVB}}$ is the spring stiffness, G_{PVB} is the shear modulus, b is the width and t_{PVB} the thickness of the PVB layer.
From horizontal equilibrium of a single beam cross section, $N_1(x) = -N_2(x) \equiv N(x)$ holds.
A moment equilibrium computation about the laft part of the beam cross section at the center of gravity of the second glass pane gives, given that the thickness of the PVB layer is disregarded in the computation

$$M = M_1 + M_2 - N h_t, \tag{29}$$

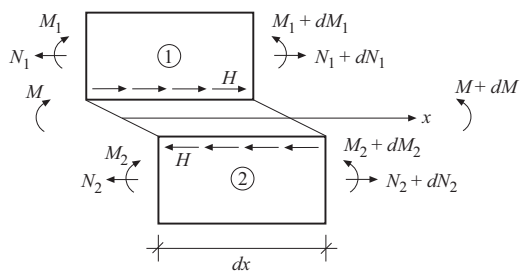

Figure 11: Forces acting on an infinitesimal laminated beam element.

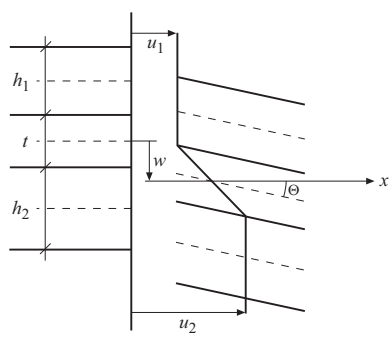

Figure 12: Displacements of a laminated beam element.

where $h_t = \frac{h_1}{2} + \frac{h_2}{2}$.
The derivation of the differential equation is based on well known structural mechanical relations and the definitions, assumptions and figures above. For brevity, the details are not given here, but the final equation is given as

$$\frac{d^2}{dx^2}N(x) - c_2 N(x) = c_1 M(x), \tag{30}$$

where the following constants are defined

$$c_1 = k_{PVB}\frac{h_t}{EI_1 + EI_2}, \tag{31}$$

and

$$c_2 = k_{PVB}(\frac{1}{EA_1} + \frac{1}{EA_2} + \frac{h_t^2}{EI_1 + EI_2}), \tag{32}$$

where E is the modulus of elasticity of glass, I_1 and I_2 are the moments of inertia of glass panes 1 and 2 respectively and A_1 and A_2 are the cross section areas of respective pane.
The total solution to this differential equation is

$$N(x) = Bsinh(\sqrt{c_2}x) + Ccosh(\sqrt{c_2}x) - \frac{c_1 R_1}{c_2}x, \tag{33}$$

where B and C are constants. The last term is the particular solution to the equation and this solution has been dervied based on the ansatz that a linear $M(x)$ corresponds to a linear particular solution. The boundary conditions $N(0) = 0$ and $(\frac{dN}{dx})_{x=l_b} = 0$ are applied to determine B and C and the final solution is obtained as

$$N(x) = \frac{c_1 R_1}{c_2\sqrt{c_2}cosh(\sqrt{c_2}l_b)}sinh(\sqrt{c_2}x) - \frac{c_1 R_1}{c_2}x. \tag{34}$$

For equal cross sectional areas of the glass beams, $A_1 = A_2 \equiv A$, $h_1 = h_2 \equiv h$ and $I_1 = I_2 \equiv I$. Under these conditions, it can be shown that $M_1(x) = M_2(x)$. Then, Equation (29) could be written as

$$M_1(x) = M_2(x) = \frac{1}{2}(M(x) + h_t N(x)). \tag{35}$$

For glass design, it is the value of the maximum tensile stress in glass parts of the beam that is of interest. Basic structural mechanic relations, [40], provides the well-known formula for the total normal stress in the x-direction, σ, for one glass pane. For the current load case, the maximum tensile tensile stress occurs at the lower surface of the laminate. Let the maximum tensile stress (evaluated at $x = l_b$) be denoted σ_{low}. At the lower surface of the laminate, $M_1(x) = M_2(x)$, $I_2 = I$ and $N_2(x) = -N_1(x) = -N(x)$. Thus,

$$\sigma_{low} = \frac{M_2(l_b)}{\frac{bh^2}{6}} - \frac{(Nl_b)}{bh}. \tag{36}$$

Note that Equation (36) is valid for beams with rectangular cross sections only.

The shear stresses are zero at the surfaces of the laminate, which means that the tensile stress in the x-direction at the lower surface of the laminate is equal to the maximum (positive) principal stress.

5.4 Modeling of Hyperelastic Materials

A brief description of hyperelastic materials is given below. The derivations are originally presented in [5] and [30]. Hyperelastic models are normally used for modeling rubber materials.

The hyperelastic material models are derived using a strain energy function to describe the characteristics of the materials. Below, the concept of strain energy function is described by the example of a non-linear elastic bar. The symbols used in the example are defined in Figure 13.

When analysing a hyperelastic material the traditional strain ($\varepsilon = \frac{u}{L}$) is replaced by the so called stretch (λ) defined as

$$\lambda = \frac{L+u}{L} = 1+\varepsilon. \tag{37}$$

The strain energy is defined as a function $W(\lambda)$, which describes the strain energy density per undeformed volume of the bar.

The total strain energy (U), is thus expressed by multiplying $W(\lambda)$ with the undeformed volume

$$U = ALW(\lambda). \tag{38}$$

The increments of work done by the external force is equal to the increment of internal work giving the energy balance equation

$$dU = Pdu. \tag{39}$$

The increment of internal work can be expressed by using $W(\lambda)$ as follows

$$dU = ALdW = AL\frac{dW}{d\lambda}d\lambda. \tag{40}$$

The definition of λ can be rewritten as

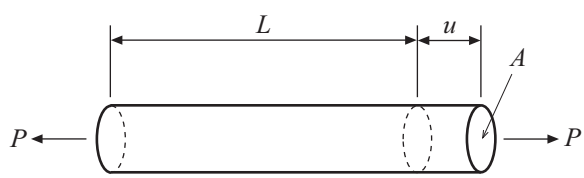

Figure 13: An elastic bar loaded in tension.

$$\lambda = \frac{L+u}{L} \leftrightarrow u = (\lambda - 1)L. \tag{41}$$

Differentiation of u gives

$$du = Ld\lambda. \tag{42}$$

Inserting Equations (40) and (42) into Equation (39) gives

$$PLd\lambda = AL\frac{dW}{d\lambda}d\lambda \rightarrow \frac{P}{A} = \frac{dW}{d\lambda}. \tag{43}$$

An expression of the stress ($\frac{P}{A}$) in the elastic bar has been derived from the strain energy function.

5.4.1 Strain Energy Function, the Neo-Hooke Model and the Mooney-Rivlin Model

The strain energy density function can be regarded as a potential function for the stresses. The measure of strains used is the left Cauchy-Green deformation tensor **B**. Thus, W can be written

$$W = W(\mathbf{B}). \tag{44}$$

The state of deformation is fully determined by the principal stretches $(\lambda_1, \lambda_2, \lambda_3)$ and the principal directions. In an isotropic material the three principal stretches are independent of the principal directions and consequently the strain energy density function can be written

$$W = W(\lambda_1, \lambda_2, \lambda_3). \tag{45}$$

The principal stretches can be obtained from the characteristic polynomial of **B**, but not very easily. The strain invariants are easier to obtain and thus the strain energy function is expressed in an easier way as a function of the three invariants,

$$W = W(I_1, I_2, I_3). \tag{46}$$

The three strain invariants can be expressed by the principal stretches

$$\begin{gathered} I_1 = \lambda_1^2 + \lambda_2^2 + \lambda_3^2 \\ I_2 = \lambda_1^2\lambda_2^2 + \lambda_1^2\lambda_3^2 + \lambda_2^2\lambda_3^2 \\ I_3 = \lambda_1^2\lambda_2^2\lambda_3^2 \end{gathered} \tag{47}$$

The third invariant expresses the change in volume and as rubber materials generally are more or less incompressible, it is assumed that no change in volume occur and thus $I_3 = 1$, giving

$$W = W(I_1, I_2). \tag{48}$$

The constitutive law for a hyperelastic, isotropic and incompressible material is derived from the strain energy density function using the energy principle in an energy balance equation in the same way as in the initial example of the elastic bar. In finite element analysis programs the most common expression used to describe the strain energy density function is the series expansion

$$W = \sum_{i=0,j=0}^{\infty} C_{ij}(I_1 - 3)^i (I_2 - 3)^j. \tag{49}$$

Most hyperelastic materials are based on this sum. They are separated by how many and which of the constants (C_{ij}) being used. For example, the Neo-Hooke material model uses the first term, C_{10}, of Equation (49) and the strain energy density function is described by

$$W = C_{10}(I_1 - 3). \tag{50}$$

As another example, for the Mooney-Rivlin model, the two first terms C_{10} and C_{01} are used to describe the strain energy density function. The expression for this function is given by

$$W = C_{10}(I_1 - 3) + C_{01}(I_2 - 3)^2. \tag{51}$$

These are two often used material models in analysis of rubber materials.

5.5 Dynamic Analysis

In dynamic analysis of a structure, the structure is subjected to dynamic (time-varying) loads. This section gives a brief introduction to dynamic analysis. The notation is taken from [17]. The simplest structural dynamic system is a so-called single-degree-of-freedom (SDF) system. An SDF system can be idealized as a mass-spring-damper system, which is illustrated in Figure 14.
In Figure 15 the forces acting on the mass are shown.
These forces are the elastic force, $f_S = ku$, the damping force, $f_D = c\dot{u}$, and the external force, $p(t)$. In the vertical direction, the gravity force mg is balanced by an equal normal force. Application of Newton's second law and rearrangement of terms gives for the horizontal direction

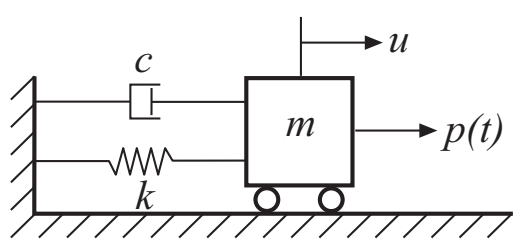

Figure 14: Mass-spring-damper system.

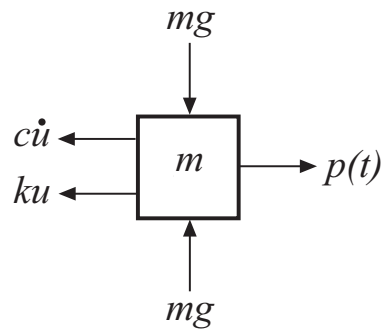

Figure 15: Free-body diagram for the mass of a mass-spring-damper system.

$$m\ddot{u} + f_D + f_S = p(t). \tag{52}$$

When substituting the relations for f_D and f_S into Equation (52), the final equation of motion of the system is obtained as

$$m\ddot{u} + c\dot{u} + ku = p(t). \tag{53}$$

The initial displacement $u(0)$ and the initial velocity $\dot{u}(0)$ must be specified for a complete definition of the problem.
In order to describe a more complex structure, more degrees of freedom are included in the model and a multi-degree-of-freedom (MDF) model is obtained. The equation of motion for this type of system is given as

$$\mathbf{m}\ddot{\mathbf{u}} + \mathbf{c}\dot{\mathbf{u}} + \mathbf{k}\mathbf{u} = \mathbf{p}(t), \tag{54}$$

where $\mathbf{m}$ is the mass matrix, $\mathbf{c}$ is the damping matrix, $\mathbf{k}$ is the stiffness matrix, $\mathbf{u}$ is the displacement vector and $\mathbf{p}$ is the load vector. For N degrees of freedom the matrices have dimensions $N \times N$ and the vectors $N \times 1$. The system can be solved for $\mathbf{u}(t)$ for given initial conditions $\mathbf{u} = \mathbf{u}(0)$ and $\dot{\mathbf{u}} = \dot{\mathbf{u}}(0)$.
When a structure is disturbed from its equilibrium position by initial displacement(s) and/or initial velocities, the structure undergoes free vibration at certain natural frequencies, ω_n. Observe that the structure vibrates at zero external force, $\mathbf{p}(t) = \mathbf{0}$. The number of natural frequencies are as many as the number of degrees of freedom of the system. Each natural frequency corresponds to a characteristic deflected shape of the structure called natural mode of vibration, ϕ_n. For an undamped ($\mathbf{c} = \mathbf{0}$) MDF-system, the free vibration in one of the natural vibration modes can be written

$$\mathbf{u}(t) = q_n(t)\phi_n, \tag{55}$$

where $q_n(t)$ is the time variation of the displacements which is described by

$$q_n(t) = A_n cos\omega_n t + B_n sin\omega_n t, \tag{56}$$

where A_n and B_n are constants that can be determined from the inital conditions of the problem. A combination of Equation (54) adjusted to the case of free vibration and without damping, Equations (55) and (56) and the exclusion of the trivial solution corresponding to $q_n(t) = 0$ yields the matrix eigenvalue problem

$$\mathbf{k}\phi_n = \omega_n^2 \mathbf{m}\phi_n. \tag{57}$$

Solving the eigenvalue problem gives the eigenfrequencies and the natural modes (eigenmodes). The natural modes form a set of N independent vectors and can thus be used as a basis for representing any displacement vector $\mathbf{u}$. The complete solution to Equation (54) for the case of undamped free vibration is then given as

$$\mathbf{u}(t) = \sum_{n=1}^{N} \phi_n (A_n cos\omega_n t + B_n sin\omega_n t). \tag{58}$$

A_n and B_n are obtained by utilizing the initial conditions of the problem, see [17].

5.6 The Rayleigh-Ritz Procedure

For some applications it is desirable to reduce the size of the MDF model with as little loss of information about the dynamic behavior of the system as possible. For these cases, model reduction techniques may be employed. Glass structures subjected to dynamic impact load may be analyzed by employing model reduction techniques. In this thesis, the Rayleigh-Ritz method is employed for model reduction. The purpose of the current section is to give a short description of the Rayleigh-Ritz method. The notation is adopted from [17].
Consider the equations of motion of an undamped system in free vibration with N degrees of freedom

$$\mathbf{m}\ddot{\mathbf{u}} + \mathbf{k}\mathbf{u} = \mathbf{0}. \tag{59}$$

The displacement field can be expressed as a linear combination of shape vectors ψ_j

$$\mathbf{u}(t) = \sum_{j=1}^{J} z_j(t)\psi_j = \Psi \mathbf{z}(t), \tag{60}$$

where $z_j(t)$ are so-called generalized coordinates and the Ritz vectors ψ_j, $j = 1, 2, ..., J$ are linearly independent vectors that satisfy the geometric boundary conditions.
The Ritz vectors are selected based on what is appropriate for the system to be analysed. Substituting Equation (60) into Equation (59) yields

$$\mathbf{m}\Psi\ddot{\mathbf{z}} + \mathbf{k}\Psi\mathbf{z} = \mathbf{0}. \tag{61}$$

Premultiplying each term by Ψ^T gives

$$\tilde{\mathbf{m}}\ddot{\mathbf{z}} + \tilde{\mathbf{k}}\mathbf{z} = \mathbf{0}, \tag{62}$$

where $\tilde{\mathbf{m}} = \Psi^T \mathbf{m} \Psi$ and $\tilde{\mathbf{k}} = \Psi^T \mathbf{k} \Psi$.
The system described by Equation (62) has J degrees of freedom $(z_1, z_2, ..., z_J)^T$ compared to the full system which has N degrees of freedom. In general, the purpose of the method is to find approximations to the lowest eigenfrequencies and eigenmodes of the system and to represent the dynamic behavior of the system by a combination of only a few of those.

5.7 Structure-acoustic Analysis

Structure-acoustic analysis can be used to model the gas filled insulated glass units. In this section, is described the theory and assumptions behind the formulation and the derivation of the finite element formulation is presented. The entire formulation is found in [43] and the notation used here stems from that work.
The structure-acoustic formulation concerns systems that consist of a flexible structure that is in contact with an enclosed acoustic cavity. The structure part is described by the differential equation of motion for a continuum body assuming small deformations and the fluid part by the acoustic wave equation. Coupling conditions at the boundary between the structure and fluid domains are applied to ensure that there is continuity in displacements and pressure between the domains.
For the structural domain, the equation of motion for a continuum body can be written

$$\tilde{\nabla}^T \sigma_s + \mathbf{b}_s = \mathbf{q}_s, \tag{63}$$

where $\mathbf{b}_s$ is the body force, $\mathbf{q}_s$ is the inertia force and the differential operator $\tilde{\nabla}$ is defined in [43]. The quantities $\mathbf{b}_s$ and $\mathbf{q}_s$ are defined as

$$\mathbf{b}_s = \begin{bmatrix} b_1^s \\ b_2^s \\ b_3^s \end{bmatrix} \tag{64}$$

and

$$\mathbf{q}_s = \rho_s \frac{\partial^2 \mathbf{u}_s}{\partial t^2}. \tag{65}$$

$\mathbf{u}_s$ is the displacement vector defined as

$$\mathbf{u}_s = \begin{bmatrix} u_1^s \\ u_2^s \\ u_3^s \end{bmatrix} \tag{66}$$

and ρ_s is the density of the material. The stresses, σ_s, are written as

$$\sigma_s = \begin{bmatrix} \sigma_{11}^s \\ \sigma_{22}^s \\ \sigma_{33}^s \\ \sigma_{12}^s \\ \sigma_{13}^s \\ \sigma_{23}^s \end{bmatrix}. \tag{67}$$

By means of the appropriate kinematic and constitutive relations and standard finite element derivations, the finite element formulation for the structural domain is obtained

$$\mathbf{M}_s\ddot{\mathbf{d}}_s + \mathbf{K}_s\mathbf{d}_s = \mathbf{f}_f + \mathbf{f}_b, \tag{68}$$

where $\mathbf{M}_s$ is the mass matrix, $\mathbf{K}_s$ is the stiffness matrix, $\mathbf{f}_f$ is the surface force vector, $\mathbf{f}_b$ is the body force vector and $\mathbf{d}_s$ are the nodal displacements.
The governing equations for the acoustic fluid are derived using the assumptions that the fluid is inviscid, only undergoes small translations and is irrotational. Thus, the governing equations are the equation of motion,

$$\rho_0 \frac{\partial^2 \mathbf{u}_f(t)}{\partial t^2} + \nabla p(t) = 0, \tag{69}$$

the continuity equation,

$$\frac{\partial \rho_f(t)}{\partial t} + \rho_0 \nabla \frac{\partial \mathbf{u}_f(t)}{\partial t} = q_f(t), \tag{70}$$

and the constitutive equation,

$$p(t) = c_0^2 \rho_f(t). \tag{71}$$

$\mathbf{u}_f(t)$ are the displacements, $p(t)$ is the dynamic pressure, $\rho_f(t)$ is the dynamic density and $q_f(t)$ is the added mass per unit volume. ρ_0 is the static density and c_0 is the speed of sound. ∇ denotes the gradient of a variable.
Differentiating Equation (70) with respect to time and substituting Equations (71) and (69) into the resulting equation gives the nonhomogeneous wave equation expressed in acoustic pressure p as

$$\frac{\partial^2 p}{\partial t^2} - c_0^2 \nabla^2 p = c_0^2 \frac{\partial q_f}{\partial t}. \tag{72}$$

The derivation of the finite element formulation for the fluid starts from Equation (72) and standard finite element derivations lead to

$$\mathbf{M}_f\ddot{\mathbf{p}}_f + \mathbf{K}_f\mathbf{p}_f = \mathbf{f}_q + \mathbf{f}_s, \tag{73}$$

where $\mathbf{M}_f$ is the mass matrix, $\mathbf{K}_f$ is the stiffness matrix, $\mathbf{f}_s$ and $\mathbf{f}_q$ are force vectors and $\mathbf{p}_f$ denotes the nodal pressures.
The kinematic coupling between the structure and fluid domains are made in the normal direction by

$$\mathbf{u}_s\mathbf{n} = \mathbf{u}_f\mathbf{n} \tag{74}$$

and through the continuity in pressure by

$$\sigma_s|_n = -p, \tag{75}$$

where $\mathbf{n}$ is a normal vector. Given that $\mathbf{n}_s$ and $\mathbf{n}_f$ are the boundary normal vectors pointing outwards from the structural and fluid domains respectively, it is defined that $\mathbf{n} = \mathbf{n}_f = -\mathbf{n}_s$.
Equation (75) can be rewritten and inserted into the term $\mathbf{f}_f$ of Equation (68). This term is then rewritten further and discretized using finite element approximations. The final format of this equation is

$$\mathbf{f}_f = \mathbf{H}\mathbf{p}_f, \tag{76}$$

where $\mathbf{H}$ is the coupling matrix, see [43].
Using Equations (69) and (74), the force term $\mathbf{f}_s$ of Equation (73) can also be rewritten. Finite element discretization and substitution of the coupling matrix $\mathbf{H}$ into the obtained expression gives the final version of the term $\mathbf{f}_s$ as

$$\mathbf{f}_s = -\rho_0 c_0^2 \mathbf{H}^T \ddot{\mathbf{d}}_s. \tag{77}$$

To summarize, the structure-acoustic system is described by the following unsymmetrical system of equations

$$\begin{bmatrix} \mathbf{M}_s & \mathbf{0} \\ \rho_0 c_0^2 \mathbf{H}^T & \mathbf{M}_f \end{bmatrix} \begin{bmatrix} \ddot{\mathbf{d}}_s \\ \ddot{\mathbf{p}}_f \end{bmatrix} + \begin{bmatrix} \mathbf{K}_s & -\mathbf{H} \\ \mathbf{0} & \mathbf{K}_f \end{bmatrix} \begin{bmatrix} \mathbf{d}_s \\ \mathbf{p}_f \end{bmatrix} = \begin{bmatrix} \mathbf{f}_b \\ \mathbf{f}_q \end{bmatrix}, \tag{78}$$

which is the standard form of the structure-acoustic formulation.

6 Application of Developed Design Methods

6.1 General

In this section an example of a glass structure with bolted joints is used in order to demonstrate the use of the two stress prediction methods applicable to bolt fixed balustrades subjected to a line load presented in the first parts of this thesis. The example comprises a laminated glass balustrade of the type presented in the part of the thesis that deals with design charts. Since the balustrade in this example has three horizontal rows with two bolts each, it is simultaneously shown how the concept of design charts can be expanded to balustrades with the increased number of bolts. The results in terms of accuracy are compared to results that are obtained when a standard finite element method is used.

6.2 Description of Test Example

The structure is a balustrade of laminated glass consisting of two glass layers with an intermediate PVB layer. The structure contains 3+3 bolt connections, which means that this example is also used to illustrate how design charts was developed for the case of 3+3 bolt connections. In Figure 16, the two dimensional geometry of the structure is displayed.
Cylindrical bolts with bolt head diameter, d_b, of 60 mm were used. The bolts are made of steel and have bushes of EPDM at the contact surfaces with the glass. The bore hole diameter, d_h, was set to 22 mm. A list of the geometry parameters with corresponding

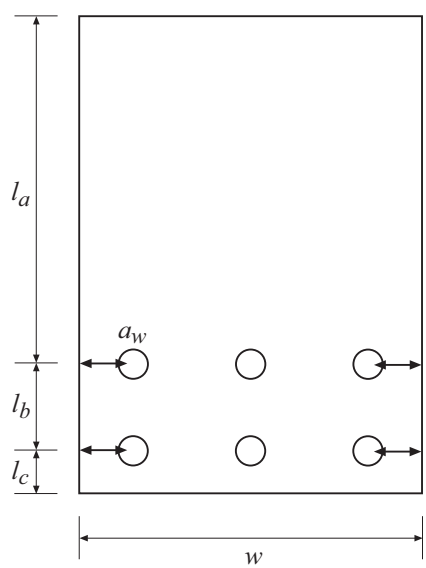

Figure 16: Two dimensional geometry of balustrade.

design values is included in Table 4. t_{PVB} is the thickness of the PVB layer, t_{EPDM} is the thickness of the EPDM layer and t_g is the glass thickness.
As an example, a horizontal (uniform) line load was applied at the upper edge of the glass balustrade. The load had the magnitude 3 kN/m. Alla materials were modeled as isotropic and linear elastic materials. In Table 5, the material parameter values are presented. E denotes modulus of elasticity and ν denotes Poisson's ratio for glass, PVB, EPDM and steel respectively.
In the coming subsections, it is described how the test example was analysed using three different methods. First, three dimensional solid elements were used in ABAQUS in order to provide a benchmark solution to which the two other methods were compared. Then, M-RESS elements were used in ABAQUS in order to illustrate the applicability of the method presented in the first part of the thesis to this test problem. Finally, design charts for balustrades with 3+3 bolt connections are introduced and it is shown how the charts were used in order to analyze the balustrade. Design charts for balustrades with 2+2 bolt connections is the topic of the second part of the thesis.

6.3 Finite Element Analysis Using Three Dimensional Solid Elements

In this subsection, second order three dimensional solid elements were used in ABAQUS in order to provide a benchmark solution to the problem presented in the former subsec-

Table 4: Design parameters for test example.

l_a	1.275 m
l_b	0.48 m
l_c	0.24 m
a_w	0.18 m
w	1.23 m
t_{PVB}	0.76 mm
t_{EPDM}	3 mm
d_h	22 mm
d_b	60 mm
t_g	12 mm

Table 5: Material parameters for test example.

E_g	70 GPa
ν_g	0.25
E_{PVB}	6.3 MPa
ν_{PVB}	0.4
E_{EPDM}	20 MPa
ν_{EPDM}	0.45
E_s	210 GPa
ν_s	0.3

tion. For each bolt, the entire bolt head consisting of a steel part and an EPDM layer was explicitly modeled. Only those bolts located at positions where equilibrium reaction forces acting on the glass occur, were included in the model. Constraints of the type tie were used between the glass pane and the EPDM layers. As boundary condition it was used that displacements are prohibited in all directions at the opposite side of the bolts. Second order three dimensional solid elements (C3D20R) were used for the glass and PVB layers. Standard linear three dimensional solid elements (C3D8R) were used for the other parts of the model. A total of about 270000 elements were used. The line load was converted to a pressure load acting on a surface of infinitely small width, since it is not possible to apply line loads in ABAQUS. The maximum principal stress occurred at the middle bolt of the upper bolt row, as is indicated in Figure 17, and took on the value 119.4 MPa.

6.4 Finite Element Analysis Using M-RESS Elements

In this subsection, the model of the previous subsection was used, but the element type of the laminated glass was selected to be M-RESS, see Section 5.2 and the first part of the thesis. A modification of the model of the former subsection was necessary. The line load was distributed to nine equidistant points and applied as concentrated forces using manual lumping. In this model, two element layers per glass layer and one element layer for the PVB layer were used. In total, around 160000 elements were used. The maximum principal stress of the glass balustrade reached 125.5 MPa.

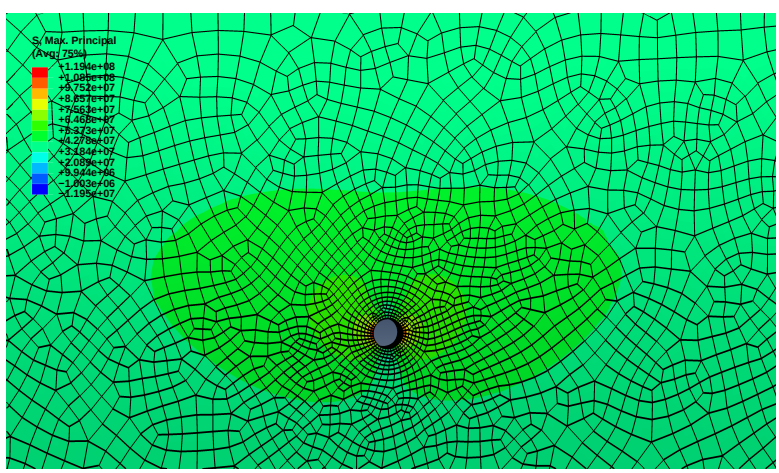

Figure 17: Maximum principal stresses for balustrade using three dimensional solid elements.

6.5 Stress Prediction Using Design Charts

In the course of writing this section, design charts for balustrades with 3+3 bolt connections were developed. The in-plane geometry of the balustrade is that of Figure 16. When comparing to the case of a balustrade with 2+2 bolt connections, the set of unknown parameters is the same. The development of the new design charts is thus a simple extension of the already developed charts. Table 6 displays the design parameters and the ranges of variation for each parameter.
Next, it is illustrated how the maximum principal stress of a glass balustrade with geometry parameters according to Table 6 and material parameters according to Table 5 was computed. First, the nominal stress value, σ_{Nom}, was computed. Analogous derivations are made in Section 5.3 and in the second part of the thesis. Here, the equations that were used are merely stated and the final answer to each equation is written out.

$$R_2 = P_{Tot}(1 + \frac{l_a}{l_b}) \tag{79}$$

gives $R_2 \approx 1.3492 \cdot 10^4$ N.

$$M(x) = \frac{R_2 l_a x}{(l_a + l_b)} \tag{80}$$

gives $M(0.48) \approx 4.7049 \cdot 10^3$ Nm.

$$N(x) = \frac{c_1 R_2 l_a}{c_2\sqrt{c_2}(l_a + l_b)cosh(\sqrt{c_2}l_b)} sinh(\sqrt{c_2}x) - \frac{c_1 R_2 l_a x}{c_2(l_a + l_b)} \tag{81}$$

gives $N(0.48) \approx -1.7426 \cdot 10^5$ N.

$$M_2(x) = \frac{1}{2}(M(x) + (h_t + t_{PVB})N(x)) \tag{82}$$

yields $M_2(0.48) \approx 1.2406 \cdot 10^3$ Nm.

Table 6: List of geometry parameters.

Parameter	Value
l_a	1.25 m
l_c	0.24 m
t_{PVB}	0.76 mm
t_{EPDM}	3 mm
l_b	0.2, 0.4, 0.8 m
a_w	0.1-($\frac{w}{2}$-0.15) m in step of 0.025 m
w	0.9-2.7 m in step of 0.3 m
d_h	15-40 mm in step of 5 mm
t_g	6, 8, 10, 12 mm
d_b	60 mm

$$\sigma_{Nom} = \frac{M_2(l_b)}{\frac{wt_g^2}{6}} - \frac{N(l_b)}{wt_g} \tag{83}$$

leads to $\sigma_{Nom} \approx 53.8$ MPa.
In Figure 18, the applicable design chart for this case is displayed. The chart was selected as the one which has parameter values closest to the actual design example.
In the diagram, $a_w = 0.18$ m was chosen on the x-axis, whereas in the case of l_b one had to interpolate between the isolines corresponding to $l_b = 0.4$ m and $l_b = 0.8$ m. The value of α which corresponded to the actual combination of parameters a_w and l_b, was read off from the diagram, which yielded $\alpha \approx 2.31$. The maximum principal stress of the balustrade was determined according to $\sigma = \alpha \cdot \sigma_{Nom} \approx 124.3$ MPa.

6.6 Results and Comparison

This subsection is devoted to a discussion and comparison of the results obtained using the various design methods discussed in this section. In Table 7, the values of maximum principal stress are presented. From the table one can conclude that the results of all three methods are sufficiently close to each other in order to classify the methods as yielding equivalent results. More rigorous comparisons of the two first methods are provided in the first part of the thesis. The result using the third method carries some uncertainties related to mesh density when constructing the chart, the selection of the design chart to match the

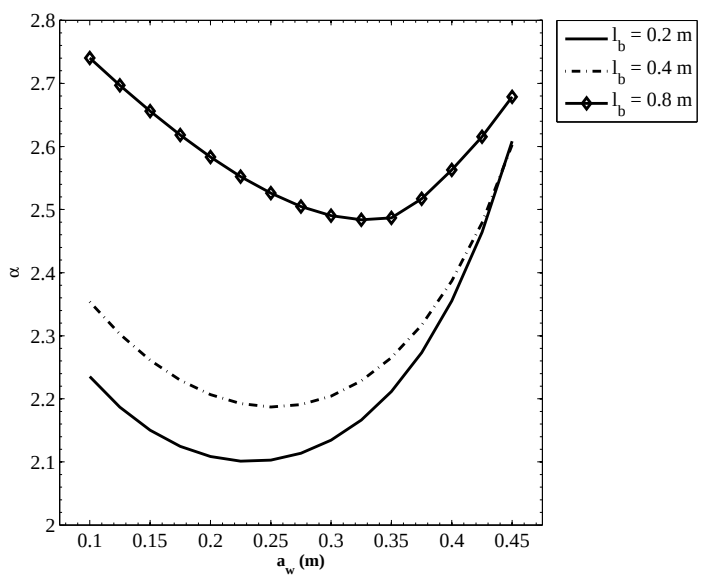

Figure 18: Design chart for $t_g = 12$ mm, $w = 1.2$ m, $d_b = 60$ mm and $d_h = 20$ mm.

Table 7: Comparison of different methods for stress prediction.

Method	Maximum principal stress (MPa)
FEM, solid elements	119.4
FEM, M-RESS	125.5
Design chart	124.3

actual set of parameters, parameter interpolation and reading off the chart. These effects do not seem to be significant given that the results are very close to those obtained using other methods.

7 Overview of Present Work

7.1 The Application of the M-RESS Element for Stress Evaluation of Advanced Laminated Glass Structures

In Paper 1, the M-RESS element was applied to typical examples of laminated glass structures and the performance regarding accuracy and computational efficiency was evaluated. The first example was a thin square plate subjected to biaxial bending through a uniformly distributed lateral load. The performance of the element was compared to standard three dimensional solid elements contained in the finite element program ABAQUS. Those elements were a linear 8-node and a quadratic 20-node element, both quadrilateral elements with reduced integration. Convergence tests were performed in terms of the vertical displacement at the center point of the bottom glass surface, w, and the in-plane stress in one direction, σ. The results were normalized to the results using the 20-node element in ABAQUS and 2 millions degrees of freedom. Defining the acceptable error to be less than or equal to 5 %, both for the displacements and the stresses, Table 8 shows the number of degrees of freedom required to reach acceptable levels of error for the elements investigated.

Apparently the 8-node solid element was not capable to represent the behavior of the structural problem. The computational advantage of using the M-RESS element instead of the 20-node solid element is well illustrated.

Further tests were dealing with real structures comprising commonly used types of joints in glass construction. The first example was adopted from [10], and comprised a square laminated glass plate with a bolted joint placed in the middle of the plate. A compressive force was applied to the joint. As an illustration of the structure, the geometry of the glass plate is shown in Figure 19.

The glass plate rested on a supporting steel frame and a rubber gasket protected the glass from direct contact with the steel. In [10], the fracture stress was evaluated experimentally for this structural problem. In Paper 1, finite element analyses of the structure were made using the M-RESS element for the modeling of the laminated glass part. As a comparison, a similar model was made using 20-node solid finite elements for the corresponding parts. The model size of the model with M-RESS elements was around 10 % of that of the model with solid elements. The maximum principal stresses were located in the upper glass layer close to the bore hole as expected. In Table 9, the maximum principal stress for the different methods is shown. For the experiments, the results presented are not the maximum principal stresses occurring in the structure since it was not possible to make experimental measurements at the correct location.

Table 8: Convergence properties of different finite elements.

Finite element	Min. number of DOFs for w	Min. number of DOFs for σ
M-RESS	300	700
8-node solid	200000	-
20-node solid	3000	3000

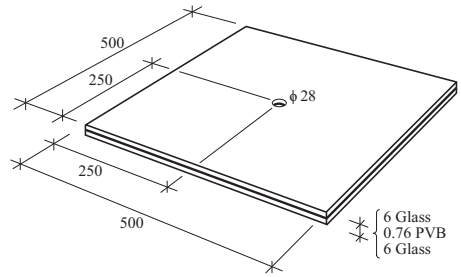

Figure 19: Geometry of glass plate.

Both of the numerical models had an error less than 15 % compared to the experimental results, and the M-RESS element predicted results that are closer to the experimental ones. With the difference in model size between the two elements, the M-RESS element is clearly a more efficient element for this kind of modeling. The 10 % error that the M-RESS element predicted is accurate enough to be used in practical design of glass structures. In Paper 1, there is a discussion relating to error sources that are related to the numerical modeling, but not to the properties of the finite elements. It is possible that the error could be further reduced without increasing the size of the model.
The second real glass structure dealt with a large glass beam that was made up by smaller glass beams through the use of adhesive joints. The structure was created and analysed experimentally and numerically in [30] and Paper 3. The aim of that work was to determine the shear capacity of an adhesive joint in a large dimension glass beam. The experimental test arrangement is displayed in Figure 20.
The test was a four-point bending test where the arrangement had been made so that pure shear stresses were obtained in the joints. In the original study, several adhesives were studied. For the demonstration of the applicability of the M-RESS element, an epoxy adhesive was used. As a comparison, a model was made using 20-node solid finite elements. The model size of the model using M-RESS elements was only 20 % of the model size of the model with solid elements. The variable used in the comparison was the ultimate displacement in the load direction at point 4 of Figure 20. The results are shown in Table 10.
Both the M-RESS element and the 20-node solid element yielded very accurate results for the present test case, but the model used for the M-RESS element was significantly more computationally efficient.

Table 9: Maximum principal stress close to bore hole.

Method	Maximum principal stress (MPa)
Experimental (mean value)	177.1
M-RESS	159.2
20-node solid	153.4

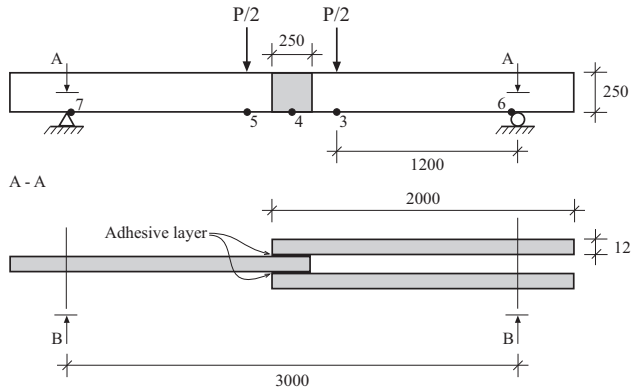

Figure 20: Test setup of four-point bending test of glass beam with adhesive joint.

Table 10: Ultimate deformations at the mid-point of the beam.

Test	Displacement (mm)
Experimental	10.00
M-RESS	10.20
20-node solid	10.24

In summary, three test cases that are relevant in the discussion regarding laminated glass structures of various support conditions have been analysed and the results consistently showed that the use of the suggested M-RESS element lead to more computationally efficient modeling at a given level of accuracy. Note that the M-RESS element is not a standard element of a commercial software package, which means that the contribution extends the abilities available in commercial finite element modeling to deal with strengh design of complex glass structure in a computationally efficient manner.

7.2 Development of Design Charts for Stress Evaluation of Laminated Glass Balustrades with Bolted Joints Subjected to a Line Load

In Paper 2, a method for evaluating the stresses in a bolt fixed laminated glass balustrade was developed. The balustrade had two rows of two bolt fixings each and was subjected to a line load. This problem could be analysed by means of finite element analysis using the M-RESS element as in Paper 1. The method developed in Paper 2 combines design charts and analytical formulas to determine the stresses. The method serves as an alternative for users that may not be so familiar with the finite element method.
The method is partly based on the analytical beam model presented in Section 5.3. By noting that the laminated glass balustrade without holes can be perceived as a beam subjected to three point bending since the loads and boundary conditions are symmetric, a

nominal stress, σ_{nom}, can be calculated. The geometry of the beam model applied to a balustrade is shown in Figure 21.
P_{Tot} is the line load, P, multiplied by the width of the balustrade, w. R_1 and R_2 are the reaction forces that represent the bolt loctions.
A finite element computation using the M-RESS element was used for the structure with holes and the maximum principal stress of the whole structure, σ, was computed. The maximum stress and the nominal stress are related through the stress concentration factors, α, by the expression $\sigma = \alpha\sigma_{Nom}$. The stress concentration factors were represented graphically in so-called design charts. For stress determination, σ_{Nom} is determined by means of derived formulas that are analogous to those derived for the analytical beam model of Section 5.3. The complete derivation is found in Paper 2. It is emphasized that an extension of the original analytical model was made to include the thickness of the PVB layer in the moment equilibrium calculations, Equation (29). In Section 6, the methods of Paper 1 and Paper 2 were compared and the method of Paper 2 was extended to the case of a balustrade with two rows of three bolt fixings each. For stress determination, it is σ that is of interest. α can be determined from the corresponding design chart, and σ is obtained through the relation between σ_{Nom} and σ. In Section 6, a sample design chart for the case of $3+3$ bolts is also displayed. Thus, for further explanation, demonstration of the method and evaluation of the results it is referred to Section 6.

7.3 Evaluation of the Shear-capacity in Adhesive Glass Joints and Development of Material Models for the Adhesives

In Paper 3 adhesive glass joints were studied. In the first part of the study, which describes the work of [30], the shear-capacity of various adhesives for connecting glass was determined experimentally. The tests were performed on small specimens and the shear-capacity was evaluated for a short-term load.
The test equipment was designed to obtain a state of pure shear in the joint. The test equipment consisted of two steel-parts that transmit the forces from the testing machine to the specimen.
The specimens in the tests consisted of two pieces of glass with dimensions 20×20 mm^2 joined together with an adhesive layer.

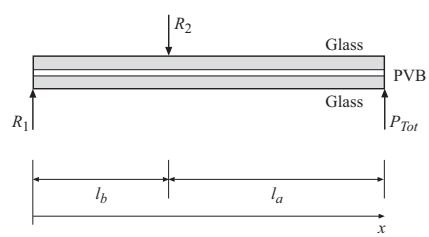

Figure 21: Beam model applied to a balustrade without holes.

The tested adhesives can be grouped into softer and stiffer adhesives. The softer adhesives contained four types of silicone based adhesives, three types of SMP (Silyl Modified Polymer) based adhesives and Bostik Multifog 2640. The stiff adhesives consisted of polyurethane adhesive, HBM Rapid Adhesive X 60, strong epoxy adhesive and UV-hardening glass-glue. The adhesive products were chosen so that a wide span of different adhesive characteristics was obtained.
Test specimens had different thickness of the adhesive layer. For the silicone glues, the thickness was 6 mm, for the SMP based adhesives and Bostik Multifog 2640, the thicknesses were 2 and 0.3 mm. The polyurethane glue and HBM Rapid adhesive X 60 had an adhesive thickness of 0.2 mm, whereas the strong epoxy and the UV-hardening glue had 0.3 mm as thickness of the adhesive.
In the tests, data on force versus displacements were collected. The shear-capacity was obtained through dividing the ultimate measured shear force by the initial surface area of the adhesive.
The results for one softer adhesive and one stiffer adhesive are presented. For the softer adhesive, one SMP based adhesive, the obtained shear-capacity was 2.3 MPa. For the stiffer adhesive, polyurethane glue, the shear-capacity was determined to 3.8 MPa.
Later, as a part of this work and the work of [30], a finite element model of the test arrangement was developed to determine the material models of the adhesives. The evaluation of the results consisted of plotting the measured data of the shear-force versus the deformation of the test series. The data was fitted to a polynomial curve and compared with the data extracted from the finite element simulations. For each adhesive, different material models were tested until a satisfying agreement was obtained. For the softer adhesives, the hyperelastic material models Neo-Hooke and Mooney-Rivlin were tested whereas the stiffer adhesives were modeled as linear elastic. For an overview of the resulting material models it is referred to Paper 3. From the respective matching material model, data on the shear-deformation was extracted and relationships between shear-stress and shear-strain were established. An initial shear modulus, G, was calculated from the shear-stress versus shear-strain diagrams and an ultimate shear-stress was determined.
Results showing the mechanical characteristics of two groups of adhesives (softer, 2 mm specimens and stiffer) are shown in Table 11. In general, the stiffer adhesives had greater stiffness (G) and ultimate shear-strength ($\tau_{avg,u}$) than the softer adhesives.
Finally, the work of [30] is described, in which a large-scale experimental test was made to determine the shear-capacity of an adhesive joint in a large dimension glass beam.
Five adhesives from the small-scale tests were chosen to be tested in the large-scale tests. The five adhesives were chosen considering the results from the finite element simulations of the corresponding test set-up. The two strongest SMP based adhesives and the

Table 11: Mechanical characteristics of adhesives.

Quantity	Softer adhesives	Stiffer adhesives
G (MPa)	0.5-1.2	83-500
$\tau_{avg,u}$ (MPa)	1.3-2.3	4-20
γ_u (%)	200-300	4-10

stiffer adhesives polyurethane glue, UV-hardening glass-glue and the strong epoxy adhesive were chosen.
The test performed was a four-point bending test of a beam that consisted of three beams made of flat-glass joined together by two adhesive joints. The test arrangement is shown in Figure 20 and creates a symmetrical beam in order to obtain pure shear- stresses in the joint. The beam had a span of three meters and every flat-glass element had dimensions 250×2000 mm and a width of 12 mm. The adhesive joints had dimensions 250×250 mm.
During the measurements, data on load and deformation of the mid-point of the beam were collected.
To investigate whether the derived material models are valid for larger joints, a finite element model was made of the large-scale test set-up. The adhesives were modeled according to the material models from the tests with the small specimens. Load-deformation graphs were determined for the tested adhesives and maximum load values were determined.
For the third SMP based adhesive, the measured data showed a less stiff behavior than the data from the simulations. After an initial deviation, the stiffness of the measured data for the polyurethane adhesive compared well with experiments. It is referred to Paper 3 for result graphs.
Looking at the principal pattern of shear-stresses in the joints, in the stiffer adhesives stress-concentrations occurred at the corners of the joints. In the softer adhesives, the stresses were more evenly distributed. This result is presented in Paper 3.
Table 12 summarizes the ultimate loads and deformations for a selection of the softer adhesives. The results were obtained from the finite element simulations. The corresponding results for the stiffer adhesives are shown in Table 13.
Overall, the softer adhesives had ultimate loads ranging between 28 and 50 kN and the stiffer adhesives had ultimate loads in the interval 10-30 kN.

Table 12: Ultimate loads and deformations at the mid-point of the beam for softer adhesives.

Adhesive	Ultimate load (kN)	Ultimate deformation (mm)
Bostik Multifog 2640	28.8	53
SMP Based Adhesive 1	49.3	51
SMP Based Adhesive 2	38.2	43
SMP Based Adhesive 3	48.8	50

Table 13: Ultimate loads and deformations at the mid-point of the beam for stiffer adhesives.

Adhesive	Ultimate load (kN)	Ultimate deformation (mm)
Strong Epoxy	30.3	10.0
Polyurethane Glue	10.3	3.5
UV-hardening Glue	22.3	7.5
HBM Rapid Adhesive X 60	20.3	7.0

7.4 Development of a Reduced Model for Evaluation of Stresses in Glass Structures Subjected to Dynamic Impact Load

The topic of Paper 4 is the development of a reduced method for evaluating stresses in glass structures subjected to dynamic impact load. The load conditions are partly prescribed in the standard SS-EN-12600, [46]. The standard describes a test to evaluate the impact strength of glass. The corresponding test arrangement is shown in Figure 22.
The arrangement consists of a glass pane held within a steel frame and an impactor consisting of a weight encased in a tire. During the test, the tire is swung in a pendulum motion into the glass pane. The dimensions of the frame are standardized to 1.95×0.887 m^2 and the weight of the impactor is prescribed to 50 kg according to the standard. When performing strength design of an arbitrary glass structure, the pendulum load as prescribed in the standard is applied.
As a starting point, a full dynamic finite element model for the case of an undamped multi-degree-of-freedom system undergoing free vibration was made for the glass part including the boundary conditions. The finite element formulation for this case is described in Section 5.5. The Rayleigh-Ritz method presented in Section 5.6 was used to reduce the number of degrees of freedom of the glass structure. Compared to existing reduced models for this load case, the inclusion of the boundary condition makes the model more flexible in applicability. Earlier contributions, for instance [44], are limited to two-sided and four-sided support conditions.
The impactor was represented by a single-degree-of-freedom system, see Section 5.5. The out-of-plane degree of freedom at the midpoint of impact of the glass pane was chosen as the reference degree of freedom, u_{ref}, to which the impactor was connected. To correctly represent the complete system, it was suggested that the degree of freedom u_i of the impactor is tied to the first generalized coordinate, z_1, of the reduced model which corresponds to the point of impact.
When connecting the impactor to the reduced model of the glass, $u_{ref} = z_1$ must be ful-

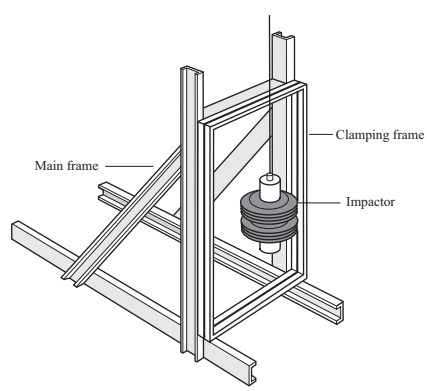

Figure 22: Test arrangement for pendulum impact test.

filled. This means that the corresponding displacement vector, ψ_1, must be normalized so that the absolute value of the out-of-plane displacement is equal to one at u_{ref} and that any other Ritz vector, ψ_j , must fulfill the condition that $u_{ref} = 0$. This can be realized from Equation (60) of Section 5.6. These conditions must always be fulfilled when creating a reduced model for the glass.
The advantages of using the Rayleigh-Ritz method to reduce the model are that for the considered design cases the Ritz vectors can be chosen based on physical intuition which might decrease the necessary amount of Ritz vectors and that excentric impact can easily be represented since the location of u_{ref} can be chosen arbitrarily.
In Paper 4, two Ritz-vectors were selected to represent the glass structure. Assembling of the subsystems representing the glass and the impactor respectively, leads to the following multi-degree-of-freedom system for the complete system

$$\begin{bmatrix} m_i & 0 & 0 \\ 0 & \tilde{m}_{11} & \tilde{m}_{12} \\ 0 & \tilde{m}_{21} & \tilde{m}_{22} \end{bmatrix} \begin{bmatrix} \ddot{u}_i \\ \ddot{z}_1 \\ \ddot{z}_2 \end{bmatrix} + \begin{bmatrix} k_i & -k_i & 0 \\ -k_i & k_i + \tilde{k}_{11} & -\tilde{k}_{12} \\ 0 & -\tilde{k}_{21} & \tilde{k}_{22} \end{bmatrix} \begin{bmatrix} u_i \\ z_1 \\ z_2 \end{bmatrix} = \begin{bmatrix} 0 \\ 0 \\ 0 \end{bmatrix}, \qquad (84)$$

where k_i and m_i represent the stiffness and mass of the impactor. $\tilde{\mathbf{m}}$ and $\tilde{\mathbf{k}}$ are the generalized mass and stiffness matrices for the glass.
For the case of central impact, the first Ritz vector corresponds to the static deformation mode of the glass. The deformed shape was constructed through applying a uniformly distributed load corresponding to the weight of the glass, Q_g, to the entire glass pane area. It is referred to Paper 4 for an explanation of how this Ritz vector was obtained for excentric load.
The second Ritz vector was constructed by means of applying a distributed force on the entire surface of the glass corresponding to the glass weight on one side of the pane and simultaneously a uniformly distributed load corresponding to the weight of the impactor, Q_i, was applied at the contact surface between the impactor and the glass but in the opposite direction. A schematic sketch of the construction of the Ritz vectors is shown in Figure 23 for the case of centrally applied impact.

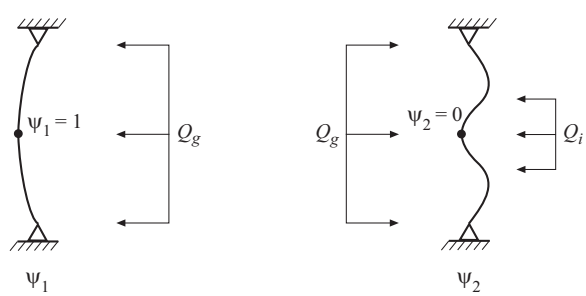

Figure 23: Construction of Ritz vectors.

Standard numerical procedures were used to solve the system of Equation (84). The corresponding stresses can be evaluated once the system has beem solved, see Papers 1, 4 and Section 5.2.3.

The model was validated using a test example corresponding to the standard SS-EN-12600, [46], which has been numerically modeled in [38]. The model in [38] is a full dynamic finite element model which is verified against experiments. The structure was four-sided supported. The impactor was dropped from a fall height of 450 mm. The lateral displacement at the middle of the glass as well at the maximum principal stress of the structure were evaluated. The most interesting results were related to the maximum principal stress. Four different models were compared. Those were the finite element model of [38] with geometrically nonlinear and linear formulations and the reduced model of Paper 4 with one and two Ritz vectors respectively. It was apparent that the reduced model based on only one Ritz vector is not appropriate to use since the stresses were around 50 % of those of the full model. The full model results were more or less the same for the geometrically linear and nonlinear formulations which means that the effect of the geometric nonlinearity was small. The reduced model developed in this paper has two Ritz vectors, and for that model the error was between 7 and 10 % compared to the full models and the stresses were smaller than for the full models.

Another test example dealt with validation of the method for the case of excentrically applied impact. Three different positions of excentric impact were investigated for four-sided supported glass. The error in terms of the maximum principal stress, σ_{max}, compared to the corresponding model from [38] was less than or equal to 10 %. For all cases considered, the error was so that it is on the safe side in strength design.

It is expected that the model behavior changes when the in-plane glass dimensions increase, see for instance [38]. Thus, a similar study was made for larger glass panes of dimensions 2×2 m^2. The results in terms of σ_{max} are displayed in Table 14.

Even for this example, the stresses for the reduced model with only one Ritz vector were much smaller than for the full model. The reduced model with two Ritz vectors had stresses that were very similar to those of the full model with linear geometry. It is implied that the included number of Ritz vectors is sufficient. The model error was almost 20 % when compared to the full model with nonlinear geometry. Since the stress was greater for this model, the model was considered sufficiently accurate, but a greater error does not make sense from the perspective of efficient material use. The geometric nonlinearity effect was significant for this case. It is likely that this effect becomes even greater with increased in-plane dimensions, so it is suggested that the reduced model applicability is limited to dimensions less than or equal to 2×2 m^2 if not nonlinear geometric effects are accounted for in the model.

The limits of the reduced model were investigated more thoroughly in Paper 4 through

Table 14: Maximum principal stress for impact load applied to a larger glass pane.

	Only Ritz vector 1	Current model
$\sigma_{max}/\sigma_{max,linear}$	0.42	0.95
$\sigma_{max}/\sigma_{max,nonlinear}$	0.52	1.18

a parametric study concerning in plane dimensions and glass thickness. The fall heights 200, 300 and 450 mm were considered. Briefly, the use of the reduced model was more critical for small glass thicknesses and large glass panes. For more detailed results, refer to Paper 4.
A final test example investigated the model applicability to a balustrade type often encountered. It was a clamped fixed laminated glass balustrade of standard dimensions and thicknesses. The fall height of the pendulum was again 450 mm. Results in terms of σ_{max} showed that the error compared to the full finite element model with nonlinear geometry was only around 3.5 %.
In summary, it was shown that the reduced model is applicable to small and medium sized glass structures when four-sided supported glass with central impact is concerned. The model performed excellently when a standard laminated glass balustrade with clamped supports was considered. The model validity for four-sided supported glass with excentric impact was also validated.

7.5 Structural Analysis of Insulated Glass Subjected to Dynamic Impact Load

Paper 5 concerns the computational modeling and analysis of insulated glass units subjected to dynamic impact load. The analyses were performed by means of the commercial finite element software ABAQUS. Structure-acoustic analysis described in Section 5.7 was used for the modeling. The load conditions and test arrangement for the pendulum impact test are described in Section 7.4 and are thus not described here. As a test of the modeling approach, the experimental results of [12] were used as a comparison. The insulated glass unit consisted of two glass panes and an intermediate air layer. Due to several differences in for instance the frame of the test rig, a more qualitative similarity of the results could be expected.
A comparison regarding the time development of the midpoint lateral displacements of the surface facing the impactor (inner) and the surface on the opposite side of the impactor (outer) showed that the model results and experimental results were in good accordance until the maximum displacements were reached. Regarding the maximum displacement, for both panes the simulation error was less than 5 % which is acceptable.
A parametric study was made regarding the in-plane dimensions of the glass, the air cavity thickness and the glass pane thickness. For the case of the in-plane dimensions, six cases were studied according to Table 15.
The glass thickness of both panes was 6 mm and the air cavity thickness was set to 12 mm. For these cases, also a structure with one glass was analyzed for comparison purposes.
In the parametric study of the influence of the air cavity thickness, the cases with cavity thicknesses 6, 12 and 18 mm were studied. The in-plane dimensions were set to 800 $\times$ 1600 mm^2 and the glass thickness was 6 mm.
In the parametric study of the influence of the glass thickness four cases were made comprising of glass thicknesses of 6, 8, 10 and 12 mm. In this study, the in-plane dimensions were 800 $\times$ 1600 mm^2 and the air cavity thickness was 12 mm.

Table 15: In-plane dimensions for the parametric study.

Case	In-plane dimensions (mm^2)
d1	800×800
d2	800×1200
d3	800×1600
d4	1200×1200
d5	1200×1600
d6	1600×1600

In terms of the center out-of-plane displacement, there was an almost 50 % increase when quadratic glass dimensions changed from the smallest to the largest. In terms of the maximum principal stress, there was a reduction of around 20 %. This can be seen from Table 16 where the maximum principal stress, σ_{max}, is displayed for various dimensions. Further it was shown that the outer pane had maximum displacements that were 70-80 % of those of the inner pane for quadratic glasses and maximum stresses that were 20-30 % of those of the inner pane for all combinations of dimensions studied.
For the cases of Table 15 an analysis was made using insulated glass versus single layered glass. The analysis was made in terms of σ_{max} and the results are displayed in Table 17 together with the results for the double glass.
In general there was only a small increase in the maximum stress when a single glass was used instead of an insulated glass. The largest increase was for the largest glass of dimensions 1600×1600 mm^2 where the maximum stress increased with around 15 %.

Table 16: Maximum principal stress for various glass pane dimensions.

Dimensions (mm^2)	σ_{max} (MPa)
800×800	192.3
800×1200	199.8
800×1600	206.3
1200×1200	187.6
1200×1600	182.3
1600×1600	156.8

Table 17: Maximum principal stress for single glass and double insulated glass for various glass pane dimensions.

Dimensions (mm^2)	σ_{max} (MPa), double glass	σ_{max} (MPa), single glass
800×800	192.3	196.8
800×1200	199.8	204.2
800×1600	206.3	213.8
1200×1200	187.6	188.6
1200×1600	182.3	197.3
1600×1600	156.8	182.2

For the parametric study with respect to the air layer thickness, results of Paper 5 indicate that the influence of the air layer is almost negligible. This also holds for the stresses of the outer pane.
For the parametric study with respect to the glass thickness, there was a clear tendency that the center displacement increased with decreasing pane thickness. The fraction of outer maximum displacement to inner maximum displacement increased when the glass pane thickness decreased. The maximum stresses also increased with decreasing pane thickness. There was a small tendency that the fraction of outer maximum stress to inner maximum stress increased as the pane thickness decreased.
In analysing a triple glass insulated unit, the decrease in maximum stress compared to the double glass unit was less than 5 %.

8 Discussion

In this section, the most important conclusions from the thesis work are presented and directions for future work are provided.

8.1 Conclusions

8.1.1 Application of the M-RESS Element for Stress Prediction in Laminated Glass

A recently developed finite element, [13], is implemented and it is proven that the performance is accurate when it comes to the modeling of thin laminated glass structures subjected to bending as well as for laminated glass with bolted and adhesive joints. The computational performance is strongly improved compared to when a standard three dimensional solid element is used. One can conclude that this element could be used in finite element analyses of complex laminated glass structures with many bolt fixings or adhesive joints.

8.1.2 Design Charts for Stress Evaluation in Laminated Glass Balustrades

A method is developed such that the maximum principal stress of a laminated glass balustrade with 2+2 bolt fixings could be determined using simple formulas and design charts. This leads to great time savings for the designer, since an investigation of the stresses of balustrades with different design parameters could be performed without finite element analyses. It is also not necessary for the designer to possess the advanced knowledge of the finite element method which is required in order to analyse advanced glass structures.

8.1.3 Shear-capacity in Adhesive Glass Joints

A test method for evaluating the shear-capacity of small-scale adhesive joints is suggested and it is concluded that the method is appropriate for the purpose. The method creates a state close to pure shear. Material models used for finite element simulations of adhesive joints subjected to short-term load can be determined with close accuracy between experiments and simulations for a group of stiff adhesives. For a group of softer SMP based adhesives, corresponding hyperelastic material models are developed and proven to be consistent with experiments for small-scale joints, whereas further research is necessary to validate the material models for large-scale joints. For small-scale joints, stiff adhesives give a stronger joint than softer adhesives. For a large joint, more soft nonlinear adhesives may give a stronger joint. With further validation, the methodology presented may be used to predict the mechanical behavior of any joint size through the combination of small specimen tests and finite element modeling.

8.1.4 Reduced Modeling for Glass Subjected to Dynamic Impact Load

A reduced finite element model for determining the maximum principal stress of a glass subjected to dynamic impact load is developed. The method is flexible because it is applicable to different support conditions as well as to both centric and excentric applied impact. The model is validated against a full finite element model and the model applicability is proven for the case of four-sided supported glass with centric impact and monolithic glass. It is shown that the model performance is improved when two Ritz vectors are used instead of one in model reduction. When the in-plane dimensions increase, the effect of geometric nonlinearity of the glass is strongly influencing the result. It is proven that the method applies to structures with excentric load positions. Further, the reduced model is very well suited for strength design of standard laminated glass balustrades with clamped fixings.

8.1.5 Analysis of Insulated Glass Subjected to Dynamic Impact Load

Structure-acoustic analysis is shown to be a useful method to analyze insulated glass subjected to dynamic impact load. For quadratic glasses, a large glass unit has a significantly larger center displacement but lower stresses than a smaller unit. For the cases of quadratic units considered in the study, the outer glass has a maximum central displacement that is 70-80 % of that of the inner glass. For all cases considered in the study, the outer glass has a maximum stress level that is 20-30 % of that of the inner glass. Further, when using a single glass instead of a double insulated glass, there is almost no difference in the maximum stress level. For a standard double insulated glass unit the air cavity thickness has only a minor influence on the stresses of the unit. The glass thickness, on the other hand, has a large influence. Both displacements and stresses increase with decreasing pane thickness. The ratio between outer and inner values of both displacements and stresses increases as the pane thickness decreases. Finally, the maximum stresses in a triple insulated glass unit are almost not reduced at all compared to the stresses of a corresponding double glass unit.

8.2 Future Work

For future work, a number of extensions can be made to the development of the design charts. The must obvious extension is to develop similar charts for balustrades with 3+3 bolt fixings. The development of these charts is to a great deal finished, which has been demonstrated in this thesis. There are possibilities for developing charts for parameter combinations that have not been taken into account, for instance considering different thicknesses of the PVB layer. Other materials for the interlayer could also be considered. It could also be interesting to consider other types of bolts and bolts for countersunk holes. An extension to include outdoor balustrades with other loading situations can also be made. Less obvious is to consider other types of connections, see [24] for an overview of different types of connections. Especially adhesive connections are of interest, since the larger contact area between the connection and the glass leads to a redistribution of the stress concentrations that glass may be subjected to. The use of glued connections also

leads to greater transparency of the structure. Furthermore, one may consider to develop similar charts for other types of structures, for instance facades.
Regarding adhesive glass joints, a number of suggestions for future work can be made. The shear-capacity of, and material models for a complementary set of adhesives may be determined. The studies may be extended to comprise long-term loads. Finally, the effect of thermal influence of the adhesive could be considered.
The model performance of the reduced model may be improved by including the effect of the geometric nonlinearity of the glass into the model. Another possible extension is to add additional Ritz vectors for representing the glass pane. Further improvement of the model could be made through including a nonlinear representation of the impactor stiffness. The model performance could be investigated for glass with other support conditions, for instance bolt fixings. Finally, further experimental investigations of glass subjected to dynamic impact load would be of interest. The influence of various types of supports, positions of impact and glass types could be investigated.
For the case of insulated glass, it could be interesting to consider different glass pane thicknesses of the inner and outer panes of the unit. The influence of different boundary conditions could also be interesting to study. Further, the effect of having another gas than air in the cavity could be analyzed. Finally, it could be of gain to perform more experimental tests of insulated glass subjected to dynamic impact load, both to increase understanding and for better model validation.

9 Summary of the Papers

9.1 Paper 1

M. Fröling and K. Persson. Computational Methods for Laminated Glass. Published in: *Journal of Engineering Mechanics*, 139, 7, 780-790, (2013).

Summary: An existing, recently developed, solid-shell finite element is proposed for the purpose of efficient and accurate modeling of laminated glass structures. The element is applied to one test example treating a thin laminated glass structure subjected to biaxial bending and the performance concerning accuracy and efficiency is compared to standard three dimensional solid elements. Further examples illustrate how the element could be applied in the modeling of laminated glass structures with bolted and adhesive joints. For these examples, experimental data for relevant quantities are provided as a comparison. It is concluded that the element is an excellent candidate for the modeling of laminated glass.

Contributions by M. Fröling
M. Fröling was the main author of the paper and wrote the manuscript. She performed the main part of the implementation work as well as the work concerning the finite element verification examples.

9.2 Paper 2

M. Fröling and K. Persson. Designing Bolt Fixed Laminated Glass with Stress Concentration Factors. Published in: *Structural Engineering International*, 23, 1, 55-60, (2013).

Summary: A general method for determining stress concentration factors for laminated glass balustrades with two plus two bolt fixings with variable positions is developed. It is demonstrated how the stress concentration factors can be presented graphically in design charts and representative charts are displayed for the case of a more specific bolt fixed balustrade type. In general, the use of simple formulas and the design charts allows the maximum principal stresses of the balustrade to be determined for any relevant combination of the variable geometry parameters involved.

Contributions by M. Fröling
M. Fröling was the main author of the paper and wrote the manuscript. She performed the main part of the implementation and contributed in developing the design method presented in the paper.

9.3 Paper 3

M. Fröling, K. Persson and O. Larsson. Shear-Capacity in Adhesive Glass Joints. Published in: Proceedings of Challenging Glass 3, Delft, The Netherlands, 2012.

Summary: The shear-capacity of adhesive glass-joints was investigated. Various stiff and soft adhesives were tested in a short-term load-case. The tests were conducted with small specimens in order to achieve a homogenous state of stress. The results of the tests were used in order to determine the material models of the adhesives. Finite element analysis of the test set-up was used for the determination of the material models. Large-scale tests were conducted to verify the material models from the tests of the small specimens. It could be concluded that with further validation, a combination of small-specimen tests and finite element simulations may allow for the determination of joint behavior for any joint size.

Contributions by M. Fröling
M. Fröling was the main author of the paper and wrote the manuscript. She performed a major part of the computational simulations and presented the paper at a conference.

9.4 Paper 4

M. Fröling, K. Persson and Per-Erik Austrell. A Reduced Model for the Design of Glass Structures Subjected to Dynamic Impulse Load. Submitted.

Summary: A reduced finite element model for determining the maximum principal stress of a glass pane subjected to dynamic impact load is developed and compared to a full dynamic finite element model. The reduced model is based on the Rayleigh-Ritz method. The Ritz vectors used are determined by simple static load-cases. The model is applicable to centrally and excentrically applied impact and to glass of various support conditions. It is demonstrated that the model performs well for various types of supported glass panes and impact applied at different locations on the glass pane. The applicability to small or medium sized glass panes is shown through a parametric investigation. For large glass panes, especially at smaller glass thicknesses, it is suggested that geometrically nonlinear behavior of the glass pane is integrated into the model to reduce the model error. Finally, it is shown that the reduced model performs excellently in the modeling of a standard laminated glass balustrade with clamp fixings. Apparently, the model is very well suited for strength design of commonly used glass structures.

Contributions by M. Fröling
M. Fröling was the main author of the paper and wrote the manuscript. She contributed in the development of the reduced model, implemented the model and performed the simulations.

9.5 Paper 5

M. Fröling and K. Persson. Numerical Analysis of Insulated Glass Subjected to Soft Body Impact. To be submitted.

Summary: Structure-acoustic analysis is performed to analyse insulated glass subjected to dynamic impact load. A parametric study is made with respect to in-plane dimensions, glass thickness and thickness of the gas layer. For quadratic panes, a larger glass has a significantly larger center displacement but lower stresses than a smaller glass. For all studied combinations of in-plane dimensions the outer glass has a maximum stress level that is between 20 and 30 % of that of the inner glass. A single layered glass unit is proven to have only marginally greater stresses than the corresponding double glass unit. The air layer thickness has almost no influence on the stresses of the insulated glass subjected to a soft body impact. It is revealed that the thickness of the glass, however, has a large influence. Both displacements and stresses increase with decreasing pane thickness. The outer glass has a maximum stress level which is between 20 and 30 % of that of the inner glass. Further, an analysis is made of a triple insulated glass unit. Apparently, the addition of a third glass pane does not impact the structural mechanical capacity of an insulated glass unit to a great extent.

Contributions by M. Fröling

M. Fröling was the main author of the paper and wrote the manuscript. She contributed with ideas regarding studies made in the paper, developed the finite element models and performed the major parts of the finite element studies.

References

[1] R.D. Adams and J.A. Harris. The Influence of Local Geometry on the Strength of Adhesive Joints. *International Journal of Adhesion and Adhesives*, **7**, 2, 69-80, (1987).

[2] R.J. Alves de Sousa, R.P.R. Cardoso, R.A. Fontes Valente, J.W. Yoon, J.J. Grácio and R.M. Natal Jorge. A New One-point Quadrature Enhanced Assumed Strain (EAS) Solid-shell Element with Multiple Integration Points Along Thickness: Part 1 - Geometrically Linear Applications. *International Journal for Numerical Methods in Engineering*, **62**, 952-977, (2005).

[3] M.Z. Aşik. Laminated Glass Plates: Revealing of Nonlinear Behavior. *Computers and Structures*, **81**, 2659-2671, (2003).

[4] M.Z. Aşik and S. Tezcan. A Mathematical Model for the Behavior of Laminated Glass Beams. *Computers and Structures*, **83**, 1742-1753, (2005).

[5] P.-E. Austrell. Modelling of Elasticity and Damping for Filled Elastomers. Report TVSM-1009, Lund University, Division of Structural Mechanics, Lund, Sweden, 1998.

[6] R.A. Behr, J.E. Minor, M.P. Linden and C.V.G.Vallabhan. Laminated Glass Units under Uniform Lateral Pressure. *Journal of Structural Engineering*, **111**, 5, 1037-1050, (1985).

[7] R.A. Behr, J.E. Minor and M.P. Linden. Load Duration and Interlayer Thickness Effects on Laminated Glass. *Journal of Structural Engineering*, **112**, 6, 1441-1453, (1986).

[8] R.A. Behr, M.J. Karson and J.E. Minor. Reliability Analysis of Window Glass Failure Pressure Data. *Struct. Safety*, **11**, 43-58, (1991).

[9] R.A. Behr, J.E. Minor and H.S. Norville. Structural Behavior of Architectural Laminated Glass. *Journal of Structural Engineering*, **119**, 1, 202-222, (1993).

[10] C. Bength. Bolt Fixings in Toughened Glass. Master's thesis, Lund University of Technology, Lund, Sweden, (2005).

[11] S.J. Bennison, A. Jagota and C.A. Smith. Fracture of Glass/polyvinylbutyral (Butacite) Laminates in Biaxial Flexure. *J. Am. Ceram. Soc.*, **82**, 7, 1761-1770, (1999).

[12] S. Brendler, A. Haufe and T. Ummenhofer. A Detailed Numerical Investigation of Insulated Glass Subjected to the Standard Pendulum Test. Proceedings of the Third LS-DYNA Forum, Bamberg, Germany, 2004.

[13] R.P.R. Cardoso, J.W. Yoon, M. Mahardika, S. Choudhry, R.J. Alves de Sousa and R.A. Fontes Valente. Enhanced Assumed Strain (EAS) and Assumed Natural Strain (ANS) Methods for One-point Quadrature Solid-shell Elements. *International Journal for Numerical Methods in Engineering*, **75**, 156-187, (2008).

[14] E. Carrera. Historical Review of Zig-Zag Theories for Multilayered Plates and Shells. *Appl. Mech. Rev.*, **56**, (2003).

[15] C. Carrick and J. Vasur. Styvhet och Hållfasthet hos Laminerat Glas. Master's thesis, Royal Institute of Technology, Stockholm, Sweden, 2002.

[16] D.J. Chen, D.K. Shah and W.S. Chan. Interfacial Stress Estimation Using Least-square Extrapolation and Local Stress Smoothing in Laminated Composites. *Computers and Structures*, **58**, 765-774, (1996).

[17] A.K. Chopra. Dynamics of Structures-Theory and Applications to Earthquake Engineering. Pearson Prentice Hall, Upper Saddle River, New Jersey, (2007).

[18] E.N. Dvorkin and K.J. Bathe. A Continuum Mechanics Based Four-node Shell Element for General Nonlinear Analysis. *Engineering and Computations*, **1**, 77-88, (1984).

[19] EN 1991-1-1:2002. Eurocode 1: Actions on Structures; Part 1-1: General Actions-Densities, Self-weight, Imposed Loads for Buildings. CEN, 2002.

[20] EN 572-1:2004. Glass in Building - Basic Soda Lime Silicate Glass Products - Part 1: Definitions and General Physical and Mechanical Properties. CEN, 2004.

[21] P. Foraboschi. Behavior and Failure Strength of Laminated Glass Beams. *Journal of Engineering Mechanics*, **12**, 1290-1301, (2007).

[22] Glafo, Glasforskningsinstitutet. Boken om glas. Allkopia, Växjö, Sweden, (2005).

[23] A.A. Griffith. The Phenomena of Rupture and Flow in Solids. *Philosophical Transactions, Series A*, **221**, 163-198, (1920).

[24] M. Haldimann, A. Luible A and M. Overend. Structural Use of Glass. Structural Engineering Documents, 10. IABSE, Zürich, Switzerland, (2008).

[25] G.A. Holzapfel. Nonlinear Solid Mechanics-A Continuum Approach for Engineering. John Wiley & Sons Ltd, Chichester, England, (2010).

[26] J.A. Hooper. On the Bending of Architectural Laminated Glass. *Int. J. Mech. Sci.*, **15**, 309-323, (1973).

[27] C.E. Inglis. Stresses In a Plate Due to the Presence of Cracks and Sharp Corners. *Transactions of the Institute of Naval Architects*, **55**, 219-241, (1913).

[28] G. Irwin. Analysis of Stresses and Strains Near the End of a Crack Traversing a Plate. *Journal of Applied Mechanics*, **24**, 361-364, (1957).

[29] I.V. Ivanov. Analysis, Modelling, and Optimization of Laminated Glasses as Plane Beam. *International Journal of Solids and Structures*, **43**, 6887-6907, (2006).

[30] O. Larsson. Shear-Capacity in Adhesive Glass Joints, Master's thesis, Lund University of Technology, Lund, Sweden, (2008).

[31] E. Le Bourhis. Glass-Mechanics and Technology. Wiley-VHC, Weinheim, Germany, (2008).

[32] W.K. Liu, Y. Guo, S. Tang and T. Belytschko. A Multiple-quadrature Eight-node Hexahedral Finite Element for Large Deformation Elastoplastic Analysis. *Computer Methods in Applied Mechanics and Engineering*, **154**, 69-132, (1998).

[33] J. Malmborg. A Finite Element Based Design Tool for Point Fixed Laminated Glass. Master's thesis, Lund University of Technology, Lund, Sweden, (2006).

[34] J.E. Minor and P.L. Reznik. Failure Strengths of Laminated Glass. *Journal of Structural Engineering*, **116**, 4, 1030-1039, (1990).

[35] H.S. Norville, K.W. King and J.L. Swofford. Behavior and Strength of Laminated Glass. *Journal of Engineering Mechanics*, **124**, 1, 46-53, (1998).

[36] N.S. Ottosen and H. Petersson. Introduction to the Finite Element Method. Prentice Hall Europe, Hemel Hempstead, England, (1992).

[37] K. Pankhardt. Investigation on Load Bearing Capacity of Glass Panes. *Periodica Polytechnica*, 52/2, 73-82, (2008).

[38] K. Persson and B. Doepker. Glass Panes Subjected to Dynamic Impact Loads. Proceedings of the XXIV A.T.I.V. Conference, Parma, Italy, 2009.

[39] Pilkington Floatglas AB. Glasfakta 2004. (2004).

[40] E.P. Popov. Engineering Mechanics of Solids, 2nd Edition, Prentice Hall, Upper Saddle River, NJ, (1991).

[41] prEN 16612:2013. Glass in building - Determination of the Load Resistance of Glass Panes by Calculation and Testing. CEN, 2013.

[42] J.N. Reddy. Mechanics of Laminated Composite Plates. Theory and analysis. CRC Press, Boca Raton, FL, (1997).

[43] G. Sandberg, P.A. Wernberg and P. Davidsson. Fundamentals of Fluid-Structure Interaction. Computational Aspects of Structural Acoustics and Vibration, CISM Courses and Lectures, G. Sandberg and R. Ohayon (eds), vol. 505. Springer, Wien, Austria, (2008).

[44] J. Schneider. Festigkeit und Bemessung punktgelagerter Gläser und stossbeanspruchter Gläser. Doctoral thesis, Technische Universität Darmstadt, Darmstadt, Germany, (2001).

[45] J.C. Simo and M.S. Rifai. A Class of Mixed Assumed Strain Methods and the Method of Incompatible Modes. *International Journal for Numerical Methods in Engineering*, **29**, 1595-1638, (1990).

[46] SS-EN-12600. Glass in building-Pendulum test-Impact test method and Classification for flat glass. Swedish Standards Institute, 2003.

[47] C.V.G. Vallabhan, J.E. Minor and S.R. Nagalla. Stresses in Layered Glass Units and Monolithic Glass Plates. *Journal of Structural Engineering*, **113**, 1, 36-43, (1987).

[48] C.V.G. Vallabhan, Y.C. Das, M. Magdi, M.Z. Aşik and J.R. Bailey. Analysis of Laminated Glass Units. *Journal of Structural Engineering*, **119**, 5, 1572-1585, (1993).

[49] A. Van Duser, A. Jagota and S.J. Bennison. Analysis of Glass/polyvinyl Butyral Laminates Subjected to Uniform Pressure. *Journal of Engineering Mechanics*, **125**, 4, 435-442, (1999).

[50] B. Weller and T. Schadow. Designing of Bonded Joints in Glass Structures. Proceedings of the 10th Glass Performance Days, Tampere, Finland, 2007.

Part 2: Appended papers

Paper 1

Computational Methods for Laminated Glass

Maria Fröling and Kent Persson

Abstract

An existing, recently developed, solid-shell finite element is proposed for the purpose of efficient and accurate modeling of laminated glass structures. The element is applied to one test example treating a thin laminated glass structure subjected to biaxial bending and the performance concerning accuracy and efficiency is compared to standard three dimensional solid elements. Further examples illustrate how the element could be applied in the modeling of laminated glass structures with bolted and adhesive joints. For these examples, experimental data for relevant quantities are provided as a comparison. It is concluded that the element is an excellent candidate for the modeling of laminated glass.

Full article available in: *Journal of Engineering Mechanics*, 139, 7, 780-790, (2013).

Paper 2

Designing Bolt Fixed Laminated Glass with Stress Concentration Factors

Maria Fröling and Kent Persson

Abstract

A general method for determining stress concentration factors for laminated glass balustrades with two plus two bolt fixings with variable positions is developed. It is demonstrated how the stress concentration factors can be presented graphically in design charts and representative charts are displayed for the case of a more specific bolt fixed balustrade type. In general, the use of simple formulas and the design charts allows the maximum principal stresses of the balustrade to be determined for any relevant combination of the variable geometry parameters involved.

Full article available in: *Structural Engineering International*, 23, 1, 55-60, (2013).

Paper 3

Shear-Capacity in Adhesive Glass Joints

Maria Fröling, Kent Persson and Oskar Larsson
Lund University, Sweden, maria.froling@construction.lth.se

The shear-capacity of adhesive glass-joints was investigated. Various stiff and soft adhesives were tested in a short-term load-case. The tests were conducted with small specimens in order to achieve a homogenous state of stress. The results of the tests were used in order to determine the material models of the adhesives. Finite element analysis of the test set-up was used for the determination of the material models. Large-scale tests were conducted to verify the material models from the tests of the small specimens. It could be concluded that with further validation, a combination of small-specimen tests and finite element simulations may allow for the determination of joint behavior for any joint size.

Keywords: Glass, Adhesive Joint, FEM, Shear-capacity

1. Introduction

Recently, there has been an increasing interest in using glass as a structural material. When constructing with glass, it is often necessary to connect different structural elements. The most common technique used for joining glass elements is to use bolted joints. The use of bolted joints leads to stress concentrations in the glass. Glass is a brittle material, which makes it sensitive to stress concentrations.

An alternative is to use adhesive joints to connect the glass elements. In general, adhesive joints are capable of distributing the stress over the surface of the joint so that stress concentrations are avoided. With many adhesives it is also possible to keep the transparency of the glass at the joint.

Adhesive joints are normally designed to be loaded in a state of shear rather than in a state of tension. This paper investigates the shear-capacity of a set of common adhesives in a short-term load-case. The adhesive products are chosen so that a wide span of different adhesive characteristics is obtained. The shear-capacity of the adhesives is tested in pure shear. From the experimental data, material models for the adhesives are determined. The material models are valid for a short-term load-case. The material models are determined through a finite element analysis of the complete test set-up. Later, the material models are verified through large-scale tests. Further information about the work could be found in [1].

2. Shear-Capacity Tests of Small Specimens

The main purpose of the tests was to determine the shear-capacity of various adhesives for connecting glass. For this reason, it is important that the tests create a situation as close as possible to a state of pure shear. In the tests, small specimens were used. Small specimens ensure a relatively homogenous state of stress and it is easier to ensure fracture in the adhesive and not in the glass. The shear-capacity was evaluated for a

short-term load, i.e. a load that was applied with a fairly high rate with the aim of causing failure in the adhesive. A constant shear strain rate at approximately 3 % per second was chosen for the tests.

2.1. Testing Equipment

To obtain a situation of pure shear in the adhesive, the test equipment was designed with the following characteristics. Firstly, all loads were applied centrically to avoid eccentricity that may cause tensile and compressive stresses to arise in the adhesive. Secondly, the adhesive had to be be able to freely expand/shrink in the direction perpendicular to the direction of the shear forces to avoid stresses caused by constraining the material strains.

A schematic drawing of the testing equipment is displayed in Figure 1. It consisted of two steel-parts that transmit the forces from the testing machine to the specimen. For stiff glues, the test equipment was loaded by compressing the steel-parts. For the softer adhesives the test equipment was loaded with tensile forces in order to allow the large deformations in the joints.

The specimens in the tests consisted of two pieces of glass with dimensions 20 × 20 mm^2 joined together with an adhesive layer. Two different specimens were used in the tests. Specimen 1 had an adhesive layer that fully covered the surface of the glass-parts and this specimen type was used for the softer adhesives. Specimen 2 had an adhesive layer of dimensions 5 × 20 mm^2. It was used to test the stiffer glues in order to reduce the applied force needed to conduct the test. The geometries of the two specimens are shown in Figure 2.

2.2. Measurements

A MTS testing machine was used to apply force to the steel-parts. Data regarding the applied force and displacements were collected every 0.5 s. In order to obtain the shear-capacity for the adhesives, $\tau_{avg,u}$, the ultimate shear force obtained from the measurements were divided by the initial surface area of the adhesive.

3. Tested Adhesives

The tested adhesives can be grouped into softer adhesives and stiffer adhesives. The softer adhesives contained four types of silicone based adhesives, three types of SMP (Silyl Modified Polymer) based adhesives and Bostik Multifog 2640. The stiff adhesives consisted of polyurethane adhesive, HBM Rapid Adhesive X 60, strong epoxy adhesive and UV-hardening glass-glue. Information about the adhesives above can be found in [2]-[5].

Test specimens had different thickness of the adhesive layer. For the silicone glues, the thickness was 6 mm, for the SMP based adhesives and Bostik Multifog 2640, the thickness was 2 and 0.3 mm. The polyurethane glue and HBM Rapid adhesive X 60 had

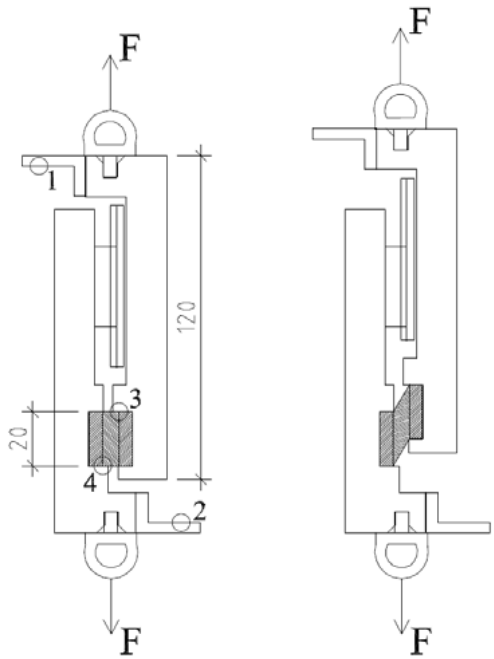

Figure 1: The test equipment used in the shear-capacity tests, tensile load.

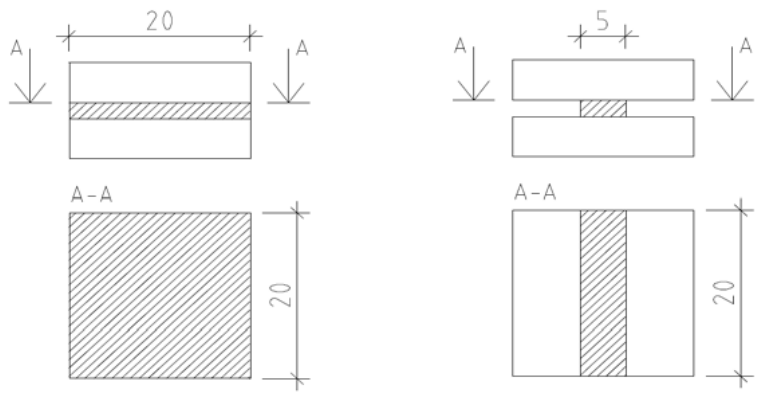

Figure 2: Drawing of the two different types of specimens.

an adhesive thickness of 0.2 mm, whereas the strong epoxy and the UV-hardening glue had 0.3 mm as thickness of the adhesive.

4. Finite Element Modeling of the Small-scale Tests

A finite element model of the entire test arrangement was developed, Figure 3, where the geometry of each of the joints was modeled. The steel-parts were modeled as linear elastic materials with the material parameters E = 210 GPa and ν = 0.3, where E denotes the modulus of elasticity and ν denotes the Poisson's ratio. Glass was modeled as linear elastic with the material parameters E = 70 GPa and ν = 0.23.

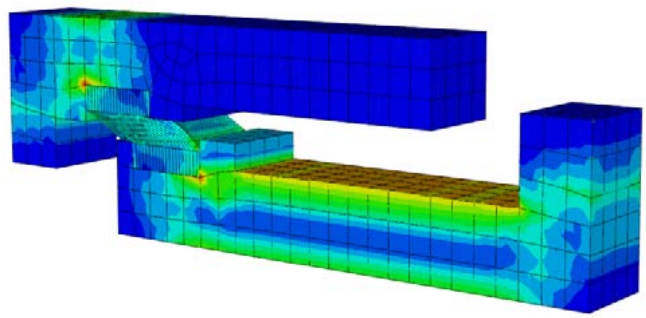

Figure 3: Finite element model of the test arrangement.

The evaluation of the results consisted of plotting the measured data of the shear-force versus the deformation of the test series. The data was fitted to a polynomial curve using the least-squares' method and compared with the data extracted from the finite element simulations. For each adhesive, different material models were tested until a satisfying agreement was obtained. For the softer adhesives, the hyperelastic material models Neo-Hooke and Mooney-Rivlin were tested whereas the stiffer adhesives were modeled as linear elastic, all with $\nu = 0.25$. From the respective matching material model, data on the shear-deformation were extracted and relationships between shear-stress and shear-strain were established.

An initial shear modulus, G, was calculated from the shear-stress versus shear-strain diagrams and an ultimate shear-stress, $\tau_{avg,u}$, was determined as the maximum value of the shear-stress for the increment closest to the average of the maximum load capacity of each adhesive.

5. Results from the Small-scale Tests

For brevity, results for one softer adhesive and one stiffer adhesive are presented. In Figure 4, experimental results and simulation results on force versus deformation for one SMP based adhesive is displayed (top). In the same figure, results from finite element simulations on average shear-stress versus shear-strain for the same adhesive are shown (bottom). The finite element results and the experimental curves coincide initially and overall the numerical and experimental results show close agreement. The material model for the adhesive was determined with good accuracy. The lower graph has a value of the maximum average shear-stress close to the experimentally obtained value of around 2.3 MPa.

In Figure 5, the corresponding graphs are shown for the polyurethane glue. There was a perfect agreement between simulations and measurements for this case. The experimental maximum value for the average shear-stress of the polyurethane adhesive was 3.8 MPa.

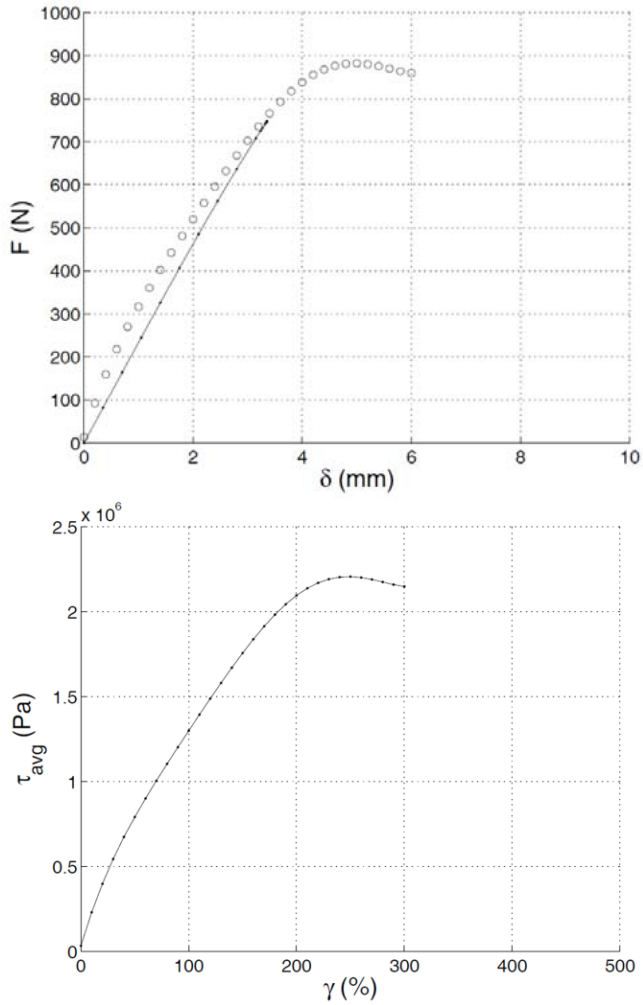

Figure 4: Results from the FE-evaluation of SMP based adhesive 3, 2 mm specimens. Top: experimental results (circles) and FE-results (line). Bottom: Average shear-stress versus shear-strain extracted from the FE-model.

As a summary of further results, diagrams showing average shear-stress versus shear-strain are displayed in Figures 6 and 7 for softer adhesives of a certain layer thickness and for stiffer adhesives respectively. From the graphs it is clear that there were differences in mechanical behavior between the adhesives within each group.

From Figure 6 it could be observed that Bostik Multifog 2640 was the softest adhesive and also had the lowest ultimate shear-strength of this group of adhesives. Among the three other adhesives of this group, Figure 6 shows that different adhesives could have similar stiffness but different ultimate strengths and vice versa.

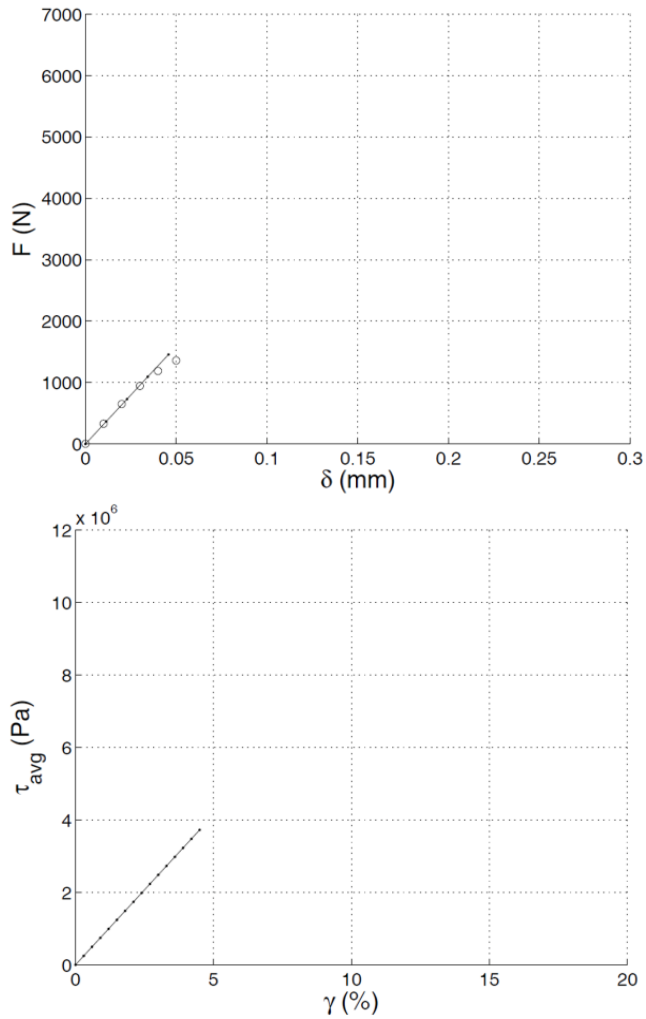

Figure 5: Results from the FE-evaluation of the polyurethane glue. Top: experimental results (circles) and FE-results (line). Bottom: average shear-stress versus shear-strain extracted from the FE-model.

From Figure 7, it could be seen that the epoxy adhesive was the stiffest adhesive and had the highest ultimate load. For the other stiff adhesives, the stiffness was quite equal but there were differences in ultimate shear-strength.

Results showing the mechanical characteristics of the two groups of adhesives (softer, 2 mm specimens and stiffer) are shown in Table 1. In general, the stiffer adhesives had greater stiffness (*G)* and ultimate shear-strength ($\tau_{avg,u}$) than the softer adhesives.

The parameters of the material models for the softer adhesives are shown in Table 2. C_{10}, C_{01} and D_1 are parameters of the material models. For the stiffer adhesives, the material model parameters are displayed in Table 3.

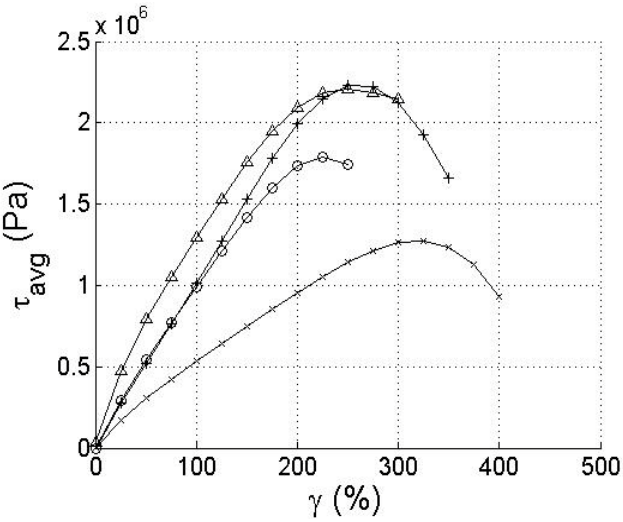

Figure 6: Shear-stress versus shear-strain for the 2 mm specimens of the softer adhesives. Bostik Multifog 2640: (x), SMP based adhesive 1: (+), 2: (o), 3: (triangle).

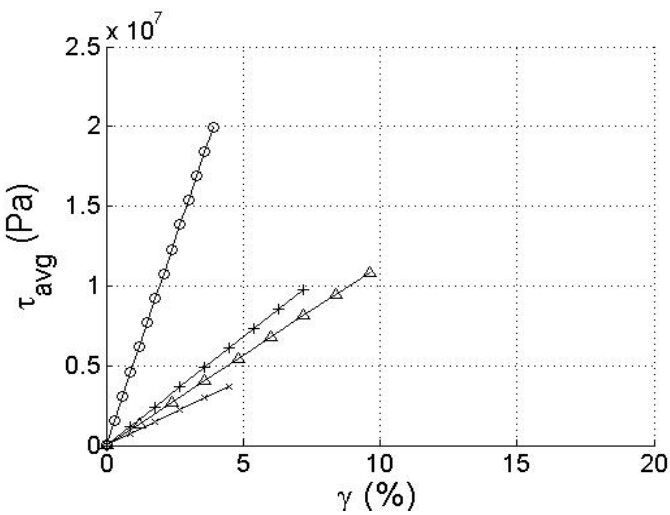

Figure 7: Shear-stress versus shear-strain for the stiffer adhesives, 0.2-0.3 mm specimens. Polyurethan glue: (x), HBM Rapid Adhesive X 60: (+), strong epoxy: (o), UV-hardening glass-glue: (triangle).

Table 1: Mechanical characteristics of adhesives.

Quantity	Softer Adhesives (2 mm Specimens)	Stiffer Adhesives
G [MPa]	0.5 - 1.2	83 - 500
$\tau_{avg,u}$ [MPa]	1.3 – 2.3	4 - 20
γ_u [%]	200 - 300	4 - 10

Table 2: Parameters of material models for softer adhesives.

Adhesive	Material Model	C_{10}	C_{01}	D_1
Silicone Based 1	Mooney-Rivlin	$51 \cdot 10^3$	$77 \cdot 10^3$	-
Silicone Based 2	Neo-Hooke	$93 \cdot 10^3$	-	-
Silicone Based 3	Neo-Hooke	$247 \cdot 10^3$	-	-
Silicone Based 4	Mooney-Rivlin	$10 \cdot 10^3$	$190 \cdot 10^3$	-
SMP Based 1	Mooney-Rivlin	$200 \cdot 10^3$	$330 \cdot 10^3$	-
SMP Based 2	Mooney-Rivlin	$100 \cdot 10^3$	$400 \cdot 10^3$	-
SMP Based 3	Mooney-Rivlin	$100 \cdot 10^3$	$500 \cdot 10^3$	-
Bostik Multifog 2640	Mooney-Rivlin	$100 \cdot 10^3$	$150 \cdot 10^3$	-

Table 3: Parameters of material models for stiffer adhesives.

Adhesive	Material Model	E [MPa]	v
Polyurethane Glue	Linear Elastic	200	0.25
HBM Rapid Adhesive X 60	Linear Elastic	320	0.25
Strong Epoxy	Linear Elastic	1500	0.25
UV-hardening Glue	Linear Elastic	300	0.25

6. Large-scale Testing

A large-scale experimental test was made with the aim of determining the shear-capacity of an adhesive joint in a large dimension glass beam.

Five adhesives from the small-scale tests were chosen to be tested in the large-scale tests. The five adhesives were chosen considering the results from the finite element simulations of the corresponding test set-up, see below. The two strongest SMP based adhesives and the stiffer adhesives polyurethane glue, UV-hardening glass-glue and the strong epoxy adhesive were chosen. When performing the tests, the deformation speed was kept constant at 10 mm/min.

6.1. Testing Equipment

The test performed was a four-point bending test of a beam that consisted of three beams made of flat-glass joined together by two adhesive joints. The test arrangement is shown in Figure 8 and creates a symmetrical beam in order to obtain pure shear-stresses in the joint. The beam had a span of three meters and every flat-glass element had dimensions 250×2000 mm and a width of 12 mm. The adhesive joints had dimensions 250×250 mm.

6.2. Measurements

Data on load and deformation of the mid-point of the beam were collected.

7. Finite Element Modeling of the Large-scale Tests

A finite element model was made of the large-scale test set-up. In the tests, the stiffer adhesives were simulated with a thickness of 0.2 mm and the softer adhesives with a thickness of 2 mm. The glass elements were modeled with a modulus of elasticity of 70

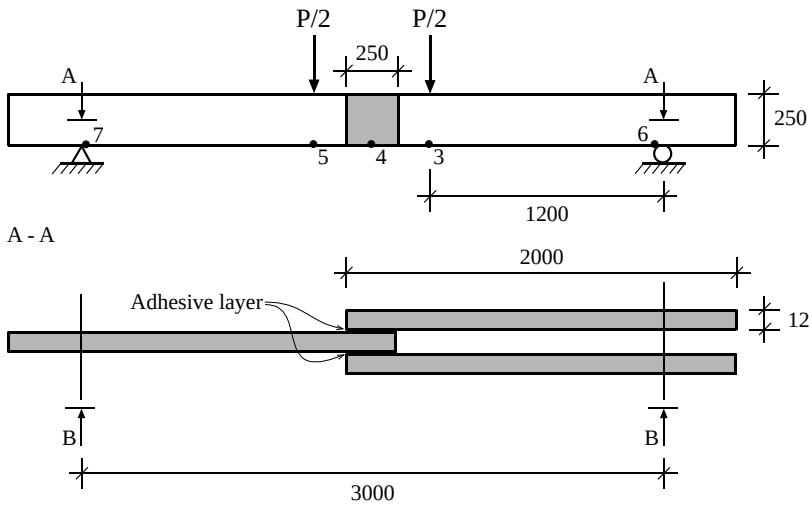

Figure 8: Test arrangement for large-scale tests.

GPa and a Poisson's ratio of 0.23. The adhesives were modeled according to the material models from the tests with the small specimens. Load-deformation graphs were determined for the tested adhesives, and maximum load values were determined and were set equal to the load that corresponded to the maximum shear-stress, τ_{max}, of each adhesive.

8. Results from the Large-scale Tests

Figure 9 displays the principal pattern of shear-stresses in the joints of the large-scale tests. In the stiffer adhesives stress-concentrations occurred at the corners of the joints. In the softer adhesives, the stresses were more evenly distributed.

In Figure 10, a graph showing load versus deformation for the third SMP based adhesive is shown. The measured data show a less stiff behavior than the data from the simulations. The measured data end at a lower load because of failure of the glass beam before the ultimate load was reached.

A load versus deformation diagram for the polyurethane adhesive is displayed in Figure 11. After an initial deviation, the stiffness of the measured data compares well with the stiffness of the results from the finite element simulations.

Table 4 summarizes the ultimate loads and deformations for a selection of the softer adhesives. The results are obtained from the finite element simulations. The corresponding results for the stiffer adhesives are shown in Table 5.

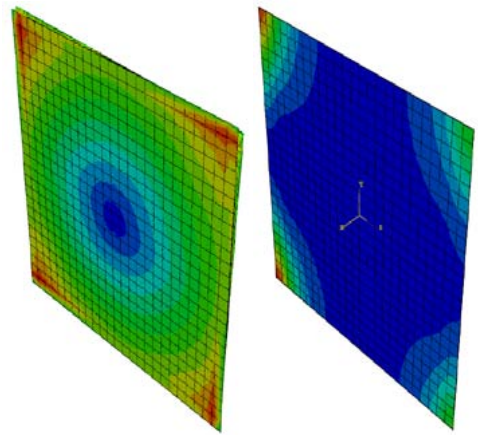

Figure 9: Principal pattern of the shear-stresses in the joints of the large-scale tests. Left: softer adhesives. Right: stiffer adhesives.

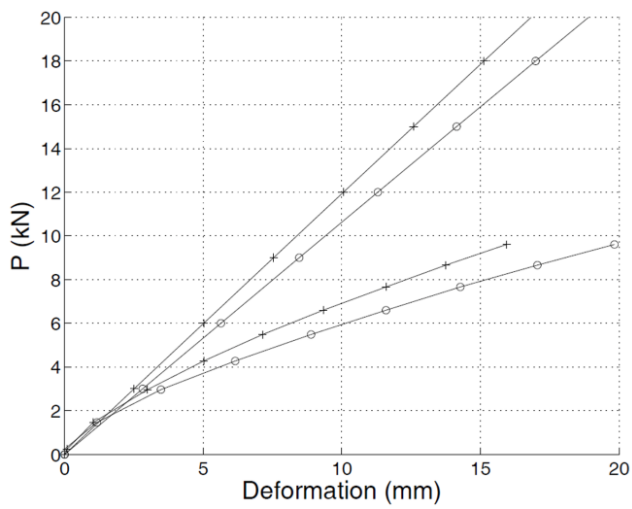

Figure 10: Comparison of load versus deformation diagrams for FE-simulations and experimental tests for the third SMP based adhesive. Top: FE-simulations. Bottom: experiments. The different points of measurements are marked: 4 (o), 5 (+). See Figure 8.

Table 4: Ultimate loads ($P = P/2 + P/2$) and deformations at the mid-point of the beam (4) for softer adhesives.

Adhesive	Ultimate Load [kN]	Ultimate Deformation [mm]
Bostik Multifog 2640	28.8	53
SMP Based Adhesive 1	49.3	51
SMP Based Adhesive 2	38.2	43
SMP Based Adhesive 3	48.8	50

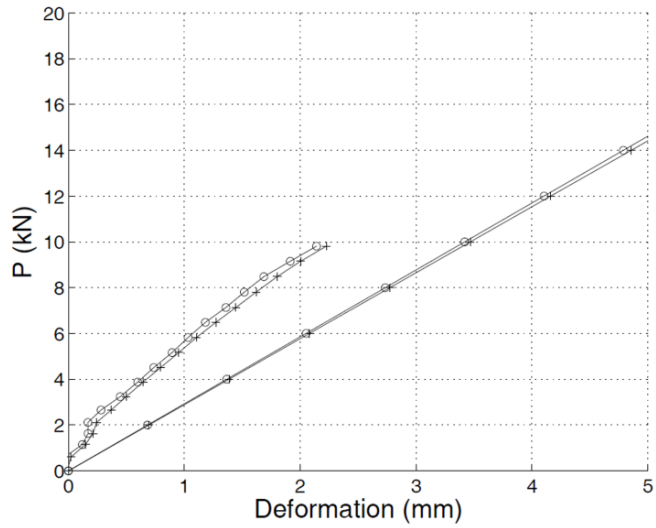

Figure 11: Comparison of load versus deformation diagrams for FE-simulations and experimental tests for the polyurethane adhesive. Top: experiments. Bottom: FE-simulations. The different points of measurements are marked: 4 (o), 5 (+). See Figure 8.

Table 5: Ultimate loads ($P = P/2 + P/2$) and deformations at the mid-point of the beam (4) for stiffer adhesives.

Adhesive	Ultimate Load [kN]	Ultimate Deformation [mm]
Strong Epoxy	30.3	10.0
Polyurethane Glue	10.3	3.5
UV-hardening Glue	22.3	7.5
HBM Rapid Adhesive X 60	20.3	7.0

Overall, the softer adhesives had ultimate loads ranging between 28 and 50 kN and the stiffer adhesives had ultimate loads in the interval 10-30 kN.

From the finite element simulations it was apparent that all the beams of the large-scale tests would suffer failure in the glass of the beam. Thus, no ultimate load of the joints could be measured by means of experimental testing. Comparing Figure 9 and the results of tables 4 and 5, the apparent stress concentrations of the stiffer adhesives reduced their ultimate load compared to the softer adhesives.

9. Conclusions

It can be concluded that the test method suggested for the small-scale tests is a functioning method for evaluating the shear-capacity of the adhesives. The method creates a state close to pure shear.

Material models valid for the short-term load-case could be determined with close accuracy between experiments and simulations for the group of stiffer adhesives. For the SMP based adhesives, the correlation between simulations and experiments is

shown to be good for the small-scale tests. For the large-scale tests, there are deviations between simulated and experimental results. An explanation of this deviation is that these adhesives were not fully hardened at the moment of the experiments. Further research is necessary to validate the material models for the SMP based adhesives for a large-scale joint.

In the small-scale tests stiffer adhesives give a stronger joint than softer adhesives. Thus, stiff adhesives may be used for small joints. From the large-scale tests it is concluded that for a large joint, a more soft adhesive may give the strongest joint.

With further validation, the methodology presented may be used to predict the mechanical behavior of any joint size through a combination of small specimen tests and finite element modeling.

10. Future Work

Further tests are conducted to investigate the shear-capacity of and to determine material models for a complementary set of adhesives. Initially, the tests are made for a short-term load-case. Later, the tests will be performed for a long-term load case and the creep parameters of the adhesives will be determined.

11. Acknowledgements

The support from The Swedish Research Council FORMAS, Glasbranschföreningen and Svensk Planglasförening is gratefully acknowledged.

12. References

[1] Larsson, Oskar, *Shear Capacity in Adhesive Glass-Joints*, Master's Thesis, Division of Structural Mechanics at Lund University of Technology, Sweden, 2008.

[2] *Product sheets of different Casco adhesives*, Akzo Nobel Bygglim AB, Casco, Stockholm, Sweden, www.casco.se

[3] *Product sheets of X 60 adhesive*, Hottinger Baldwin Messtechnik, Darmstadt, Germany, www.hbm.com

[4] *Product sheets of different Bostik adhesives*, Bostik AB, Helsingborg, Sweden, www.bostik.se

[5] www.sika.com

Paper 4

A Reduced Model for the Design of Glass Structures Subjected to Dynamic Impulse Load

Maria Fröling, Kent Persson and Per-Erik Austrell

Abstract

A reduced finite element model for determining the maximum principal stress of a glass pane subjected to dynamic impact load is developed and compared to a full dynamic finite element model. The reduced model is based on the Rayleigh-Ritz method. The Ritz vectors used are determined by simple static load-cases. The model is applicable to centrally and excentrically applied impact and to glass of various support conditions. It is demonstrated that the model performs well for various types of supported glass panes and impact applied at different locations on the glass pane. The applicability to small or medium sized glass panes is shown through a parametric investigation. For large glass panes, especially at smaller glass thicknesses, it is suggested that geometrically nonlinear behavior of the glass pane is integrated into the model to reduce the model error. Finally, it is shown that the reduced model performs excellently in the modeling of a standard laminated glass balustrade with clamp fixings. Apparently, the model is very well suited for strength design of commonly used glass structures.

1 Introduction

When performing strength design of glass structures, dynamic impact load is one of the load cases that often need to be included in the analysis. Since glass is a brittle material, it is sensitive to impact load and it is necessary to accurately determine the stress distribution in the glass due to this load case. Most often strength design of glass structures subjected to dynamic impact load is performed by means of experimental tests. The European standard EN-12600, [26], is available to classify glass for impact strength. Other authors, ([25], [11]), have confirmed that this test yields reproducible results and that the test is easy to perform. However, when performing strength design of glass structures, the properties of the structure may be different from those prescribed in the standard. It is possible to apply the impact load according to the standard to a glass structure. In [19] several experimental tests of glass panes of various sizes and support conditions subjected to dynamic impact load are performed and data for calibration and development of analytical and numerical models are extracted. The process of experimental testing is, however, time consuming when considering parameter variation in strength design.

An alternative to experimental tests is to use finite element simulations. Several authors have demonstrated the applicability of full transient finite element simulations in order to

simulate the application of impact load to glass structures, ([21], [22], [20], [23], [24], [27]). However, finite element modeling of transient impact load is advanced, time consuming and may require access to advanced commercial finite element programs.

In the design process it is important that the design tools used are such that alternative designs may be tested in an interactive fashion. This put on a demand that the methods applied are very time-efficient.

To make the model more computationally efficient the size of the finite element model can be reduced by means of model reduction techniques. Several methods that are variants of the Rayleigh-Ritz procedure, [4], are available. The methods can be subdivided into the following main categories, [9],: generalised coordinate methods, condensation methods and component mode synthesis. When generalised coordinates are introduced, the system is described using only a few deflection shapes of the original system where for example eigenvectors, [4], Lanczos vectors, [6], and Ritz vectors, [2], may be utilized. Condensation methods involves removing the degrees of freedom that are not necessary in order to describe the dynamic behavior of the system. This can be accomplished using for example static (Guyan) condensation, [14], or dynamic condensation, see for instance [15]. In component mode synthesis, [8], the domain of the problem is divided into subdomains and each subdomain is described by a different set of basis vectors.

Reduced modeling of glass subjected to dynamic impact load was addressed in ([22], [23], [24], [27]). In [22], a two-degree-of-freedom model, [7], was developed and compared to numerical and experimental results. The applicability of the model is limited to four-sided and two-sided supported glass panes. In the above categorization of reduction methods, the method is using generalized coordinates using Ritz vectors for representation of the glass pane. One Ritz vector was used in the modeling of the glass, i.e. the static deformation mode. It was noted that when the glass panes have larger width than two meters, the use of the static deformation mode of the glass yields an unrealistic representation of the dynamic behavior of the glass.

The contributions in [23] and [24] develop different formats of the reduced model of [22]. In [23] it was pointed out that the method presented is only applicable to a limited geometric range.

Comparison was made between the simplified approach of [24], a full transient finite element model and experiments, [27]. For two values of the fall height, and a fixed sized glass plate, the simplified approach yielded satisfying results. The verification was made with a panel width less than two meters.

In this work, a reduced finite element model for strength design of glass structures subjected to dynamic impact load is developed. The Rayleigh-Ritz procedure using generalized coordinates and Ritz vectors is used for modeling the glass pane. Comparing the use of Ritz vectors to the use of for instance eigenvectors, there is the possibility to construct

the Ritz vectors to account for the physical behavior of the system such as the position of the load. Thus, fewer vectors may be used for an accurate representation of the system. The model is similar to the model of for instance [22], but this model includes an additional Ritz vector in the representation of the glass pane, which means that the model error is reduced especially for off-center loading. The second Ritz vector is constructed through considering knowledge about the physical behavior of the system and the resulting vector is a key feature of the present model. The developed model is intended for integration into a glass design computer program, [17], which allows fast and accurate strength design of glass structures. The entire procedure is finite element based and in the resulting program the user only has to give input data. The procedure is valid for different fall heights of the impactor, various support conditions and locations of the impact. Initially, the accuracy of the model reduction technique is demonstrated for the case of centrally applied impact and four-sided supported glass. Later, it is demonstrated that the model is applicable to excentrically applied load cases. A final example illustrates the applicability of the model to a standard laminated glass balustrade with clamp fixings. It is a subject for future work to evaluate the model performance for the types of support conditions not covered in this study and to make further experimental verification.

2 A Pendulum Impact Test for Classifying Glass for Impact Strength

The experimental test method used for classifying glass for impact strength, [26], is shown in Figure 1 (a). The arrangement consists of a glass pane held within a steel frame and an impactor consisting of a weight encased in two tires. Between the steel frame and the glass there are rubber strips. During the test, the tire is swung in a pendulum motion into the glass pane. The dimensions of the frame are standardized to 1.95×0.887 m^2 and the weight of the impactor is 50 kg according to the standard. The test is considered as a soft impact with a long pulse time, Figure 1 (b).

3 A Reduced Model for Glass Panes Subjected to Dynamic Impact Loads

In the reduced dynamic modeling of the glass pane, including the supports, the Rayleigh-Ritz method, [7], was adopted. Consequently, the displacements, $\mathbf{u}(t)$, were expressed as a linear combination of shape (Ritz) vectors ψ_j:

$$\mathbf{u}(t) = \sum_{j=1}^{J} z_j(t)\psi_j = \Psi \mathbf{z}(t), \tag{1}$$

where $z_j(t)$ are the generalized coordinates.

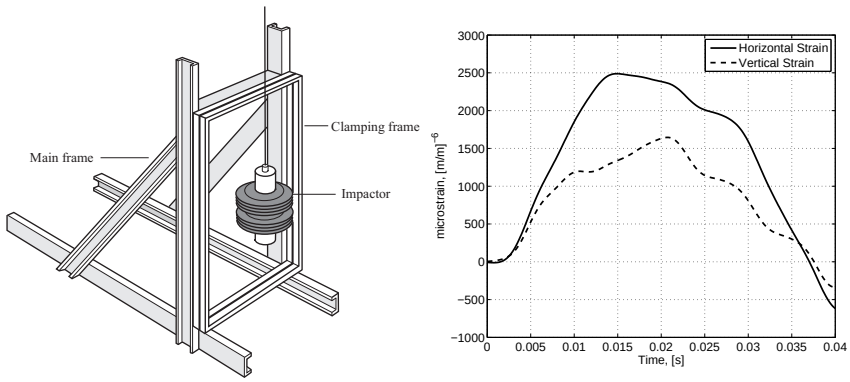

Figure 1: Test arrangement for pendulum impact test (a) and example of result (b).

The glass pane together with the supports can be represented as a multi-degree-of-freedom system with one degree of freedom for each Ritz vector. The equations of motion for an undamped multi-degree-of-freedom system in free vibration are given as, [7],

$$\mathbf{m}\ddot{\mathbf{u}} + \mathbf{k}\mathbf{u} = \mathbf{0}, \tag{2}$$

where $\mathbf{m}$ is the mass matrix and $\mathbf{k}$ is the stiffness matrix. Substituting (1) into (2) yields

$$\mathbf{m}\Psi\ddot{\mathbf{z}} + \mathbf{k}\Psi\mathbf{z} = \mathbf{0}. \tag{3}$$

Premultiplying each term in (4) by Ψ^T yields

$$\tilde{\mathbf{m}}\ddot{\mathbf{z}} + \tilde{\mathbf{k}}\mathbf{z} = \mathbf{0}, \tag{4}$$

where $\tilde{\mathbf{m}} = \Psi^T\mathbf{m}\Psi$ and $\tilde{\mathbf{k}} = \Psi^T\mathbf{k}\Psi$. $\tilde{\mathbf{m}}$ and $\tilde{\mathbf{k}}$ are the generalized mass and stiffness matrices.

The impactor is suggested to be represented by a single-degree-of-freedom system, [7],

$$\mathbf{m}_i = \begin{bmatrix} m_i & 0 \\ 0 & 0 \end{bmatrix}, \tag{5}$$

$$\mathbf{k}_i = \begin{bmatrix} k_i & -k_i \\ -k_i & k_i \end{bmatrix}, \tag{6}$$

and the corresponding degree of freedom u_i, where m_i and k_i are the mass and stiffness of the impactor.

The out-of-plane degree of freedom of the full finite element model at the point of impact of the glass pane was chosen as the reference degree of freedom, u_{ref}, to which the impactor was connected. However, the impactor was connected to the reduced model of

the glass and not to the full model in order to create the complete reduced system. This is not trivial since the generalized coordinates, $[z_1,...,z_J]^T$, do generally not represent physical degrees of freedom of the glass. To correctly represent the complete system, it was suggested that the degree of freedom u_i of the impactor is tied to the first generalized coordinate, z_1, which corresponds to the point of impact. The system representing the impactor can be assembled into the system representing the glass to form the total system. The system variables are $\bar{\mathbf{z}} = [u_i, z_1, ..., z_J]^T$.

When connecting the impactor to the reduced model of the glass, $u_{ref} = z_1$ must be fulfilled. This means that the corresponding displacement vector, ψ_1, must be normalized so that the absolute value of the out-of-plane displacement is equal to one at u_{ref} and that any other Ritz vector, ψ_j , must fulfill the condition that $u_{ref} = 0$. This can be realized from equation (1).

When selecting the Ritz vectors several procedures are available, see [7]. In principle any of the methods for model reduction can be used given that the conditions above are fulfilled. For the design cases considered, the first Ritz vectors of the glass can easily be visualized and this information was used when suggesting a novel procedure for choosing the Ritz vectors of the glass. The method is general in the sense that the location of u_{ref} can be chosen arbitrarily in order to represent excentric impact. For simplicity, the description of the method is made for central impact. A further advantage of the method is the option to freely choose the deformed shapes of the Ritz vectors based on physical intuition. This might decrease the necessary amount of Ritz vectors to obtain a decently accurate representation of the glass.

In this work, two Ritz-vectors were selected to represent the glass structure. Combining equations (5)-(6) and making sure that the impactor is connected to z_1 in the assembling, the following multi-degree-of-freedom system is obtained

$$\begin{bmatrix} m_i & 0 & 0 \\ 0 & \tilde{m}_{11} & \tilde{m}_{12} \\ 0 & \tilde{m}_{21} & \tilde{m}_{22} \end{bmatrix} \begin{bmatrix} \ddot{u}_i \\ \ddot{z}_1 \\ \ddot{z}_2 \end{bmatrix} + \begin{bmatrix} k_i & -k_i & 0 \\ -k_i & k_i + \tilde{k}_{11} & -\tilde{k}_{12} \\ 0 & -\tilde{k}_{21} & \tilde{k}_{22} \end{bmatrix} \begin{bmatrix} u_i \\ z_1 \\ z_2 \end{bmatrix} = \begin{bmatrix} 0 \\ 0 \\ 0 \end{bmatrix}. \qquad (7)$$

For the case of central impact, the first Ritz vector corresponds to the static deformation mode of the glass. The deformed shape was constructed through applying a uniformly distributed load corresponding to the weight of the glass, Q_g, to the entire glass pane area. Variations of construction of this mode are shown in Figure 2.

The load Q_g can be applied either to the entire glass pane area, or to the contact surface, A, between the glass and the impactor. The method shown in figure 2 c) is a combination of these cases.

The second Ritz vector was constructed by means of applying a distributed force on the entire surface of the glass corresponding to the glass weight on one side of the pane and

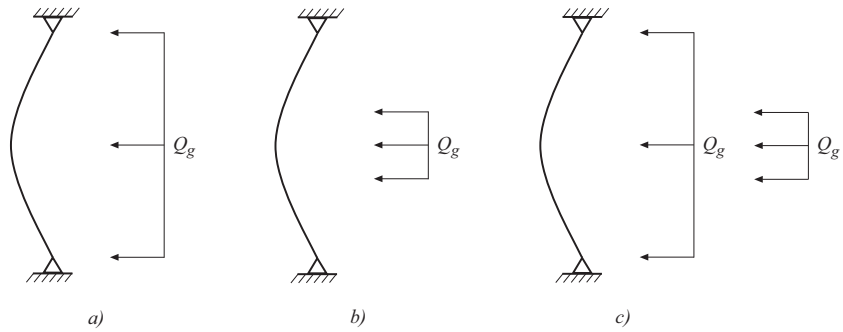

Figure 2: Methods of construction for Ritz vector 1.

simultaneously a uniformly distributed load corresponding to the weight of the impactor, Q_i, was applied at the contact surface between the impactor and the glass but in the opposite direction. A schematic sketch of the construction of the Ritz vectors is shown in Figure 3 for the case of centrally applied impact.

The two Ritz vectors are determined by solving a static finite element model for two load cases. When adding additional Ritz vectors there is a trade-off between increasing the accuracy and decreasing the computational efficiency.

A simple contact condition is assumed where the solution is valid only until the contact force between the glass and the impactor change signs. When the contact force becomes negative, the impactor is disassembled from the model.

The system is solved using the Newmark procedure, ([4], [7]), as implemented in [3] by means of Matlab. Initial values for $\bar{\mathbf{z}}$ and $\dot{\bar{\mathbf{z}}}$ are required.

Once $\mathbf{u}(t)$ has been determined, the stresses, $\boldsymbol{\sigma}(t)$, of the glass can be evaluated as, [12],

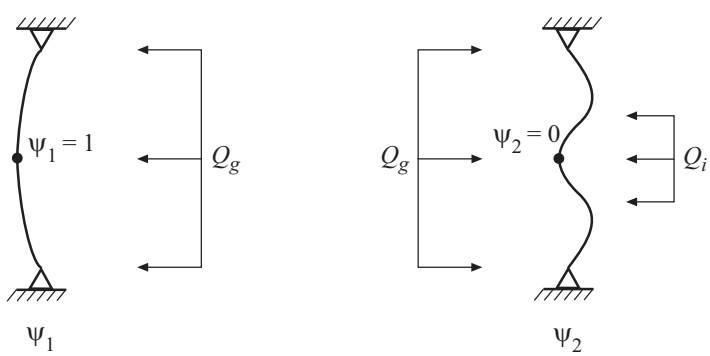

Figure 3: Construction of Ritz vectors.

$$\sigma(t) = \mathbf{D}\tilde{\varepsilon}(t) = \mathbf{D} \cdot [\hat{\mathbf{B}}_{\mathbf{u}} \hat{\mathbf{B}}_{\alpha}] \begin{bmatrix} \mathbf{u}(t) \\ \alpha \end{bmatrix}. \tag{8}$$

$\mathbf{D}$ is the constitutive matrix, $\hat{\mathbf{B}}_{\mathbf{u}}$ is the standard finite element method strain-displacement matrix, $\hat{\mathbf{B}}_{\alpha}$ is the enhanced strain-displacement matrix and α is the enhanced strain field.

The maximum principal stress, $\sigma_{max}(t)$, is the quantity normally used in strength design of glass and the goal is to obtain a decent result in terms of the maximum of this variable, σ_{max}.

4 Model Validation

The model was validated using a baseline test example corresponding to the standard SS-EN-12600, [26], and to the example described in [20]. In [20], the case of centrally applied impact of four-sided supported glass is analysed using a full dynamic finite element model that is validated by experiments. Consequently, a full finite element model of a four-sided supported monolithic glass pane was made in Matlab and the in-plane geometry of the glass is displayed in Figure 4. The area A is the contact area between the impactor and the glass. The steel frame was not modeled but the corresponding degrees of freedom of the rubber strips were fixed in all directions. The rubber was modeled by means of a spring model, see [18].

The glass was modeled by means of a solid-shell element, ([5], [1]), which has proven accurate and efficient for modeling of glass and laminated glass, [12]. The solid-shell element has quadrilateral in-plane geometry and therefore a quadrilateral mesh generator was employed. In the finite element analysis, the mesh generator and the finite element

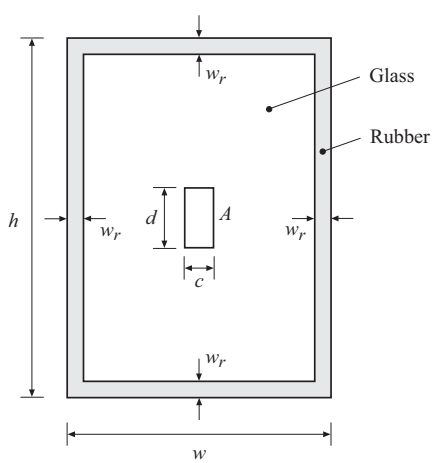

Figure 4: Two-dimensional geometry of glass pane.

program Calfem of Austrell et al. (2004), [3], and Lorentzon (2010), [16], were used together with Matlab.

Isotropic linear elastic material properties were assumed for both glass and rubber. The material parameters that are required are the modulus of elasticity, E, the Poisson's ratio, ν, and the mass density, ρ. The values of these parameters were adopted from [20]. The parameter values are displayed in Table 1.

The choice of the geometry parameters shown in Figure 4 is presented in Table 2. The out-of-plane thickness for the glass, t_g, and rubber, t_r, were both chosen to be 10 mm. The initial values of $\bar{\mathbf{z}}$ were zeroes and the initial velocity of the impactor was -2.97 m/s corresponding to a fall height of 450 mm. 450 mm is the maximum fall height used in strength design of structures subjected to dynamic impulse load in Sweden, according to a relation derived in for instance [22]. The impactor stiffness, k_i, was determined by means of the finite element program ABAQUS/CAE through a static compression of the impactor onto a rigid surface and extraction of a load displacement relation for the impactor. This relation is nonlinear, but a linear approximation of the relation gives a constant value of the stiffness. The dimensions of the contact area, A, have been determined from the model of [20] at the moment of maximum lateral displacement of the glass. A summary of the model scalar parameters is given in Table 2.

For this case of central impact, it has been investigated that the method of construction of the first Ritz vector does not impact the results. Therefore, for the cases of central impact in this work, method a) of Figure 2 is chosen. For the cases of excentric impact, method b) is chosen because there is a small shift of location of the peak value of deformation which can be better represented by method b).

As a first version of the model only geometrically linear analysis was considered. The finite element model of the glass contained a total of about 56000 degrees of freedom. This was determined from a convergence study. Standard parameter values were used for the Newmark procedure, [4]. The size of the time step used in the Newmark procedure was determined by means of a convergence analysis and set to 0.625 ms.

Table 1: Material parameters for the finite element model.

Material	E [MPa]	ν	ρ [kg/m^3]
Glass	78000	0.2	2700
Rubber	15	0.44	1250

Table 2: Model parameters for baseline case.

h [m]	w [m]	d [m]	c [m]	w_r [m]	t_g [m]	m_i [kg]	k_i [kN/m]	t_r [m]
1.95	0.887	0.2	0.18	0.02	0.01	50	400	0.01

For evaluation, the midpoint lateral displacement, $u_{ref}(t)$, and the maximum principal stress, $\sigma_{max}(t)$, of the glass were calculated. The same quantities were determined by using the current reduced model with only the first Ritz vector, and through the model of [20] using geometrically linear and nonlinear formulations. The simulation results are presented in Figures 5 and 6.

From Figures 5 and 6 a number of observations can be made. First of all, the effect of geometric nonlinearity is more or less negligible in this case concerning the stresses. The model based on only Ritz vector 1 is underestimating the stress by around 50 % and does not seem to be trustworthy in strength design. The reduced model based on two Ritz vectors is underestimating the stresses by around 10 % in case of the geometric linear model and by around 7 % in case of the geometric nonlinear model. The current model error of between 7 and 10 % in terms of stresses is likely to give accuracy enough in strength design of glass so that a safe design is ensured and providing optimized material use.

5 Model Validity for Excentrically Applied Load

In this section, the model developed in this paper is validated for excentrically applied load cases. The test cases are extensions of the baseline case of section 4, but three dif-

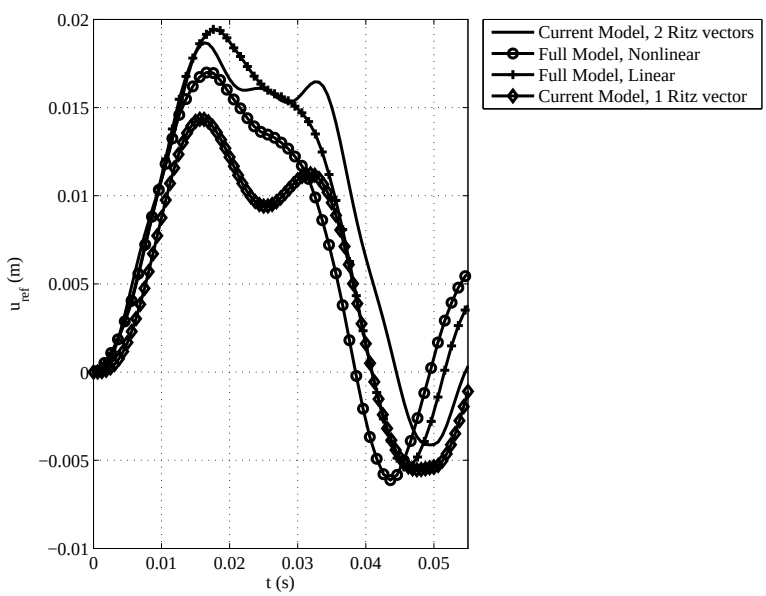

Figure 5: Lateral displacement of the midpoint of the glass versus time for the baseline case.

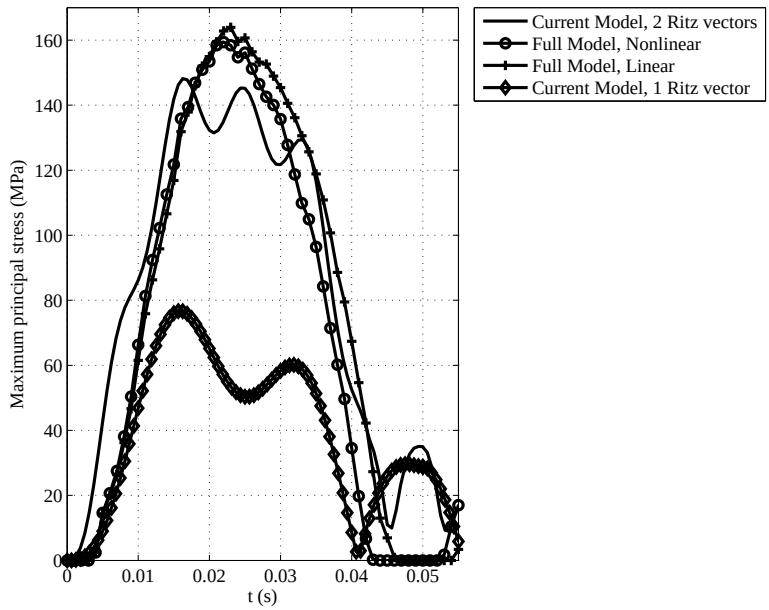

Figure 6: Maximum principal stress at the center of the glass pane versus time for the baseline case.

ferent load cases are considered. The load cases are illustrated in Figure 7.

The load cases are numbered 1 to 3. The horizontal and vertical distances between the midpoint of the glass and the midpoints of the areas A are given in the figure. All other model features were as for the baseline case. The same load cases were modeled in ABAQUS using the model in [20]. The ratio between σ_{max} obtained using the reduced model and $\sigma_{max,nonlinear}$ obtained using the full FE-model are presented in Table 3.

For all three load cases, σ_{max} was greater than for the corresponding quantity obtained using ABAQUS. That means that the results are on the safe side in glass design. The greatest error was around 10 % and was obtained for load case 1. A 10 % error on the safe side is considered acceptable. For load case 3, the results were identical to the ones obtained using ABAQUS. Conclusively, the reduced model is well capable of modeling

Table 3: Maximum principal stress for excentric load cases.

Load case	$\sigma_{max}/\sigma_{max,nonlinear}$
1	1.10
2	1.03
3	1.00

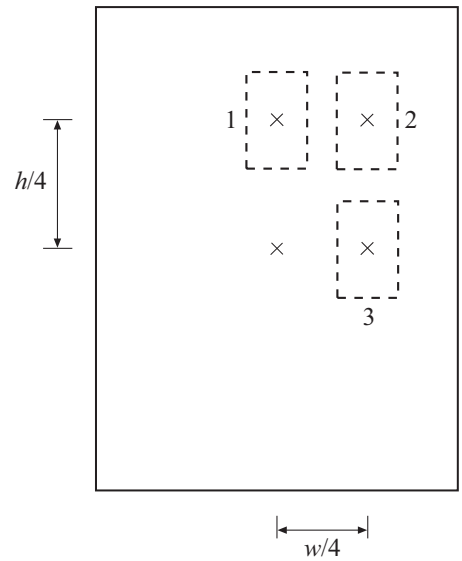

Figure 7: Load positions for excentric load cases.

excentric load, at least for the positions considered in this section.

6 Model Validity for Various Glass Pane Dimensions

In, for instance, [20] an observation was made that a different behavior of the full dynamic finite element solution was obtained when the in-plane glass pane dimensions increase. Firstly, the deformed shapes of the glass are more complicated when the pane is larger and secondly, it is well known that the influence of the geometric nonlinearity increases as the in-plane glass size increases. As an illustration, the baseline case with in-plane glass pane dimensions 2×2 m^2 was analysed. The model results in terms of σ_{max} were compared to those from the model of [20] for geometric linear and nonlinear analyses, as well as to those of the current model by only considering ψ_1. The results are presented in Table 4.

The model based on only ψ_1 is apparently not valid. The model based on two Ritz vectors is performing excellent compared to the full geometrically linear model and has an error slightly under 20 % compared to the full geometrically nonlinear model. The stress is

Table 4: Maximum principal stress for larger glass pane.

	Only Ritz vector 1	Current model
$\sigma_{max}/\sigma_{max,linear}$	0.42	0.95
$\sigma_{max}/\sigma_{max,nonlinear}$	0.52	1.18

greater for the current model compared to the full model which means that the current model results are on the safe side from a strength design perspective. Since the glass dimensions are rather large, the geometric nonlinear effect is significant for this case. The reduced model replicates very well its full linear counterpart, which implies that the use of two Ritz vectors is sufficient.

In order to test the model validity for different glass pane dimensions, the combinations of the parameters $t_g = [6, 8, 10, 12]$ mm and $h \times w = [1 \times 1, 1.25 \times 1.25, 1.5 \times 1.5, 1.75 \times 1.75, 2 \times 2]$ m^2 were investigated. The analyses focused on the difference in the value of σ_{max} between the model used in [20] and the model presented in this paper. The solution of the current model was considered acceptable when the relative error was less than 15 % for results that were not on the safe side and less than 20 % for results that were on the safe side. The fall heights 200, 300 and 450 mm were considered. Table 5 presents the parameter combinations and indicates at which maximum fall height the model is valid for respective case. In general there is a tendency that for a small glass thickness combined with a large glass pane size a lower maximum fall height is allowed. For the glass with the smallest thickness, the maximum possible fall height never exceeds 300 mm. The error bounds chosen will affect the results and Table 5 more generally illustrates the limitations that various glass pane dimensions put on the suggested method.

7 Application to a Clamp Fixed Glass Balustrade

To demonstrate the applicability of the suggested method in strength design the method was applied to a real glass structure. The test example consisted of a laminated glass balustrade with four clamp fixings. A laminated glass with two glass panes and an intermediate polyvinylbutyral (PVB) layer was considered. The two-dimensional geometry of the balustrade is shown in Figure 8. The dimensions of the contact area A was the same as for the baseline case. The in-plane dimensions were $h = w = 1.2$ m. All the other dimensions of the balustrade have been chosen considering a real glass balustrade of standard type. The distance e was set to 0.24 m, the clamp fixings were quadratic with a side length, f, of 0.025 m, the glass thickness, t_g, was set to 6 mm and the PVB layer thickness, t_{PVB}, was equal to 0.76 mm. The clamp fixings consisted of rubber parts and

Table 5: Maximum fall height for which the linear model is valid for different parameter combinations.

t_g [mm] $h \times w$ [m^2]	6	8	10	12
1×1	200 mm	450 mm	450 mm	450 mm
1.25×1.25	200 mm	450 mm	450 mm	450 mm
1.5×1.5	300 mm	450 mm	450 mm	450 mm
1.75×1.75	200 mm	450 mm	450 mm	450 mm
2×2	-	-	450 mm	450 mm

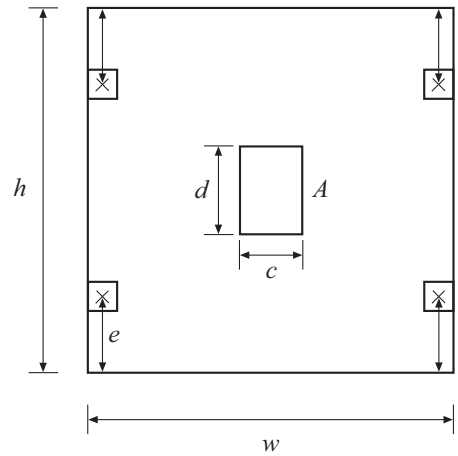

Figure 8: Two-dimensional geometry of glass balustrade.

steel parts. Only the rubber parts were modeled and the thickness of the rubber, t_r, was set to 3 mm. The modeling of the rubber was made as in the case of the rubber frame of the baseline case. The degrees of freedom on the side of a rubber part that is not in contact with the glass were set to be fixed.

Alla materials were assumed to be linear elastic and the material parameters for glass and rubber are given in Table 1. For PVB, the modulus of elasticity was set to 6 MPa that may be valid for a high strain-rate load case as an impact. The Poisson's ratio was set to 0.43 as in [13]. The mass density of PVB was 1.1 kg/m^3, [10].

In the full finite element model, as a special feature of the solid-shell element ([5], [1]), only one element layer per material layer was required. Altogether, around 30000 degrees of freedom were used.

Further modeling features were as in the baseline case above.

A comparison between the reduced model and the full FE-model in terms of σ_{max} resulted in a model error of only around 3.5 %.

8 Conclusions and Future Work

In this paper, a reduced finite element model for determining the maximum principal stress of a glass pane subjected to dynamic impact load is developed. The aim is to integrate the model into a glass design program for easy, fast and accurate strength design of glass structures. In the model development, a method for constructing Ritz vectors for use

in the Rayleigh-Ritz method is suggested and the resulting combination of Ritz vectors is unique and the choice of the second Ritz vector is a novelty. The method is also flexible in that it is applicable to different support conditions as well as to both centrally and excentrally applied impact. The model is made so that the support conditions are directly included.

The model performance is evaluated for four-sided supported glass panes with centrally applied impact and monolithic glass. It is proven that the model performs well for a baseline test case compared to a full geometrically nonlinear finite element model. It is shown how the model performance is improved when two Ritz vectors are used instead of one in modal reduction.

When in-plane glass dimensions increase and the glass pane thickness decreases, geometrically nonlinear behavior of the glass is having a larger impact on the result. Comparisons to both nonlinear and linear full finite element model results indicate that the modal reduction method is valid, but that the geometric nonlinearity of the glass gives rise to a relatively large error between the reduced model and the full nonlinear model. A parametric study with respect to pane dimensions investigates the limitations of the use of the reduced model. It is recommended that the reduced model is not used for larger glass panes than considered in this study and that lower fall heights are used for thin glasses than for thicker glasses.

The applicability of the model to glass structures with excentric load positions is demonstrated.

It is shown that the reduced model is very well suited for strength design of standard laminated glass balustrades with clamped fixings, even without compensating for the geometric nonlinearity effect. Most likely, the structures used in strength design are of dimensions and support conditions such that the reduced model is well applicable.

It is a subject for future work to include the effect of the geometric nonlinearity of the glass pane into the current model. For instance, [1] provides an extension to nonlinear behavior for the finite element formulation used. Another possible extension is to add additional Ritz vectors for representing the glass pane. The constant value of the impactor stiffness is a simplification. For further improvement of the results of the reduced model, a nonlinear representation of the impactor stiffness could be included.

In future development, it could be evaluated by means of test examples how well the reduced model represents the application to glass with other support conditions, for instance bolt fixed glass. As was shown for the case of glass with clamped fixings, it is expected that the effect of nonlinear behavior of the glass would be smaller for these other support conditions and for these cases our model may be directly applicable for all pane sizes without including the effect of nonlinear geometry.

Finally, it could be interesting to make an experimental investigation of glass structures subjected to dynamic impact load. For this investigation, different types of supports, different positions of the impact and both single layered and laminated glasses could be used.

References

[1] R.J. Alves de Sousa, R.P.R. Cardoso, R.A. Fontes Valente, J.-W. Yoon, J.J. Grácio and R.M. Natal Jorge. A New One-point Quadrature Enhanced Assumed Strain (EAS) Solid-shell Element with Multiple Integration Points Along Thickness-Part II: Nonlinear Applications. International Journal for Numerical Methods in Engineering, 67, 160-188, (2006).

[2] R.R. Arnold, R.L. Citerley, M. Chargin and D. Galant. Application of Ritz Vectors for Dynamic Analysis of Large Structures. Computers and Structures, 21, 3, 461-467, (1985).

[3] P.E. Austrell, O. Dahlblom, J. Lindemann, A. Olsson, K.G. Olsson, K. Persson, H. Petersson, M. Ristinmaa, G. Sandberg and P.A. Wernberg. CALFEM-A Finite Element Toolbox, Version 3.4. KFS, Lund, Sweden, 2004.

[4] K.-J. Bathe. Finite Element Procedures. Prentice Hall, Upper Saddle River, NJ, 2006.

[5] R.P.R. Cardoso, J.W. Yoon, M. Mahardika, S. Choudhry, R.J. Alves de Sousa and R.A. Fontes Valente. Enhanced Assumed Strain (EAS) and Assumed Natural Strain (ANS) Methods for One-point Quadrature Solid-shell Elements. International Journal for Numerical Methods in Engineering, 75, 156-187, (2008).

[6] H.C. Chen and L. Taylor. Solution of Eigenproblems for Damped Structural Systems by the Lanczos Algorithm. Computers and Structures, 30, 1/2, 151-161, (1988).

[7] A.K. Chopra. Dynamics of Structures-Theory and Applications to Earthquake Engineering. Pearson Prentice Hall, Upper Saddle River, NJ, 2007.

[8] R.R. Craig. Structural Dynamics; An Introduction to Computer Methods. John Wiley & Sons Inc., New York, NY, 1981.

[9] P. Davidsson. Structure-acoustic Analysis; Finite Element Modelling and Reduction Methods. Doctoral thesis, Lund University of Technology, Lund, Sweden, 2004.

[10] L.R. Dharani, F. Ji, R.A. Behr, J.E. Minor and P.A. Kremer. Breakage Prediction of Laminated Glass using the "Sacrificial Ply" Design Concept. Journal of Architectural Engineering, 10, 4, 126-135, (2004).

[11] M. Dubru, J.C. Nugue and G. van Marcke de Lummen. Toughened Glass: Mechanical Properties and EN 12600 Behaviour. Proceedings of Glass Processing Days, Tampere, Finland, 2005.

[12] M. Fröling and K. Persson. Computational Methods for Laminated Glass. Journal of Engineering Mechanics, 139, 7, 780-790, (2013)

[13] M. Fröling and K. Persson. Designing Bolt Fixed Laminated Glass with Stress Concentration Factors. Structural Engineering International, 23, 1, 55-60, (2013).

[14] R. Guyan. Reduction of Stiffness and Mass Matrices. AIAA, 3, 380, (1965).

[15] A.Y.T. Leung. An Accurate Method of Dynamic Condensation in Structural Analysis. International Journal for Numerical Methods in Engineering, 12, 1705-1715, (1978).

[16] J. Lorentzon. CALFEM Meshing Module. Division of Structural Mechanics and Division of Solid Mechanics, Lund University of Technology, Lund, Sweden, 2010.

[17] J. Malmborg. A Finite Element Based Design Tool for Point Fixed Laminated Glass. Master's thesis, Lund University of Technology, Lund, Sweden, 2006.

[18] N.S. Ottosen and H. Petersson. Introduction to the Finite Element Method. Prentice Hall Europe, Hemel Hempstead, England, 1992.

[19] A. Pacios, S. Postigo and C. Huerta. Relationship Between Characteristic Parameters of Impact Test for Safety Glasses. Stahlbau Spezial-Glasbau, 8, 1, 61-66, (2011).

[20] K. Persson and B. Doepker. Glass Panes Subjected to Dynamic Impact Loads. Proceedings of the XXIV A.T.I.V. Conference, Parma, Italy, 2009.

[21] R. Rück and M. Weschler. Numerical Simulation of the Pendulum Test with a Glass Plate. Otto-Graf-Journal, 11, 109-122, (2000).

[22] J. Schneider. Festigkeit und Bemessung punktgelagerter Gläser und stossbeanspruchter Gläser. Doctoral thesis, Technische Universität Darmstadt, Darmstadt, Germany, 2001.

[23] J. Schneider and S. Schula. Transient Impact Simulation and a Simplified Mechanical Model for Soft Body Impact on Glass Panes. Proceedings of the Engineered Transparency Conference, Düsseldorf, Germany, 2010.

[24] J. Schneider, S. Schula and A. Burmeister. Zwei Verfahren zum rechnerischen Nachweis der dynamischen Beanspruchung von Verglasungen durch weichen Stoss. Stahlbau, 80, 81-87, (2011).

[25] F. Serruys, G. van Marcke de Lummen and J. B. Waldron. CEN-Impact Test prEN 12600. Proceedings of Glass Processing Days, Tampere, Finland, 1999.

[26] SS-EN-12600. Glass in building-Pendulum test-Impact test method and Classification for flat glass. Swedish Standards Institute, 2003.

[27] B. Weller, S. Reich and P. Krampe. Zwei Verfahren zum rechnerischen Nachweis der dynamischen Beanspruchung von Verglasungen durch weichen Stoss. Teil 2: Numerische Vergleichungsberechnungen und experimentelle Verifikation. Stahlbau Spezial-Konstruktiver Glasbau, 88-92, (2011).

Paper 5

Numerical Analysis of Insulated Glass Subjected to Soft Body Impact

Maria Fröling and Kent Persson

Abstract

Structure-acoustic analysis is performed to analyse insulated glass subjected to dynamic impact load. A parametric study is made with respect to in-plane dimensions, glass thickness and thickness of the gas layer. For quadratic panes, a larger glass has a significantly larger center displacement but lower stresses than a smaller glass. For all studied combinations of in-plane dimensions the outer glass has a maximum stress level that is between 20 and 30 % of that of the inner glass. A single layered glass unit is proven to have only marginally greater stresses than the corresponding double glass unit. The air layer thickness has almost no influence on the stresses of the insulated glass subjected to a soft body impact. It is revealed that the thickness of the glass, however, has a large influence. Both displacements and stresses increase with decreasing pane thickness. The outer glass has a maximum stress level which is between 20 and 30 % of that of the inner glass. Further, an analysis is made of a triple insulated glass unit. Apparently, the addition of a third glass pane does not impact the structural mechanical capacity of an insulated glass unit to a great extent.

1 Introduction

Insulating glass consists of two or more glass panes with air or gas filled space(s) in between. Insulating glass units are favorable for use in buildings due to for instance the thermal insulating properties that the insulating glass possesses.

Studies of the structural mechanical behavior of insulated glass are scarce in the literature. Vallabhan and Chou (1986), [14], present a theoretical model of an insulating glass unit subjected to lateral (wind) load. An analysis was made of the load sharing between the inner and the outer glass and it was studied how the load sharing is affected by varying the temperature of the gas layer. Wörner et al. (1993), [17], made a simpler theoretical method for the load sharing analysis of a double insulated glass unit subjected to lateral load. The model is more suitable for design than the model in [14]. Vallabhan et al. (1990), [15], included the modeling of the silicone sealants that are used as connections between the glass plates of an insulating glass unit and between the glass unit and the supporting mullion. The insulated glass unit was subjected to lateral load. Both the stresses in the glass plates and the forces in the sealants were studied.

All of the previously mentioned studies deal with lateral (wind) load. Also important in the strength design of glass structures is dynamic impact load. The conditions for dealing with dynamic impact load in strength design are partly prescribed in the European and Swedish standard SS-EN-12600, [13]. Experimental and numerical studies of glass subjected to dynamic impact load were described in for instance ([12], [2], [7], [9], [5],[10], [11], [16], [3]). Experimental and numerical studies with special focus on insulated glass subjected to dynamic impact load are provided in [6] and [1].

In [1], the air filled tires of the pendulum and the air layer between the glass panes were modeled by means of the so-called uniform pressure approach. The parts of the pendulum were modeled with shell elements. The control volume concept with an equation of state for ideal gases was used for the simulation of the internal pressure of the tires and for simulating the behavior of the air space of the glass unit. The clamping framework, which was supported with diagonals, was included in the model. The study described the time development of the middle lateral displacement of the inner and outer surfaces of the insulated glass unit and comparisons with experiments were made. The model seemed to well replicate experimental data.

In this work, structure-acoustic analysis, [8], is used in the finite element modeling of insulated glass subjected to dynamic impact load. In this approach, the gas filled space is modeled by means of the acoustic wave equation and the interaction between the glass and the gas filled space is taken into account. A numerical example is made that simulates the pendulum impact test of the European and Swedish standard SS-EN-12600, [13], available to classify glass for impact strength. The test arrangement of this test is displayed in Figure 1.

A glass unit is held within a steel frame and an impactor consisting of a steel weight encased in tires is dropped from a fall height in a pendulum motion towards the glass. In order to protect the glass, there are rubber strips between the steel frame and the glass. The weight of the impactor is prescribed to 50 kg.

The commercial finite element software ABAQUS is adopted for the simulations. One of the purposes is to demonstrate the applicability of structure-acoustic analysis to this test problem. The supporting frame, and the modeling of the frame, are different from that in [1]. The approach presented serves as a useful alternative to analyse the structural problem. Further analyses are made than in [1]. Parametric studies are made with respect to the in-plane glass dimensions, the glass thickness and the air layer thickness. The studied variables are the out-of-plane displacement in the middle of the glass pane and the maximum principal stress. To conclude, a triple insulated glass unit is studied in terms of stresses.

Figure 1: Test arrangement for pendulum impact test.

2 Structure-acoustic Analysis

Structure-acoustic analysis as formulated in [8] investigates the analysis of structure-acoustic systems consisting of a flexible structure that is in contact with an enclosed cavity.

The structure is described by the differential equation of motion for a continuum body under the assumption of small deformations and the fluid behavior is captured by the acoustic wave equation. The latter equation has been derived using the following conditions for a compressible fluid: the fluid is inviscid, irrotational and undergoes small translations. The formulation enforces continuity in displacements and pressure at the boundary between the structure and fluid domains. The governing equations can be written as

$$\tilde{\nabla}^T \boldsymbol{\sigma}_s + \mathbf{b}_s = \rho_s \frac{\partial^2 \mathbf{u}_s}{\partial t^2}, \tag{1}$$

$$\frac{\partial^2 p}{\partial t^2} - c_0^2 \nabla^2 p = c_0^2 \frac{\partial q_f}{\partial t}, \tag{2}$$

$$u_s|_n = u_f|_n, \tag{3}$$

$$\boldsymbol{\sigma}_s|_n = -p, \tag{4}$$

where equations (1) and (2) govern the structure and fluid behavior respectively and equations (3) and (4) state the coupling conditions through the kinematic and static boundary

conditions. $\mathbf{u}_s$ are the displacements and $\mathbf{b}_s$ is the body force. It is defined that

$$\mathbf{u}_s = \begin{bmatrix} u_1^s \\ u_2^s \\ u_3^s \end{bmatrix}, \tag{5}$$

and

$$\mathbf{b}_s = \begin{bmatrix} b_1^s \\ b_2^s \\ b_3^s \end{bmatrix}. \tag{6}$$

$\mathbf{q}_s$ is the inertia force given as

$$\mathbf{q}_s = \rho_s \frac{\partial^2 \mathbf{u}_s}{\partial t^2}, \tag{7}$$

where ρ_s is the density of the material. The differential operator $\tilde{\nabla}$ is defined in [8]. For the fluid, p is the dynamic pressure, c_0 is the speed of sound and q_f is the added fluid mass per unit volume. The operator ∇ is defined in [8].

Standard finite element derivations lead to the following finite element formulation for the structural domain

$$\mathbf{M}_s \ddot{\mathbf{d}}_s + \mathbf{K}_s \mathbf{d}_s = \mathbf{f}_f + \mathbf{f}_b, \tag{8}$$

where $\mathbf{M}_s$ is the mass matrix, $\mathbf{K}_s$ is the stiffness matrix, $\mathbf{f}_f$ is the surface force vector, $\mathbf{f}_b$ is the body force vector and $\mathbf{d}_s$ are the nodal displacements.

Similar finite element derivations as for the structure part yields the finite element formulation for the fluid domain as follows:

$$\mathbf{M}_f \ddot{\mathbf{p}}_f + \mathbf{K}_f \mathbf{p}_f = \mathbf{f}_q + \mathbf{f}_s, \tag{9}$$

where $\mathbf{M}_f$ is the mass matrix, $\mathbf{K}_f$ is the stiffness matrix, $\mathbf{f}_s$ and $\mathbf{f}_q$ are force vectors and $\mathbf{p}_f$ denotes the nodal pressures.

To obtain the finite element formulation of the coupled structure-acoustic system, a few operations are needed. Equation (4) can be rewritten and inserted into the surface force term of equation (8). This term is then rewritten and the final format is given as follows

$$\mathbf{f}_f = \mathbf{H}\mathbf{p}_f, \tag{10}$$

where $\mathbf{H}$ is the coupling matrix, see [8]. The term $\mathbf{f}_s$ of equation (9) is also rewritten. The relation

$$\nabla p = -\rho_0 \frac{\partial^2 \mathbf{u}_f(t)}{\partial t^2}, \tag{11}$$

and the boundary condition in equation (3) are used. Finite element discretization and introduction of the coupling matrix $\mathbf{H}$ leads to the final version of the term $\mathbf{f}_s$ as

$$\mathbf{f}_s = -\rho_0 c_0^2 \mathbf{H}^T \ddot{\mathbf{d}}_s. \tag{12}$$

The final structure-acoustic problem is described by the following unsymmetrical system of equations

$$\begin{bmatrix} \mathbf{M}_s & \mathbf{0} \\ \rho_0 c_0^2 \mathbf{H}^T & \mathbf{M}_f \end{bmatrix} \begin{bmatrix} \ddot{\mathbf{d}}_s \\ \ddot{\mathbf{p}}_f \end{bmatrix} + \begin{bmatrix} \mathbf{K}_s & -\mathbf{H} \\ \mathbf{0} & \mathbf{K}_f \end{bmatrix} \begin{bmatrix} \mathbf{d}_s \\ \mathbf{p}_f \end{bmatrix} = \begin{bmatrix} \mathbf{f}_b \\ \mathbf{f}_q \end{bmatrix}, \tag{13}$$

which is the standard form of the FSI formulation.

Note that this implementation does not take into account the static pressure of the air. Moreover, in ABAQUS the fluid layer is not remeshed automatically to account for large deformations of the structure.

3 Model Validation

Two slightly different versions of the same model are developed in this paper. In this section it is described how the model adopted in Section 4 compares to the experimental data of [1] when the same in-plane dimensions and thicknesses of the material layers as in [1] are adopted. The comparison is presented in Figure 2. The result variables are the center out-of-plane displacements of the inner (closest to the impactor) and the outer panes. In the figure the inner pane is termed front and the outer is termed back.

From the figure it appears as the model results and experimental results are in good accordance until the maximum displacements are reached. The experimental maximum values are greater than the simulated ones, but for both panes the simulation error is less than 5 % which is acceptable. The peak values are occurring earlier in the simulations, but the time difference is maximum around 3 ms for the outer pane. In the experiments the whole

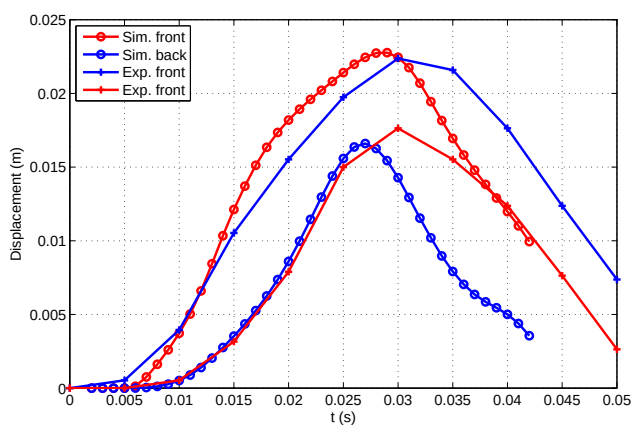

Figure 2: Comparison between model data and experimental data.

movement lasts longer than in the simulations. In [1], the support frame is different than for the current model and in [1] it is emphasized that the modeling of the frame contains all details for accurate simulation results to be obtained. In [1], close accuracy between experiments and simulations is obtained. There are further modeling differences between the model in this paper and the model in [1]. This can explain some of the discrepancies between the model results of this model and the experiments. In strength design, the maximum values of the design variables are of primary importance. For the case of maximum values, the model developed here has good accuracy, albeit the difference between the structures. Finally, the model in this paper stems from an experimentally validated model for single layered glass subjected to soft body impact, [5].

4 Parametric Study

4.1 General

In this section, parameter studies with respect to several relevant parameters were carried out for insulated glass consisting of two glass panes and a sealed cavity subjected to dynamic impact load. A case was constructed based on the model for single glass subjected to dynamic impact load by Persson and Doepker (2009), [5]. That model was extended to comprise double insulated glass. In the parametric study, the in-plane dimensions, the glass thickness and the air layer thickness were varied.

The test arrangement was modeled in ABAQUS. All parts were explicitly modeled apart from the clamping frame. The displacements of the sides of the rubber strips facing the frame were prescribed to zero in all directions. The material properties of the structure were adopted from [5] and the properties of the air were taken from [4]. A summary of the material parameters is given in Table 1. E denotes modulus of elasticity, ν is the Poisson's ratio, ρ denotes density and D is the bulk modulus.

The pendulum was swung from a fall height of 450 mm. The modeling of the parts, except for the air layer and the spacer, is described in [5]. For the air part, an 8-node linear acoustic brick element was used. Three element layers were used in the thickness direction of the air part. Totally around 100000 elements were contained in the model.

Table 1: Material parameters for pendulum impact test.

Material	E (MPa)	ν	ρ (kg/m^3)	D (MPa)
Glass	78000	0.2	2700	-
Air	-	-	1.2	0.142
Spacer	50	0.2	1000	-
Pendulum rubber	2	0.3	900	-
Pendulum steel	210000	0.3	7800	-
Frame rubber	15	0.44	1250	-

The coupling condition between the air and the glass was set through a surface based tie constraint.

The parametric study was investigating the influence of the in-plane dimensions of the insulated glass unit, the air layer thickness and the glass pane thickness. In the parametric study of the influence of the in-plane dimensions, six cases were analyzed as shown in Table 2.

The glass thickness of both panes was 6 mm and the air cavity thickness was set to 12 mm. For these cases, also a structure with one glass was analyzed for comparison purposes.

In the parametric study of the influence of the air cavity thickness, the cases with cavity thicknesses 6, 12 and 18 mm were studied. The in-plane dimensions were set to 800 $\times$ 1600 mm^2 and the glass thickness was 6 mm. In the parametric study of the influence of the glass thickness four cases were made comprising of glass thicknesses of 6, 8, 10 and 12 mm. In this study, the in-plane dimensions were 800 $\times$ 1600 mm^2 and the air cavity thickness was 12 mm.

For all studies, the result variables of interest were the out-of-plane displacement at the center of the glass and the maximum principal stress. The main interest was to compare displacements and stresses between the outer and inner glass panes.

4.2 Influence of the In-plane Dimensions of the Insulated Glass Unit

In this subsection, the results from the parametric study with respect to the in-plane dimensions are reported. Figure 3 shows the time history of the center out-of-plane displacement of the inner and outer panes for quadratic shaped insulated glass units of various dimensions.

There is a significant increase in the maximum displacement when the dimensions change from the smallest to the largest. The increase is almost 50 %. The results in terms of the maximum principal stress of the whole unit, σ_{max}, are displayed in Table 3. The values are reported for all combinations of dimensions in Table 2.

Table 2: In-plane dimensions for the parametric study.

Case	In-plane dimensions (mm^2)
d1	800 $\times$ 800
d2	800 $\times$ 1200
d3	800 $\times$ 1600
d4	1200 $\times$ 1200
d5	1200 $\times$1600
d6	1600 $\times$ 1600

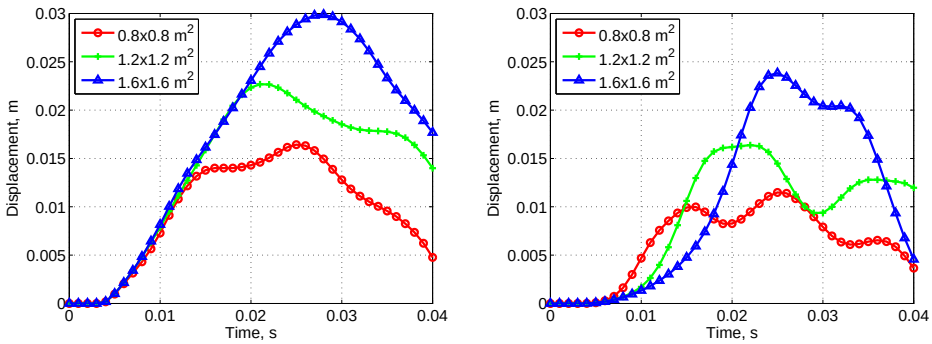

Figure 3: Time history of center displacement for quadratic insulated glasses. Inner glass to the left (a) and outer glass to the right (b).

Table 3: Maximum principal stress for various glass pane dimensions.

Dimensions (mm^2)	σ_{max} (MPa)
800×800	192.3
800×1200	199.8
800×1600	206.3
1200×1200	187.6
1200×1600	182.3
1600×1600	156.8

The time history of the maximum principal stress is shown in Figure 4 for the inner and outer panes of quadratic insulated glass of various dimensions.

From the Table 3 and Figure 4 it can be realized that there is a reduction in σ_{max} by almost 20 % when the dimensions increase from the smallest to the largest. There is a change in the behavior of the solution when the largest pane is considered. There are two subsequent stress peaks instead of one and the maximum is occurring later than for the smaller glasses. This is due to the different eigenfrequencies of the impactor and the glass panes.

For rectangular insulated glass units, the effect of increasing the length of one of the sides of the pane can be extracted by fixing the length of the other side of the pane. In Figure 5, the length of one of the sides is fixed to 800 mm and the time history of the center out-of-plane displacement of the inner pane is shown for various lengths of the variable side.

When the length of the variable side is increased from 800 to 1600 mm there is an increase in maximum displacement of around 25 %.

From the results in Table 3 it can be noted that when the length of one side of the pane is fixed to 800 mm there is a maximum increase in σ_{max} of only around 7 % if the length of the other side of the pane is varied from 800 to 1600 mm. From Table 3 it is apparent that if the length of the fixed side of the pane is 1600 mm, σ_{max} decreases with around 25 % when the length of the variable side increases from 800 mm to 1600 mm.

In Figure 3 (b) the time history of the center out-of-plane displacement of the outer pane is shown for quadratic insulated glasses of various dimensions. The maximum displacement is more than doubled when the pane size increases from the smallest to the largest and the solutions for the different pane sizes display different behaviors. The difference in behavior can partly be explained by the fact that the pressure is transferred by means of a pressure wave that travels through the unit. Compared to the maximum displacements of the inner pane, the outer displacements are 70-80 % of the inner displacements and the

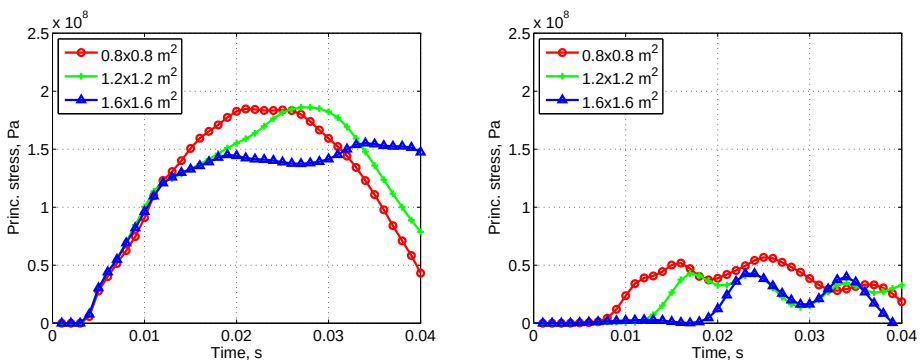

Figure 4: Time history of maximum principal stress for quadratic insulated glasses. Inner glass to the left (a) and outer glass to the right (b).

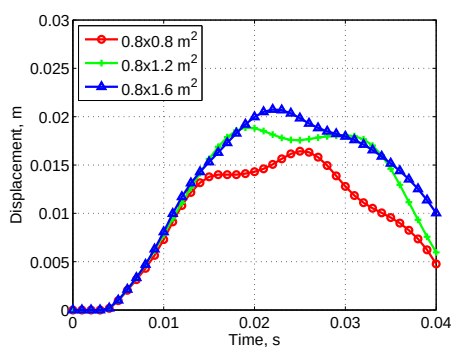

Figure 5: Time history of center displacement for rectangular insulated glasses.

ratio between outer and inner displacement is greatest for the largest dimensions.

In Table 4 the maximum principal stress for the outer glass is displayed for the various dimensions of the glass pane.

The time history of the maximum principal stress for the outer pane of quadratic insulated glass units of various dimensions is shown in Figure 4 (b). The maximum stress of the outer glass is 20 to 30 % of maximum stress of the inner glass as presented in Table 2. When rectangular glasses with one of the side lengths set to 800 mm are considered, the maximum stress of the outer glass is around 30 % of the maximum stresses of the inner glass irrespective of the length of the other side. For the largest glasses, the maximum stress of the outer glass is rather around 25 % of the maximum stresses of the inner glass.

A comparison of insulated glass and single glass in terms of σ_{max} is made in Table 5 for various dimensions of the glass.

In general there is only a small increase in the maximum stress when a single glass is used instead of an insulated glass. The largest increase is for the largest glass of dimensions 1600×1600 mm^2 where the maximum stress increases with around 15 %.

4.3 Influence of the Air Layer Thickness

In this subsection, the results from the parametric study with respect to the air cavity thickness are reported. The time history of the center out-of-plane displacement is shown in Figure 6 for varying air cavity thickness.

The corresponding results for the maximum principal stress are displayed in Figure 7 for both the inner and the outer panes.

In terms of both displacements and stresses, and for both the inner and outer panes in terms of the stresses, the influence of the air layer thickness is almost negligible.

Table 4: Maximum principal stress for outer glass for various glass pane dimensions.

Dimensions (mm^2)	Maximum principal stress (MPa)
800×800	56.8
800×1200	57.4
800×1600	63.0
1200×1200	42.4
1200×1600	42.6
1600×1600	42.7

Table 5: Maximum principal stress for single glass and double insulated glass for various glass pane dimensions.

Dimensions (mm^2)	σ_{max} (MPa), double glass	σ_{max} (MPa), single glass
800 × 800	192.3	196.8
800 × 1200	199.8	204.2
800 × 1600	206.3	213.8
1200 × 1200	187.6	188.6
1200 × 1600	182.3	197.3
1600 × 1600	156.8	182.2

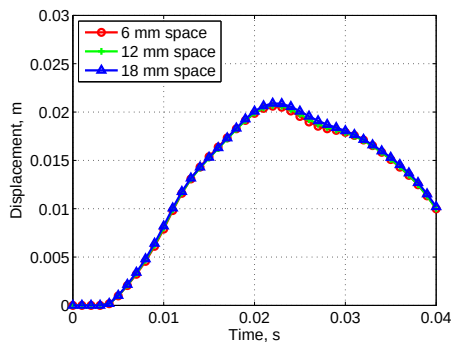

Figure 6: Time history of center displacement for insulated glasses of varied cavity thickness.

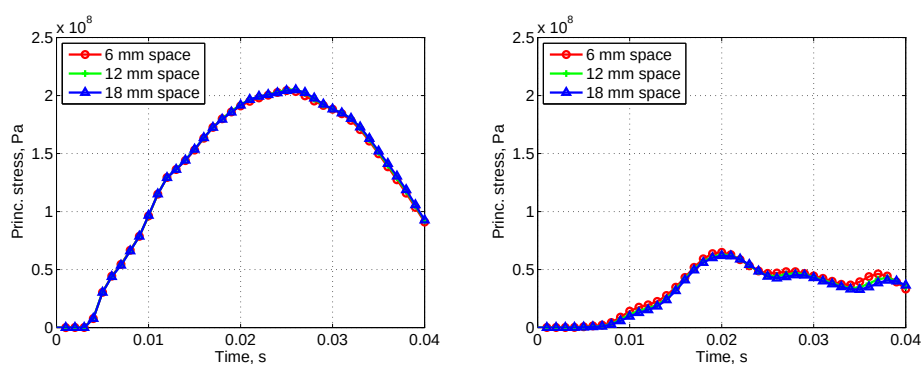

Figure 7: Time history of maximum principal stress for insulated glasses of varied cavity thickness. Inner glass to the left (a) and outer glass to the right (b).

4.4 Influence of the Glass Thickness

This subsection reports the results of the parametric study with respect to the glass thickness. Figure 8 shows the time history of the center out-of-plane displacement for the inner

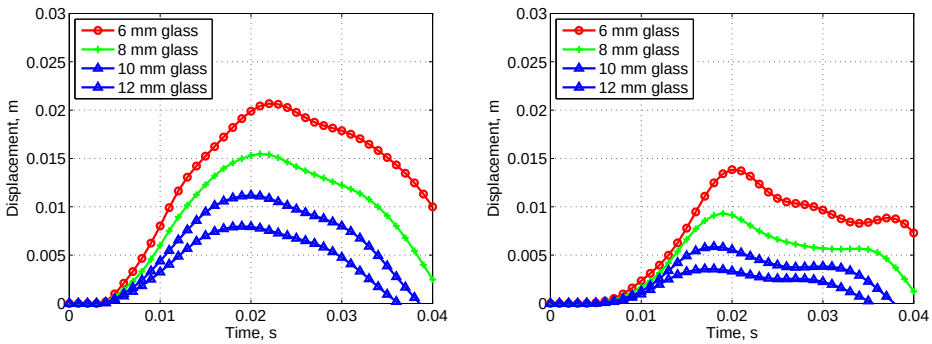

Figure 8: Time history of center displacement for insulated glasses of varied glass thickness. Inner glass to the left (a) and outer glass to the right (b).

and outer panes of insulated glasses of various glass thicknesses.

The displacements increase with decreasing pane thickness. When the pane thickness is 12 mm, the maximum displacement is around 40 % of the maximum displacement for the case with glass pane thickness of 6 mm. For the thinnest glass, the outer pane has a maximum displacement that is around 65 % of the maximum displacement of the inner pane. For the thickest glass, this relation is around 40 %. Apparently the fraction of outer maximum displacement to inner maximum displacement increases when the glass pane thickness decreases.

The time history of the maximum principal stresses for the inner and outer panes of insulated glasses of various glass thickness is shown in Figure 9.

The maximum stresses increase with decreasing pane thickness. For a pane thickness of 12 mm, the maximum stress is around 60 % of the maximum stress when the pane thickness is 6 mm. The outer pane has maximum stresses between 20 and 30 % of the maximum stresses of the inner pane. There is a small tendency that the value of this fraction increases as the glass pane thickness decreases.

5 Analysis of Insulated Glass with Three Glass Layers

In some applications, triple insulated glass is used. In this section, the aim was to evaluate the structural performance of a triple insulated glass unit. The performance was evaluated in terms of the maximum principal stress. For this examination, a slightly different model was adopted. The in-plane dimensions were the same as in [1], namely a height of 2056 mm and a width of 1050 mm. The thickness of the glass was set to 7.75 mm and the thickness of the air layer was set to 16 mm in line with [1]. Some material parameters

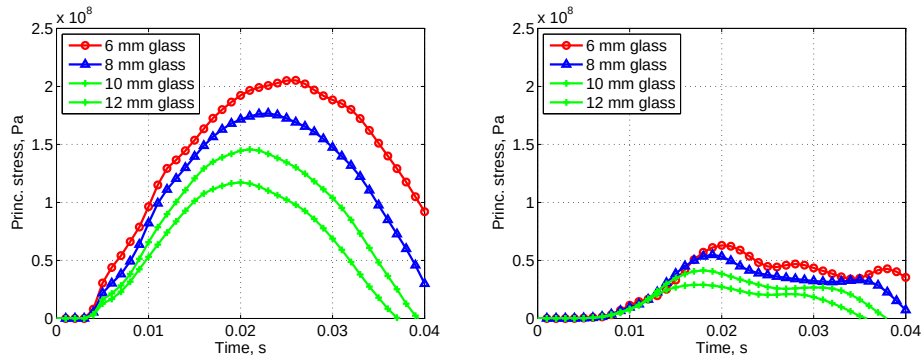

Figure 9: Time history of maximum principal stress for insulated glasses of varied glass thickness. Inner glass to the left (a) and outer glass to the right (b).

were changed compared to in Table 1. To the extent possible, the material parameters were set as in [1]. The values of the material parameters that were changed are E = 70000 MPa, ν = 0.23 and ρ = 2500 kg/m^3 for the glass and ν = 0.23 for the frame rubber. The spacer was not explicitly modeled, but the air parts were set to be rigidly supported on the sides facing the frame.

The results in terms of σ_{max} are displayed in Table 6.

The inner glass pane has a stress level that is less than 5 % lower than that of the inner glass pane of that which arises in a double glass unit modeled in a similar fashion. This value is 154.8 MPa. It is noteworthy that the middle glass has a very low value of the maximum stress. For this case, the maximum stress is not located in the middle of the glass pane. The outer glass has a stress level which is slightly greater than the outer glass of the corresponding double glass unit, 56.7 MPa. When it comes to strength design, it seems like there is little to be gained to add a third glass pane to the insulating unit.

6 Conclusions and Future Work

In this paper, structural-acoustic analysis is used to develop a finite element model of an insulated glass unit subjected to dynamic impact load. The method is suggested as a use-

Table 6: Maximum principal stress (MPa) of glass panes for triple glass.

Pane	σ_{max}
Inner	150.7
Middle	8.6
Outer	58.3

ful means to analyze this type of problem.

A parametric study is made in terms of the in-plane dimensions of the unit. For quadratic glasses, a larger glass unit has significantly larger center displacement but lower stresses than a smaller unit. The outer glass has maximum center displacement that is 70-80 % of the maximum center displacement of the inner glass. For all combinations of dimensions the outer glass has a maximum stress level that is between 20 and 30 % of the maximum stress level of the inner glass. When a single layer glass is used instead of a double insulated glass unit, there is only a small increase in the stress level. It appears as the structural mechanical gain of using insulated glass instead of single layered glass is almost negligible.

For a standard double insulated glass unit, a parametric study with respect to the air layer thickness is made. Apparently, the air layer thickness has a minor influence on the structural mechanical behavior of the studied glass unit.

Further, a parametric study that investigates the influence of the glass thickness on the structural behavior of the insulated glass is made. The glass thickness seems to be a relevant design variable in strength design of insulated glass. Both displacements and stresses increase with decreasing pane thickness. In terms of maximum stresses, the difference between using the thickest and thinnest glass in the study is around 40 %. The ratio between outer and inner values of both displacements and stresses increases as the pane thickness decreases and for the stresses the value of this ratio ranges between 20 and 30 %.

Finally, a triple insulated glass unit is analysed in terms of stresses. The maximum stresses of the unit are almost not reduced at all compared to the maximum stresses of a corresponding double glass unit. The outer glass pane has a stress level which largely is comparable to that of the outer glass of the corresponding double glass unit. An interesting result is that the middle pane has very low stresses and the maximum stress of that pane is not located in the middle of the pane. From a strength design perspective a triple glass unit does not seem to give an added value compared to a two glass unit, but may instead increase the cost.

The present analysis can be extended in several ways. It could be interesting to consider different glass pane thicknesses of the inner and outer panes of one unit. The influence of different boundary conditions can also be interesting to study. A further extension is to have another gas than air in the insulated unit. It would also be of interest to vary the impactor fall height.

The current framework of modeling may also be used to investigate other types of research questions relating to for instance sound insulation properties.

Experimental results on insulated glass units are scarce. Further experimental tests would shed light on the structural mechanical properties of insulated glass and serve as an aid in

validating the numerical results.

References

[1] S. Brendler, A. Haufe and T. Ummenhofer. A Detailed Numerical Investigation of Insulated Glass Subjected to the Standard Pendulum Test. Proceedings of the Third LS-DYNA Forum, Bamberg, Germany, 2004.

[2] M. Dubru, J.C. Nugue and G. van Marcke de Lummen. Toughened Glass: Mechanical Properties and EN 12600 Behaviour. Proceedings of Glass Processing Days, Tampere, Finland, 2005.

[3] M. Fröling, K. Persson and P.-E. Austrell. A Reduced Model for Glass Structures Subjected to Dynamic Impact Loads. Proceedings of the TU0905 COST Action Mid-term Conference on Structural Glass, Poreč, Croatia, 2013.

[4] F.P. Mechel. Formulas of Acoustics. Springer-Verlag, Berlin Heidelberg, Germany, (2002).

[5] K. Persson and B. Doepker. Glass Panes Subjected to Dynamic Impact Loads. Proceedings of the XXIV A.T.I.V. Conference, Parma, Italy, 2009.

[6] R. Rück. Tragverhalten von Mehrscheiben-Isolerglas. Doctoral thesis, Otto-Graf-Institut, Universität Stuttgart, Germany, 2002.

[7] R. Rück and M. Weschler. Numerical Simulation of the Pendulum Test with a Glass Plate. Otto-Graf-Journal, 11, 109-122, (2000).

[8] G. Sandberg, P.A. Wernberg and P. Davidsson. Fundamentals of Fluid-Structure Interaction. Computational Aspects of Structural Acoustics and Vibration, CISM Courses and Lectures, G. Sandberg and R. Ohayon (eds), vol. 505. Springer, Wien, Austria, (2008).

[9] J. Schneider. Festigkeit und Bemessung punktgelagerter Gläser und stossbeanspruchter Gläser. Doctoral thesis, Technische Universität Darmstadt, Darmstadt, Germany, 2001.

[10] J. Schneider and S. Schula. Transient Impact Simulation and a Simplified Mechanical Model for Soft Body Impact on Glass Panes. Proceedings of the Engineered Transparency Conference, Düsseldorf, Germany, 2010.

[11] J. Schneider, S. Schula and A. Burmeister. Zwei Verfahren zum rechnerischen Nachweis der dynamischen Beanspruchung von Verglasungen durch weichen Stoss. Stahlbau, 80, 81-87, (2011).

[12] F. Serruys, G. van Marcke de Lummen and J.B. Waldron. CEN-Impact Test prEN 12600. Proceedings of Glass Processing Days, Tampere, Finland, 1999.

[13] SS-EN-12600. Glass in building-Pendulum test-Impact test method and Classification for flat glass. Swedish Standards Institute, 2003.

[14] C.V.G. Vallabhan and G.D. Chou. Interactive Nonlinear Analysis of Insulated Glass Units. Journal of Structural Engineering, 112, 6, (1986).

[15] C.V.G. Vallabhan, G.D. Chou and J.E. Minor. Seal Forces in Structural Glazing Systems. Journal of Structural Engineering, 116, 4, 1080-1089, (1990).

[16] B. Weller, S. Reich and P. Krampe. Zwei Verfahren zum rechnerischen Nachweis der dynamischen Beanspruchung von Verglasungen durch weichen Stoss. Teil 2: Numerische Vergleichungsberechnungen und experimentelle Verifikation. Stahlbau Spezial-Konstruktiver Glasbau, 88-92, (2011).

[17] J.-D. Wörner, X. Shen and B. Sagmeister. Determination of Load Sharing in Insulating Glass Units. Journal if Engineering Mechanics, 119, 2, 386-392, (1993).